

INVESTIGATION OF ACTIVE SUSPENSION SYSTEM IN
A MULTI-BODY QUARTER CAR MODEL

HIMADRI SHASTRY

**INVESTIGATION OF ACTIVE SUSPENSION SYSTEM IN A MULTI-BODY
QUARTER CAR MODEL**

by

© Himadri Shastry

A Thesis submitted to the

School of Graduate Studies

in partial fulfillment of the requirements for the degree of

Master of Engineering

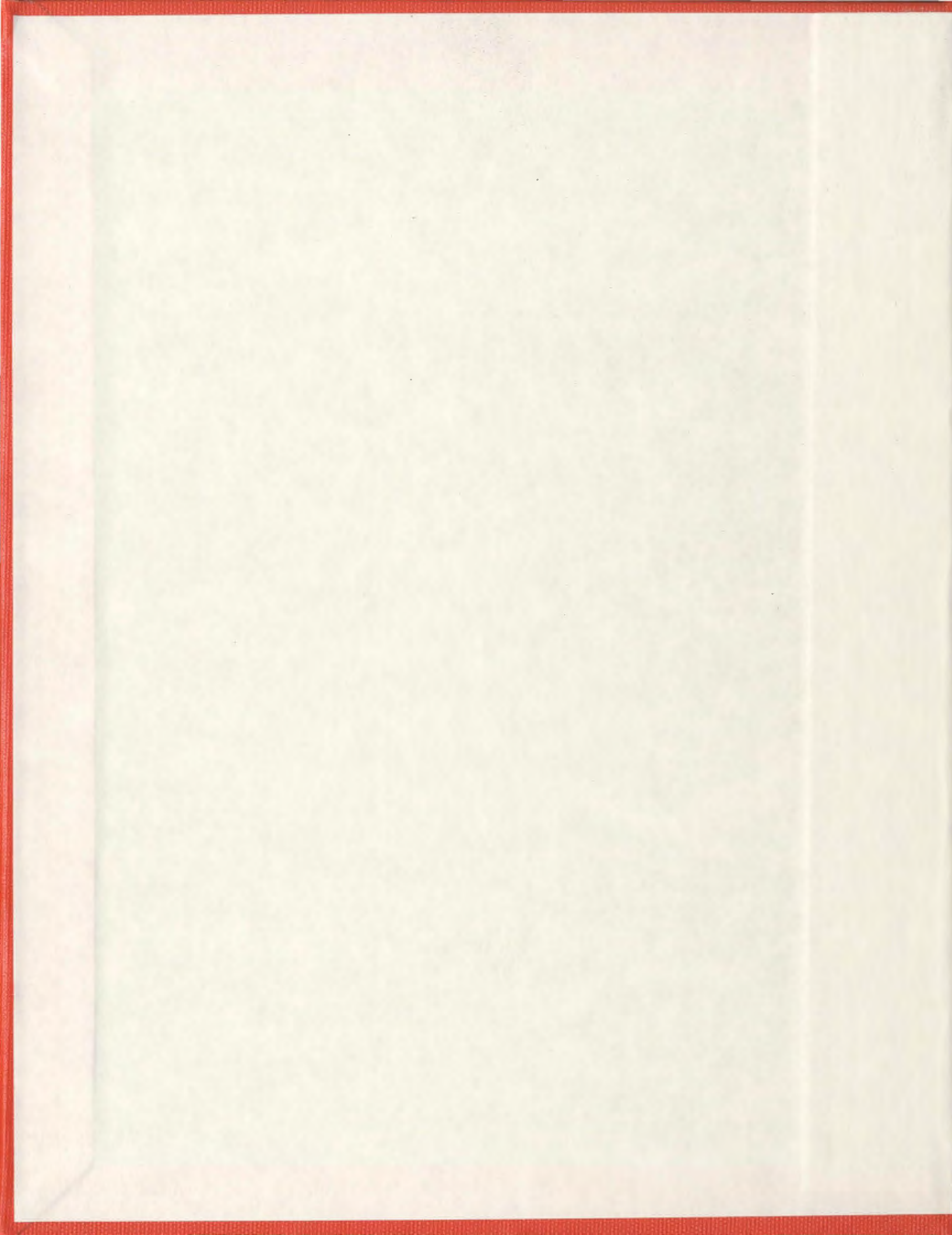
Faculty of Engineering and Applied Sciences

Memorial University of Newfoundland

January 2013

St. John's

Newfoundland



ABSTRACT

Technological advancements in the automotive industry have led to various improvements in vehicle safety, ride quality and aesthetics. Vehicle safety is one of the foremost issues that the automotive industry is constantly working on to reduce the risk of injury and discomfort to passengers. Humans are sensitive to vibrations and excessive vibrations can cause injury or discomfort such as back pain, fatigue, mental stress and unseating of passengers. Road holding and vehicle stability is affected by road disturbances, suspension characteristics and directional motion of the vehicle. Ride quality is also influenced by vibrations induced from the road as well as imbalances in the tire/wheel assembly. In order to analyze and suppress vehicle vibrations and increase vehicle safety, a non-linear multi-body quarter car model and a linear quarter car model have been developed using bond graph methodology.

Active suspension system has been developed in this research using a linear quadratic controller and applied to the linear quarter car and the multi-body model. The multi-body model has been characterized to obtain the parameters for suspension and damping coefficients that can be used in the linear quarter car model. Non-linearity has been introduced in the multi-body model with the use of non-linear components (springs and dampers) and/or use of geometric non-linearity of the suspension. A gain factor is applied to the actuator force of the active suspension system of the multi-body model to compensate for the kinematic differences between the linear model and the non-linear model. A comparison study is performed in frequency and time domain for both the models and four cases have been developed to study the effectiveness of the linear

quadratic controller on the multi-body model as well as the linear quarter car model. The results show that the multi-body model performs better than the linear quarter car model when there is low geometric non-linearity. When component non-linearity and high geometric non-linearity are introduced in the multi-body model, the performance of the linear quadratic controller deteriorates in comparison to the linear quarter car, particularly for the ride quality scenarios. The active suspension system for the multi-body model performs better than the passive system in all the four cases.

The research winds up with a discussion on how the objectives outlined in the study have been attained and recommendations for future work.

ACKNOWLEDGEMENTS

I would like to thank my thesis adviser Dr. Geoff Rideout for providing me the opportunity to work under his esteemed guidance. Throughout these two years at Memorial University of Newfoundland, he has been a source of inspiration and provided me encouragement and motivation in my graduate courses and research. I have a high regard for him and his encouraging attitude towards students which inspires me to excel in studies and thereafter.

I would also like to take this opportunity to thank Mustafizur Rahman and Keith Wakeham for providing the help and support whenever I needed and encouragement to do well in my research.

Last but not the least, I would like to thank my family who has provided me the support and back-up in every walks of life. Without their love and caring this would not have been possible.

Table of Contents

ABSTRACT	ii
ACKNOWLEDGEMENTS	iv
Table of Contents	v
List of Tables	vii
List of Figures	viii
List of Symbols, Nomenclature or Abbreviations	xii
Symbols.....	xii
Abbreviations.....	xiii
List of Appendices	xiv
Chapter 1: Introduction and Background.....	1
1.1 Introduction.....	1
1.2 Objective	2
1.3 Research Outline	3
Chapter 2: Literature Review	5
2.1 Research Background	5
2.1.1 Types of Vehicle Models	7
2.1.2 Types of Suspension	9
2.2 Multi-body Vehicle Models	13
2.3 Controller Design	15
2.4 Bond Graph Modeling	18
Chapter 3: Multi-body Control Arm Suspension Model	20
3.1 Overview	20
3.2 Bond Graph Background	20
3.3 SLA Suspension.....	24
3.4 Multi-body Quarter Car Model	24
3.4.1 Non-linear Component Addition	41
3.5 Conclusion	43
Chapter 4: Equivalent Quarter Car Suspension Model	45
4.1 Overview	45
4.2 MATLAB/Simulink model for quarter car	46
4.3 Bond graph model for quarter car	48
4.4 Method of determining quarter car parameters.....	49

4.5 Simulation results for quarter car model.....	54
4.6 Comparison of Multi-body vs. Quarter Car Results	56
4.7 Conclusion	58
Chapter 5: Active Suspension Controller Design and Simulation.....	60
5.1 Overview.....	60
5.2 LQR Controller Design.....	62
5.3 Frequency Domain Analysis.....	67
Ride quality test for quarter car	68
Road holding test for quarter car	70
5.3.1 Open loop test	71
Ride quality test for multi-body model	75
Road holding test for multi-body model	76
5.4 Time Domain Analysis	77
Case 1: Linear components with low suspension deflection (5 cm).....	77
Road holding.....	86
Case 2: Non-linear components with low suspension deflection (5 cm).....	90
Case 3: Linear components with high suspension deflection (16 cm).....	97
Case 4: Non-linear components with high suspension deflection (16 cm).....	106
5.5 Summary of Results	112
5.6 Conclusion	116
Chapter 6: Conclusions and Future Work.....	117
6.1 Conclusion	117
6.2 Quarter Car Model	117
6.2.1 Future Work	117
6.3 Controller Design.....	118
6.3.1 Future Work	118
References.....	121

List of Tables

Table 1: Simulation parameters for quarter car model	37
Table 2: Initialization parameters for the multi-body model	39
Table 3: Quarter car parameters.....	53
Table 4: Bond graph eigenvalues for quarter car.....	56
Table 5: Ride quality (peak amplitudes) summary for four cases	113
Table 6: Road holding (peak amplitudes) summary for four cases	114
Table 7: Road holding (settling times) summary for four cases.....	115

List of Figures

Figure 1: Pin joint (A) and pin-in-slot (B) [46]	6
Figure 2: Quarter car model [1]	7
Figure 3: Half car model [1]	8
Figure 4: Full car model [1]	8
Figure 5: Hotchkiss rear suspension [5].....	10
Figure 6: Trailing arms suspension [5]	11
Figure 7: MacPherson strut [5]	12
Figure 8: Double wishbone/SLA suspension [5]	12
Figure 9: Bond graph constitutive laws and symbols [35]	22
Figure 10: Causal stroke placement [35]	23
Figure 11: Bond graph example scenario [35].....	23
Figure 12: SLA suspension [1]	24
Figure 13: SLA suspension model in bond graph [21]	25
Figure 14: 3-D motion of a rigid body [2]	26
Figure 15: Generalized rigid body and frames of references	27
Figure 16: Generalized vector A	28
Figure 17: Co-ordinate system location for multi-body model.....	29
Figure 18: EJS for body 5 of multi-body quarter car model.....	31
Figure 19: Full multi-body quarter car model.....	33
Figure 20: EJS sub-model body 4	34
Figure 21: Tire sub-model.....	34
Figure 22: EJS submodel body 3	35
Figure 23: Suspension (spring and damper)	36
Figure 24: String multi-body quarter car model (Solidworks)	38
Figure 25: Sprung mass acceleration MB model – Passive mode	40
Figure 26: Suspension states MB model – Passive mode	40
Figure 27: Non-linearity due to large suspension deflection	41
Figure 28: Effect of non-linear spring on MB model	42
Figure 29: Bi-linear damper for MB model	43

Figure 30: 2 DOF quarter car model.....	45
Figure 31: Simulink model with state-space matrix design.....	47
Figure 32: Notation for bond graph equation formulation.....	48
Figure 33: Slow sinusoidal test for stiffness coefficient.....	50
Figure 34: Sinusoidal test for stiffness coefficient.....	51
Figure 35: Work diagram for damping coefficient.....	52
Figure 36: Force-velocity deflection curve for damping coefficient.....	53
Figure 37: Pole-zero plots for Simulink model.....	55
Figure 38: Road input (8 cm).....	56
Figure 39: Sprung mass acceleration for MB & QC model (Passive mode).....	57
Figure 40: Suspension deflection for MB & QC model (Passive mode).....	57
Figure 41: Tire deflection for MB & QC model (Passive mode).....	58
Figure 42: Overview of cases for studying active suspension system.....	62
Figure 43: Road profile – 5 cm bump.....	67
Figure 44: Sprung mass acceleration bode plot for QC model (highly rated ride quality).....	68
Figure 45: Sprung mass acceleration bode plot for QC model (moderately rated ride quality).....	69
Figure 46: Suspension deflection bode plot for QC model (highly rated road holding).....	70
Figure 47: Tire deflection bode plot for QC model (highly rated road holding).....	70
Figure 48: Open loop test illustration.....	71
Figure 49: Open loop test for MB model.....	72
Figure 50: Open loop test (2) for MB model.....	73
Figure 51: Sprung mass acceleration bode plot for MB model (Passive state).....	74
Figure 52: Sprung mass acceleration bode plot for MB model (highly rated ride quality).....	75
Figure 53: Sprung mass acceleration bode plot for MB model (moderately rated ride quality).....	75
Figure 54: Suspension deflection bode plot for MB model (highly rated road holding).....	76
Figure 55: Tire deflection bode plot for MB model (highly rated road holding).....	76
Figure 56: Road profile – 5 cm bump.....	78
Figure 57: Case 1 – Sprung mass acceleration for MB and QC models (highly rated ride quality).....	79

Figure 58: Case 1- QC model active vs. passive states (highly rated ride quality)	79
Figure 59: Case 1- MB model active vs. passive states (highly rated ride quality).....	80
Figure 60: Case 1 - PI (highly rated ride quality)	81
Figure 61: Case 1 - Sprung mass acceleration (highly rated ride quality).....	81
Figure 62: Case 1 – MB vs. QC model in active state (highly rated ride quality).....	82
Figure 63: Case 1 - Sprung mass acceleration for MB and QC models (moderately rated ride quality)	83
Figure 64: Case 1- QC model active vs. passive states (moderately rated ride quality)....	83
Figure 65: Case 1- MB model active vs. passive states (moderately rated ride quality) ...	84
Figure 66: Case 1 - PI (moderately rated ride quality)	85
Figure 67: Case 1 - Sprung mass acceleration (moderately rated ride quality)	85
Figure 68: Case 1 - MB vs. QC model in active state (moderately rated ride quality).....	86
Figure 69: Case 1 – QC model active vs. passive states (road holding)	87
Figure 70: Case 1 - MB model active vs. passive states (road holding)	87
Figure 71: Case 1 - PI (road holding)	88
Figure 72: Case 1 - Suspension deflection (road holding).....	88
Figure 73: Case 1 - Tire deflection (road holding)	89
Figure 74: Case 2 – Sprung mass acceleration for MB and QC models (ride quality).....	91
Figure 75: Case 2- MB model active vs. passive states (ride quality)	91
Figure 76: Case 2 - PI (ride quality)	92
Figure 77: Case 2 - Sprung mass acceleration (ride quality)	92
Figure 78: Case 2 – MB vs. QC model in active state (ride quality)	93
Figure 79: Case 2 - MB model active vs. passive states (road holding)	94
Figure 80: Case 2 - PI (road holding)	95
Figure 81: Case 2 - Suspension deflection (road holding).....	95
Figure 82: Case 2 - Tire deflection (road holding)	96
Figure 83: Case 3 - Road profile – 16 cm bump.....	97
Figure 84: Case 3 – Sprung mass acceleration for MB and QC models (ride quality).....	98
Figure 85: Case 3- QC model active vs. passive states (ride quality).....	99
Figure 86: Case 3- MB model active vs. passive states (ride quality)	100
Figure 87: Case 3 - PI (ride quality)	100
Figure 88: Case 3 - Sprung mass acceleration (ride quality)	101

Figure 89: Case 3 – MB vs. QC model in active state (ride quality).....	101
Figure 90: Case 3 – QC model active vs. passive states (road holding).....	102
Figure 91: Case 3 - MB model active vs. passive states (road holding).....	103
Figure 92: Case 3 - PI (road holding)	103
Figure 93: Case 3 - Suspension deflection (road holding).....	104
Figure 94: Case 3 - Tire deflection (road holding)	105
Figure 95: Case 4 – Sprung mass acceleration for MB and QC models (ride quality)....	107
Figure 96: Case 4 - MB model active vs. passive states (ride quality).....	107
Figure 97: Case 4 - PI (ride quality)	108
Figure 98: Case 4 - Sprung mass acceleration (ride quality)	108
Figure 99: Case 4 – MB vs. QC model in active state (ride quality).....	109
Figure 100: Case 4 - MB model active vs. passive states (road holding).....	110
Figure 101: Case 4 - PI (road holding)	110
Figure 102: Case 4 - Suspension deflection (road holding).....	111
Figure 103: Case 4 - Tire deflection (road holding)	112

List of Symbols, Nomenclature or Abbreviations

Symbols

a = acceleration of the rigid body G

F = force acting on the rigid body G

P = momentum of the rigid body G

r = a general vector in frame of reference 2

v_G = velocity of the center of mass G

v_A = velocity of point A on the rigid body G

${}^1\vec{v}_G$ = velocity of the center of mass G in frame of reference 1

2v_G = velocity of the center of mass G in frame of reference 2

${}^2v_{GX}$ = velocity of the center of mass G in x direction in frame of reference 2

${}^2v_{GY}$ = velocity of the center of mass G in y direction in frame of reference 2

${}^2\dot{v}_{GX}$ = acceleration of the center of mass G in x direction in frame of reference 2

${}^2\dot{v}_{GY}$ = acceleration of the center of mass G in y direction in frame of reference 2

${}^0X, {}^0Y$ = global coordinates for multi – body model

G_5 = center of mass of body 5 for multi – body model

${}^5X, {}^5Y$ = local coordinates of body 5 for multi – body model

θ_5 = initial orientation of body 5 for multi – body model

R_{01} = rotation matrix from frame of reference 0 to 1 for multi – body model

Abbreviations

DAQ – Data acquisition

DOF – Degree of freedom

EJS – Euler junction structure

FPGA – Field programmable gate array

LQR – Linear quadratic regulator

LVDT – Linear variable differential transformer

MB – Multi-body (Non-linear quarter car model)

MRAC – Model reference adaptive control

MTS – Material testing systems

PI – Performance index

QC – Quarter car (Unidirectional linear quarter car model)

SLA – Short long arm (suspension)

SI – System identification

List of Appendices

A	MATLAB/SimMechanics Multi-body Model	126
B	LQR Controller Gains	128
C	Bond Graph States	131

Chapter 1: Introduction and Background

1.1 Introduction

One of the most important objectives of automotive industry today is to make safer vehicles. In order to accomplish that modeling is done even more so to shorten the design and development cycle and models are developed of varied complexity and various scenarios are tested. The two main objectives for vehicle dynamics related to vibrations are to maintain the ride quality and road holding. These competing objectives, the details of which have been discussed in Section 5.1, pose a challenge for designing a controller since the performance of one affects the other [1].

Studies have been conducted on vehicle models for quarter, half and full cars but these models typically show linear behavior [12, 13, and 14]. Even if there is non-linearity in the system model, the components used in the model are often linear [30, 31]. Different kinds of controllers are developed and applied on these linear models and their performances are analyzed [10, 11, 15]. Simulations have been performed in various modeling environments such as MATLAB/Simulink [13], bond graphs (20-Sim) [25, 28] and CarSim [20] etc. To simulate a 2-D non-linear suspension design, a bond graph based multi-body quarter car model has been developed in this research using 20-sim [21] software. 20-sim software is a modeling and simulation program which possess multi-domain (electrical, mechanical, hydraulics) modeling capabilities [21]. The complexity of the multi-body model is increased by adding non-linearity to the system in various ways. The non-linearity in the multi-body model is of two types: component non-linearity due to springs and dampers and geometric non-linearity due to suspension travel. A linear

unidirectional quarter car model has also been developed using bond graph method. Both these models are compared to each other in passive mode for differences in system responses. Bond graph modeling facilitates multi-body modeling and it also provides multi-energy domain capabilities. The system equations can also be formulated by using bond graph method. The second important aspect of this thesis is to develop a linear controller using state space method that can be applied to both the models so that it suppresses the vibrations experienced by the vehicle or provides good road holding. This approach will determine the limits of a linear controller applied to a non-linear multi-body model. Various controllers have been used in the literature [8, 10, 11, and 15] but there has been little comparison between non-linear and linear models. Also, a comprehensive literature has not revealed prior work on how the linear controller performs for non-linear model in passive and active mode. These issues have been addressed in this research. A linear quadratic controller has been applied to both the models and the response of the vehicle states has been compared in the frequency and the time domain.

The study concludes by providing a summary of the objectives attained in this research and the scope of future work.

1.2 Objective

The objective of this thesis is to design a multi-body quarter car model using bond graph method and apply a controller to investigate the performance of active suspension system when the vehicle is undergoing road perturbations. The quarter car model will be introduced with two main kinds of nonlinearities: component and geometric. A linear

quadratic regulator (LQR) controller will be designed to assess its performance on an inherently non-linear system for ride quality as well as road holding scenarios. The controller performance will also be tested on a linear quarter car model.

The controller will then be compared for performance on the multi-body quarter car model and the linear quarter car model in active and passive states in frequency and time domain. This would ascertain the limitations of the controller on the multi-body model.

The future works will consist of validating the simulation models and the controller performance on a quarter car test-bed by real-time testing.

1.3 Research Outline

Chapter 1 provides an introduction and background study on the topic of vehicle dynamics. It provides a brief outline of the current state of research in vehicle dynamics and the motivation for this thesis in developing a non-linear multi-body model and applying a linear controller to analyze its performance. Further it discusses the need for a quarter car test rig to test and verify the simulation results.

Chapter 2 provides a documentation of the existing literature related to car models and basics of vehicle dynamics. It also discusses different types of control schemes implemented in simulation and hardware realizations of suspension models.

Chapter 3 provides a brief introduction to bond graph methodology related to multi-body modelling of vehicles. It provides an overview of the short long arm suspension and a detailed description of the multi-body quarter car model developed in this research. Non-linearity is also introduced in the model related to the components i.e. the spring and damper and geometric due to the suspension travel.

Chapter 4 provides an equivalent quarter car model using the bond graph method and MATLAB/Simulink. The suspension parameters for the linear model are determined by numerical experiments on the multi-body model. The equations related to the linear quarter car are also introduced in this section and simulations for multi-body model and linear quarter car are compared with each other in passive mode.

Chapter 5 introduces the optimal control derivation i.e. the linear quadratic regulator approach. Then simulation is performed in the frequency domain to show the benefits of active suspension control for ride quality and road holding properties in the linear quarter car and the multi-body model. Then a comparison between the two models is done in time domain with four different case scenarios. The case scenarios are based on increasing complexity of the multi-body model in terms of nonlinearities due to components and geometry.

Chapter 6 provides a background on what problems were encountered in the quarter car test rig and the hardware changes that were implemented on it. It provides documentation on the hardware and software changes that were made to improve the test-bed. Passive tests were performed on the test-bed to show how the experiments agree with the simulation.

Chapter 7 provides the conclusion, recommendations and scope of future work related to this research.

Chapter 2: Literature Review

2.1 Research Background

The automotive industry has been constantly looking for new technologies and innovative ideas to produce safer and better cars. There has been research going on in academic as well as industrial domains to better study dynamics of vehicles. A poor ride quality affects passengers' ability to drive safely. The implications of poor ride quality could be detrimental to the safety of passengers by causing injury or discomfort, fatigue, unseating and customer dissatisfaction. Research in vehicle dynamics has been constantly trying to find solutions to make it safer for passengers to drive their vehicles. The suspension characteristics of a vehicle play an important role in the vehicle dynamics. There are some key terms in vehicle dynamics to be noted before further discussion on advanced topics–

Sprung mass – The overall mass of the vehicle built on the chassis and supported by the suspension system.

Unsprung mass – This consists of the overall mass of the suspension system, wheel spindle and tires.

Ride frequency – The natural frequency of resonance experienced by a passenger sitting in a car, when it is traversing over a given road profile.

Wheel hop frequency – The frequency at which the tire starts to resonate due to the road input.

Passive suspension system – A passive suspension system consists of un-actuated spring and damper components in a vehicle.

Active suspension system – An active suspension system consists of the passive system (spring and damper) and also an actuator which exerts additional force on the suspension and helps in suppressing the vibrations experienced by a vehicle.

Semi-active system – A semi-active suspension system does not transfer independent force on the suspension, rather it provides variable damping or spring adjustability in real time.

Jounce and rebound – Jounce is the compression and rebound is the extension of the suspension components.

Some other important terms have been defined here-

Demultiplexor (demux) – A demux is a device which accepts a single input vector signal and separates it into multiple scalar output signals [44].

Pin-joint – A 1-DOF joint between two bodies, where each of the body is free on any axis with respect to each other.

Pin-in-slot – This type of joint allows sliding motion between the bodies and allows the bodies to pivot with respect to each other.

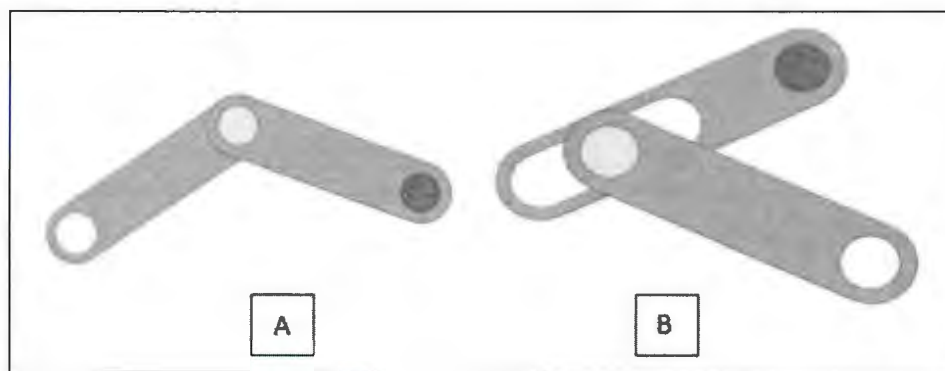


Figure 1: Pin joint (A) and pin-in-slot (B) [46]

2.1.1 Types of Vehicle Models

There are various types of vehicle models that can be analysed to describe the dynamics of the vehicle [1]. Vehicle models can be categorised in various levels of complexity. A 2-DOF 'quarter car' model as shown in Figure 2 represents each corner of a vehicle. The sprung mass is composed of the weight of the vehicle at one corner m_s and the unsprung mass is composed of the weight due to the axle and tire m_u . The suspension is characterized by a spring k_s , damper b_s and an actuator F_a in case of active suspension.

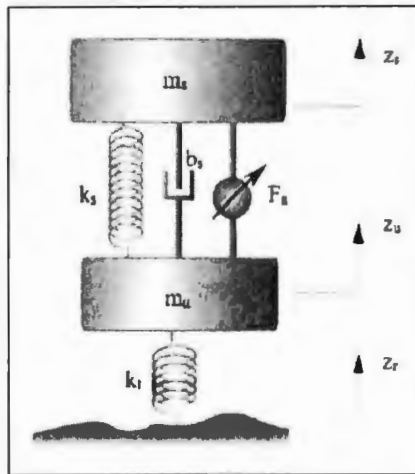


Figure 2: Quarter car model [1]

A 4-DOF half car model is shown in Figure 3. In this case, the pitch and heave of the vehicle can be calculated as well as the vertical translation of the front and the rear axles. The vehicle is assumed to be dissected halfway going from front to back of the car. So, the spring and damper elements of the car are concentrated on the left and right side of the model.

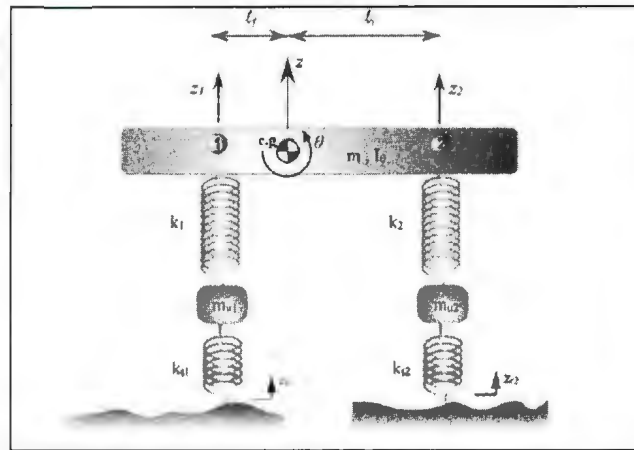


Figure 3: Half car model [1]

A full car model having 7-DOF is the most complex to design and it can provide the heave, pitch and roll of the vehicle body and the vertical motions at each corner of the vehicle. In this case, we can vary the road input that is experienced by the vehicle for the front and rear tires. A full car model is shown in Figure 4.

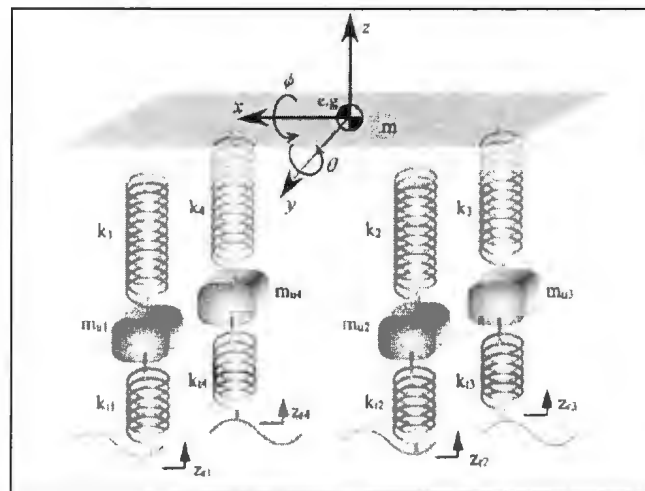


Figure 4: Full car model [1]

2.1.2 Types of Suspension

The passive suspension is made up of spring and damper components. The spring supports the static weight of the vehicle and handles the load applied on it at any corner which could be due to passengers, luggage or weight transfer while cornering. The damper prevents the suspension to vibrate erratically when it encounters an uneven road or bumps and maintain contact of the vehicle on the road.

The suspensions in a vehicle serve two main objectives of maintaining the ride quality and have a good road holding, which are often competing with each other. The ride quality of the vehicle is defined as the vibrations experienced by the passengers in the vehicle. The role of the suspension is to suppress these vibrations so that it provides excellent ride quality. In a vehicle model, it is measured by sprung mass acceleration (\ddot{z}_s). Road holding is a very important aspect of vehicle dynamics as it involves cornering, braking and traction abilities of a vehicle. The suspension also provides road holding properties to a vehicle as it can be quantified in terms of the tire deflection ($z_u - z_r$) performance [1].

Good road holding of a vehicle is also provided by the suspension and it can classified as the roll and pitch accelerations of the vehicle. For a good road holding, these parameters should be minimized. The suspension supports the weight of the vehicle as well as the passengers. This can be quantified as suspension deflection ($z_s - z_u$) performance [1].

The rattle space is the space available for suspension deflection in a vehicle.

There are two main types of suspensions: dependent and independent systems. In dependent systems, the motion of the wheel on one side of the vehicle is transferred to the

wheel on the other side. This has an adverse effect on the vehicle performance and hence it has been replaced by independent suspensions in passenger vehicles. In independent systems, the motion of one wheel is not transferred to the other wheel and each suspension acts independently [5].

There are two types of solid axle or dependent suspensions, which have been described -

Hotchkiss Rear Suspension

This kind of dependent suspension system consists of leaf springs which support the axles. The movement of these leaf springs is restricted to vertical motion. At one of the leaf springs, there is a pin connection to enable the vertical motion and the other end consists of pivot links as shown in Figure 5.

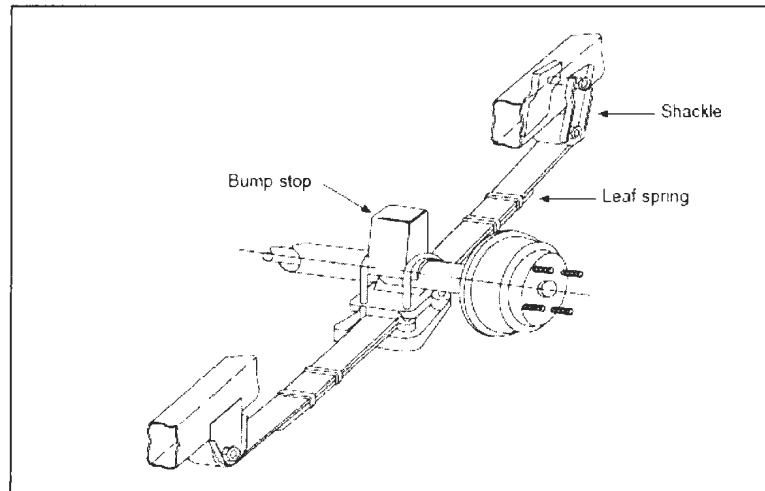


Figure 5: Hotchkiss rear suspension [5]

This kind of suspension is very simple to build and also has a rugged architecture. The problem with this kind of suspension is that the leaf springs cannot have unrestricted

flexibility, which degrades the ride quality in vehicles equipped with Hotchkiss rear suspension systems [5].

Trailing Arms Suspension

This is a rigid axle configuration where coil or air springs can be used, and the movement is restricted to vertical motion and rolling motion, shown in Figure 6. This four link design provides advantage in the choice of roll center selection, anti-squat and anti-dive geometry. The lateral movement in this suspension is not possible due to the rigid joint of the trailing arms to the wheel [5].

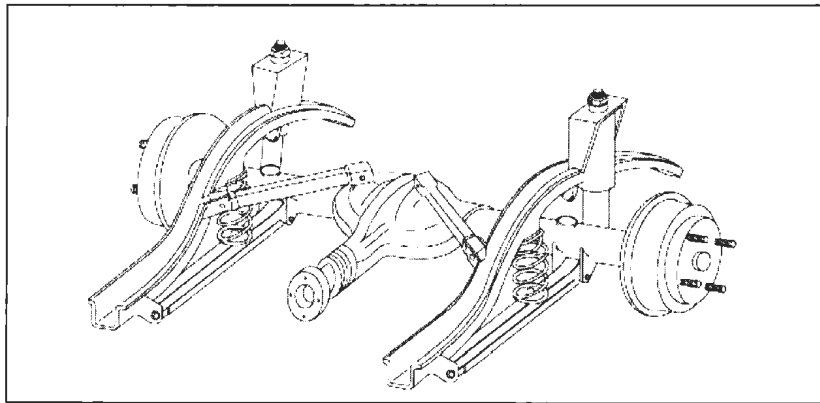


Figure 6: Trailing arms suspension [5]

The main types of independent suspension have been summarized below

MacPherson Strut

This type of suspension can move vertically due to the telescopic link, laterally due to the transverse arms and longitudinally due to the extension link, depicted in Figure 7. The spring can be attached in parallel to the damper or it could be integrated with the damper itself.

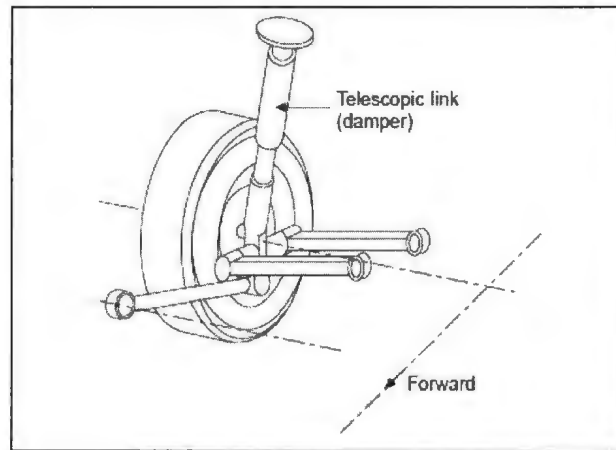


Figure 7: MacPherson strut [5]

The main disadvantage of this type of suspension is that the height adjustment becomes an issue when a low bonnet line vehicle style is required by the designer [5].

Double Wishbone/SLA

This type of suspension resembles a four bar mechanism as shown in Figure 8, with the spring and damper components attached between two A-arms, the lower one longer than the upper links to accommodate space requirements. A knuckle is attached at the centre of the coupler link (lower A-arm) which provides vertical motion to the knuckle.

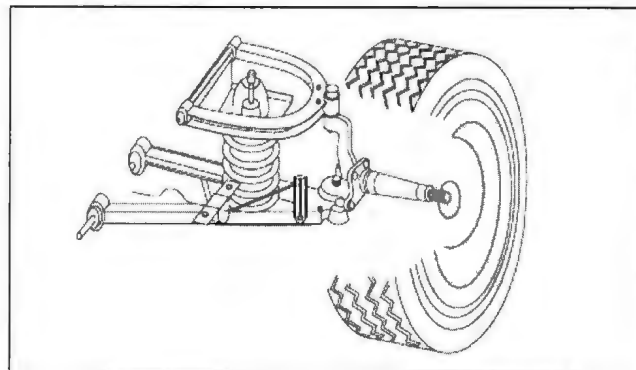


Figure 8: Double wishbone/SLA suspension [5]

The multi-body model developed in this research is based on a SLA suspension system as it can sustain high transverse and longitudinal loads and has found its application in high performance vehicles such as Alfa Romeo, Honda and Mercedes Benz [5]. The kinematic links in this type of suspension can be tuned easily and the effect of each of the links can also be calculated using a simple four-bar mechanism. This makes it advantageous in an analytical point of view. It also provides significant geometric non-linearity which is useful in this research to analyse the performance of the controller in later sections.

2.2 Multi-body Vehicle Models

This section provides documentation on multi-body vehicle models that are found in literature. Prior work on multi-body modeling of vehicles have been identified and discussed according to their applicability and usefulness in this research.

Sandu et al. [12] have performed a multi-body simulation on a MacPherson strut suspension system. Using a quarter car test rig, they have identified the system using system identification (SI) techniques. They compared a linear and non-linear quarter car system. The model generated using SI process is used for control purposes of the quarter car test rig. The linear and non-linear models are compared with the experimental results. It showed that the sprung mass accelerations of both linear and non-linear models are very close to each other. The description of a kinematic non-linear model is useful since the model in this thesis is also based on a multi-body model with kinematic non-linearity.

Crolla et al. [13] showed a co-simulation approach in analyzing the dynamic responses of a vehicle. In this paper, a multi-body simulation model of a full car is generated using Visual Nastran. MATLAB is used to integrate the model with its inputs and outputs and the controller. This co-simulation approach is adopted so that the different vehicle subsystems i.e. vehicle models, suspension types, and tyre models can be validated individually. A lumped parameter full vehicle model is used to identify the system rather than using quarter car models, which does not account for non-linearity. The results showed that the response of the sprung mass acceleration for a semi-active suspension system is affected greatly but the response of the unsprung mass remains largely unaffected. However, different tyre models affect the loads applied to the hub of a vehicle. A semi-active system improves vehicle body response but has significant effect on the unsprung mass response and the force applied on the suspension. This paper shows integration of the multi-body simulation approach with control strategy using MATLAB and Visual Nastran.

Mantaras et al. [14] provided documentation of kinematic modeling of a MacPherson strut with constraint equations for the various links of the mechanism. It used two different frames of references; body fixed and inertial frames. Once the constraint equations are formulated, the spatial geometry of the suspension system is determined. Using MATLAB/Simulink, the equations are solved and the model is validated. This paper provides a kinematic model of MacPherson suspension and it permits optimization of the suspension geometry. The basics of multi-body modeling are provided in this paper

like using two frames of references and Euler's parameters, which will be helpful in the modeling of SLA suspension in this research.

This thesis develops a multi-body model based on a different vehicle suspension configuration (SLA suspension) due to its advantages as discussed in Section 2.1. The model has kinematic non-linearity similar to that of the MacPherson strut [12] as well as component non-linearity. The SLA suspension is developed using bond graph approach, where it is easier to build a multi-body models compared to the cumbersome process described in [14] using MATLAB/Simulink. This research also develops a linear quadratic controller to assess the performance of the active suspension system, unlike both papers [12] and [14]. The results of controller design are assessed for the multi-body model and compared with the linear quarter car model in this research, similar to the methodology adopted in [13]. This thesis uses 20-sim [21] for bond graph modeling and MATLAB for initial validation of the linear quarter car model, the inspiration of which comes from [13] where two different modeling environments are used.

2.3 Controller Design

This section provides different control architectures in the literature and their application to different vehicle models. It also shows various kinds of software approaches used in modeling the system or the controller.

Hrovat [8] discussed various types of suspension designs with increasing complexity and how LQR controller performs in comparison to the passive suspension. A 1-DOF quarter car model was developed, wheel hop was measured using a 2-DOF quarter car model,

pitch and heave were measured by a 2-DOF half car model and a full 7-DOF comprehensive vehicle model was also developed in this paper. The paper concluded with successful implementation of optimal control in quarter car models, further developing 2-DOF quarter car models and other vehicle models with higher complexities.

Hrovat [10] developed a linear quadratic regulator (LQR) controller for a linear quarter car suspension system and a non-linear hydraulic actuator. The dynamic equations of the quarter car model and hydraulic actuator are generated and using the LQR approach, a cost function is calculated and solved to obtain the optimal gains. The results show marked improvement of active suspension systems over the passive systems. The sprung mass acceleration is reduced in an active suspension system with optimal feedback gains. The body displacement is also reduced for the LQR active suspension system in comparison to a passive system.

Esmailzadeh and Fahimi [15] presented an optimal active suspension system for a linear 7 DOF vehicle model. The state equations for the 7 DOF model are generated and a cost function is also determined for optimum control. An adaptive control system is discussed for implementation of model reference adaptive control (MRAC) by utilizing the optimal control model as the basic system model for the vehicle. This ensures that the controller always tries to approach the optimal performance of the system. The paper concludes with simulations showing that the optimal control and MRAC control perform much better than the passive system.

Crolla et al. [11] used a Kalman filter for state estimation of a fully active suspension system of a quarter car model. Using the state space equations a system model is generated and a cost function is used to calculate the optimal gains for the system. Then an observer is designed using the optimal gains, which in the case of a Kalman filter estimates the states of the system. A filtered gaussian white noise is used the road input. The closed loop system using the optimal Kalman estimation process is compared with a full state feedback. The model works very well with different road inputs and the Kalman filter is able to predict the states with little loss of performance.

Hrovat [8] and [10] develops a basic and effective controller linear quadratic regulator and its performance is tested on various vehicle models. But the literature rarely discusses the application of a linear LQR controller on a multi-body model to see how it performs in comparison to a linear quarter car model and also in terms of their active and passive states. Here, a linear LQR controller is designed and it is applied to both the multi-body quarter car model as well the linear quarter car model and their performance is analysed in various scenarios. The two papers by Crolla et. al. [11] and Ezmailzadeh and Fahimi [15] discuss some of the advanced non-linear controllers which have been applied to linear vehicle models. Such controllers could also be tested on the multi-body models; however their added complexity may not be justified if an LQR controller works on a non-linear plant.

2.4 Bond Graph Modeling

In this section, some of the modelling procedure performed using the bond graph method have been outlined. Since this research involves the development of a multi-body quarter car model, study of bond graph literature would provide further insight on the feasibility and advantages of this method.

Pacejka [28] developed a multi-body modeling procedure for vehicle systems using bond graphs. It describes the problems in multi-body modeling and how bond graph method can be used to eliminate these problems and make modeling for multi-body systems easier. It provides examples by describing dynamics of a rigid body in a body fixed frame and calculating the body motions. Then the inertial frame is discussed to calculate the position and orientation of the rigid body. Next, it describes the combination of two different bodies in bond graph and goes on to develop constraint equations for a car-caravan model.

Margolis et al. [30] developed a non-linear full car model using the bond graph method to investigate longitudinal dynamics. This paper is crucial in demonstrating how the instrumentation (sensors, actuators and controls) are applied to the whole vehicle model in bond graph. Due to the advantage of having multi-domain capability, the bond graph method is suited to model analysis or simulation. A simple PI control was applied to the model and the yaw rate response was analysed for steering control and brake control.

Jahromi et al. [9] discussed the characterization of a rubber isolator for frequency dependent parameters of the stiffness and damping in an oil drill string. In this paper stiffness and damping parameters were found using an experimental setup to test the rubber isolators used to suppress vibrations in sonic head drilling machines. The force-displacement curve provided the spring stiffness. Once the spring force was deducted from the total force, the damping force-velocity curve provided the damping coefficient. The area of the work diagram (force-displacement curve) was also used to calculate the damping coefficient.

Rideout and Hadi [28] and Margolis and Shim [30] develop vehicle models using bond graph method and employ controllers on it to study vehicle dynamics. The study shows that using the bond-graph method to develop multi-body models is much more intuitive than using other widely used software like MATLAB/Simulink. The bond graph method can be used to define different frames of references for a 2-D or a 3-D model using Euler junction structure, which has been discussed in Section 3.2. Also the paper by Jahromi et al. [9] is useful in providing a method to characterize the multi-body model with stiffness and damping coefficients using sinusoidal excitation, which has been conducted in Section 4.4. This is performed to obtain the suspension parameters for the linear quarter car model.

The next chapter develops a multi-body quarter car model using bond graph method and the model is explained in detail.

Chapter 3: Multi-body Control Arm Suspension Model

3.1 Overview

A multi-body model for a quarter car using SLA suspension has been developed using bond graph method. The significance of such a model is that it accounts for the geometrical non-linear nature of the quarter car; the modeling of which is not typical in the literature. A detailed description of the multi-body model has been presented. This type of model could also encompass component non-linearity as has been discussed later in this chapter. After the modeling is complete, it is verified by conducting simulations and analysing the system response in passive state.

3.2 Bond Graph Background

Bond graph methodology has been used in this research to design the multi-body quarter car model and perform simulations. Bond graphs are an energy flow based method which has the capability of combining components of different domains that make up a system [3]. The forces acting on the system can be represented with an effort source Se and the velocities experienced by the system with a flow source Sf . Generalized effort e and flow f are defined by the time derivatives of generalized variables momentum p and displacement q . Two or more elements can be combined together in a junction, which are power conserving nodes [2]. In bond graph methodology two types of junctions are present, “0-junction” and “1-junction”. “0-junction” represents common effort nodes, where the flow of the connecting bonds adds up to zero. Similarly, “1-junction” represents common flow nodes, where the effort of the connecting bonds adds up to zero

[34]. The inertial elements acting on the system, for example the mass of the system can be denoted by $I:m$, which store kinetic energy. The moment of inertia of rotational elements in the system can be denoted by $I:J$. The 0- and 1- junctions can be appended with various energy dissipative or energy storing components such as resistive elements R or capacitive elements C . Some other power conserving elements could also be used in the formation of a system, such as a transformer TF , which is used to transfer energy from one point to another in the same energy domain and/or a gyrator GY , which is used to transfer energy from one point to another in a different domain. In case the parameter is not constant but varying, these power conserving elements could be modified to modulated transformers MTF and modulated gyrators MGY . Figure 9 shows the symbols and constitutive laws for the various elements that have been discussed.

	SYMBOL	CONSTITUTIVE LAW (LINEAR)	CAUSALITY CONSTRAINTS
SOURCES			
Flow	$Sf \mapsto$	$f = f(t)$	fixed flow out
Effort	$Se \dashrightarrow$	$e = e(t)$	fixed effort out
ENERGETIC ELEMENTS			
Inertia	$\dashrightarrow I$	$f = \frac{1}{I} \int e dt$	preferred integral
	$\mapsto I$	$e = I \frac{df}{dt}$	
Capacitor	$\mapsto C$	$e = \frac{1}{C} \int f dt$	preferred integral
	$\dashrightarrow C$	$f = C \frac{de}{dt}$	
Resistor	$\mapsto R$	$e = Rf$	none
	$\dashrightarrow R$	$f = \frac{1}{R} e$	
2-PORT ELEMENTS			
Transformer	$\begin{array}{c} 1 \dashrightarrow TF \dashrightarrow 2 \\ n \end{array}$	$e_2 = n e_1$ $f_1 = n f_2$	effort in-effort out or flow in- flow out
Modulated Transformer	$\begin{array}{c} \downarrow \theta \\ \dashrightarrow MTF \dashrightarrow \\ n(\theta) \end{array}$	$e_2 = n(\theta) e_1$ $f_1 = n(\theta) f_2$	
Gyator	$\begin{array}{c} 1 \mapsto GY \dashrightarrow 2 \\ n \end{array}$	$e_2 = n f_1$ $e_1 = n f_2$	flow in-flow out or effort in-effort out
Modulated Gyator	$\begin{array}{c} \downarrow \theta \\ \mapsto MGY \dashrightarrow \\ n(\theta) \end{array}$	$e_2 = n(\theta) f_1$ $e_1 = n(\theta) f_2$	
CONSTRAINT NODES			
1-junction	$\begin{array}{c} 1 \dashrightarrow 1 \dashrightarrow 2 \\ \vee_3 \end{array}$	$e_2 = e_1 - e_3$ $f_1 = f_2$ $f_3 = f_2$	one flow input
0-junction	$\begin{array}{c} 1 \mapsto 0 \mapsto 2 \\ \vee_3 \end{array}$	$f_2 = f_1 - f_3$ $e_1 = e_2$ $e_3 = e_2$	one effort input

Figure 9: Bond graph constitutive laws and symbols [35]

The positive direction of power is defined in the direction of the half arrow (power bond) [34]. In bond graph, the direction of inputs and outputs is designated by a causal stroke (normal to the power bond). The possible causality that results in the input or the output of the connecting elements is defined by the causal stroke. As an example, the effect of causal stroke placement is illustrated by Figure 10.

$$\begin{array}{l} f = \Phi_A(e) \quad \mathbf{A} \xrightarrow[e]{f} \mathbf{B} \quad e = \Phi_B(f) \\ e = \Phi_{A^{-1}}(f) \quad \mathbf{A} \xrightarrow[e]{f} \mathbf{B} \quad f = \Phi_{B^{-1}}(e) \end{array}$$

Figure 10: Causal stroke placement [35]

Bond graph provides easy inspection of causality between inputs and outputs and to detect algebraic loops and dependent states [2]. For example, a mechanical and electrical system is shown and a bond graph is generated for both the systems in Figure 11. The generalized effort e can be the force $F(t)$ or voltage supply $V(t)$ and the generalized flow f can be either the velocity or the current. The mass M and inductance L act as inertial elements I , the resistive element is the damper B and the resistor R and the capacitive element is the spring K and the capacitor C for the mechanical and the electrical system respectively.

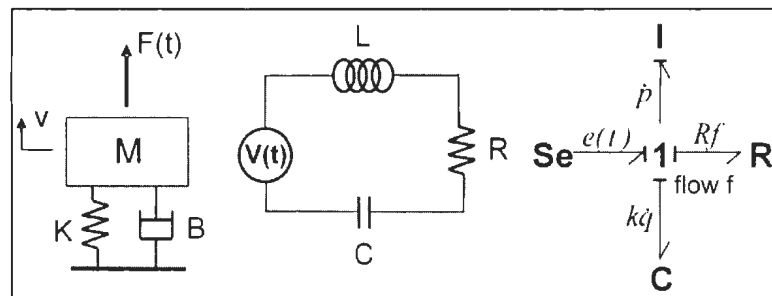


Figure 11: Bond graph example scenario [35]

3.3 SLA Suspension

As discussed previously, double wishbone suspension or as commonly called short long arm suspension (SLA) forms the basis of the non-linear quarter car model in this thesis. SLA suspension has a short upper arm due to space constraints and a longer lower arm as shown in Figure 12. The springs and dampers are attached in between these arms. The set-up can be approximated as a planar four-bar mechanism, if the steering link is omitted [1].



Figure 12: SLA suspension [1]

This type of suspension design possesses superior strength in terms of load handling capabilities and dynamic characteristics [29].

3.4 Multi-body Quarter Car Model

The multi-body quarter car model formulation is based on a bond graph approach that has previously been described and a planar approximation is shown in Figure 13, developed

using 20-Sim [21]. Two types of co-ordinate systems are used in this model. One is the inertial coordinate system which is the global co-ordinate system XY , which neither accelerates nor rotates [3]. Another is the body fixed coordinate system which is attached to each of the bodies and uses a moving coordinate system [3]. The need for a moving coordinate system in vehicle dynamics arises to describe the motion of the vehicle easily since the body-fixed coordinate system translates and rotates with its attachment to a rigid body and its inertial properties are not affected by this motion. Body-fixed coordinate system can only represent the linear and angular velocities as well as accelerations but the position of the body cannot be conveniently expressed in this coordinate system [3].

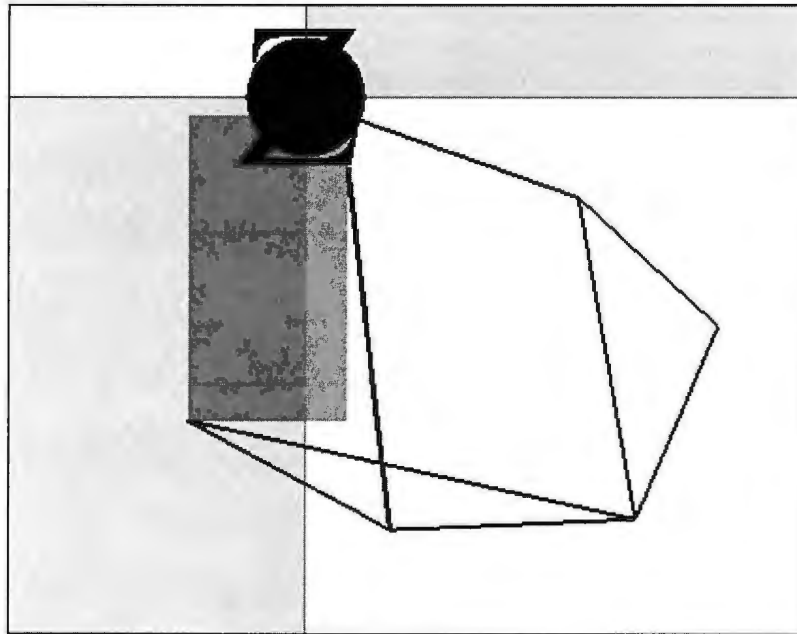


Figure 13: SLA suspension model in bond graph [21]

Figure 15 (B) shows a rigid body in 2-D motion with center of mass G located in a body fixed frame of reference 2. The inertial coordinate system is located in frame of reference

1 as shown in Figure 15 (A). For a generalized rigid body in 3-D motion of mass m as shown in Figure 14, the dynamic principles for any type of coordinate frames can be described by the following equations. The force \vec{F} acting on the body is defined by change in its momentum \vec{P} . The body has an absolute velocity \vec{v} and absolute angular velocity $\vec{\omega}$. The inertial coordinates are X, Y and Z and the body-fixed coordinates are x, y and z attached to the center of mass G .

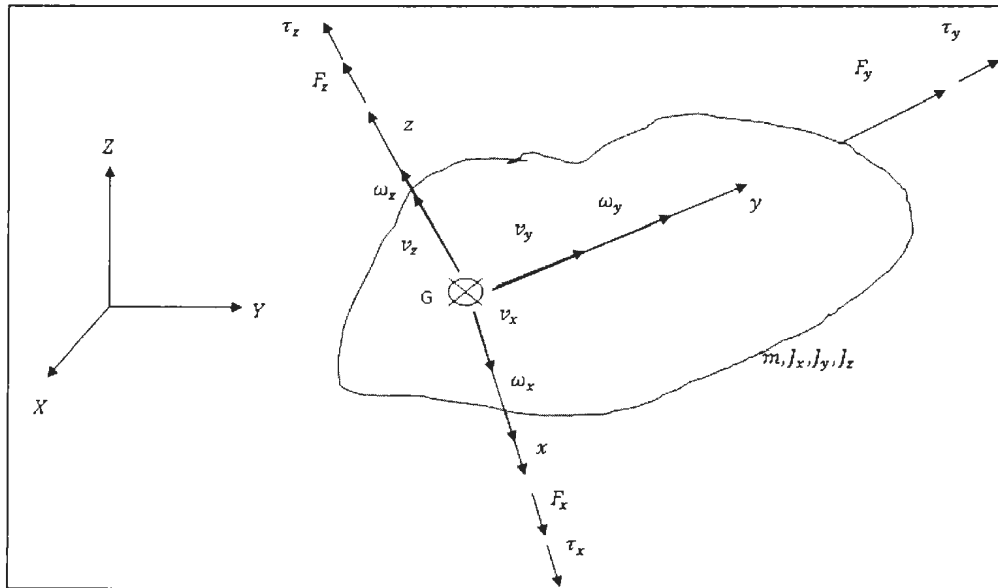


Figure 14: 3-D motion of a rigid body [2]

$$\vec{F} = \frac{d}{dt}(\vec{P}) = m\vec{a}$$

$$\vec{F} = \frac{d}{dt}(m\vec{v}_G) + \vec{\omega} \times (m\vec{v}_G)$$

$$\vec{F} = \begin{bmatrix} m & {}^2\dot{v}_{GX} \\ m & {}^2\dot{v}_{GY} \end{bmatrix} + \vec{\omega} \times m \begin{bmatrix} {}^2v_{GX} \\ {}^2v_{GY} \end{bmatrix}$$

$$\vec{F} = m \begin{bmatrix} {}^2\dot{v}_{GX} \\ {}^2\dot{v}_{GY} \end{bmatrix} + \vec{\omega} \times m \begin{bmatrix} {}^2v_{GX} \\ {}^2v_{GY} \end{bmatrix}$$

$$\begin{aligned}\vec{F}_X &= m {}^2\dot{v}_{GX} + \vec{\omega} \times m {}^2v_{GX} \\ \vec{F}_Y &= m {}^2\dot{v}_{GY} + \vec{\omega} \times m {}^2v_{GY} \\ \vec{F}_X &= m {}^2\dot{v}_{GX} + \omega \hat{k} \times m {}^2v_{GX} \hat{i} = m {}^2\dot{v}_{GX} - m \omega {}^2v_{GY} \\ \vec{F}_Y &= m {}^2\dot{v}_{GY} + \omega \hat{k} \times m {}^2v_{GY} \hat{j} = m {}^2\dot{v}_{GY} + m \omega {}^2v_{GX} \\ \vec{F} &= m \begin{bmatrix} {}^2\dot{v}_{GX} \\ {}^2\dot{v}_{GY} \end{bmatrix} + m \begin{bmatrix} -\omega {}^2v_{GY} \\ \omega {}^2v_{GX} \end{bmatrix} \quad (3.4.1)\end{aligned}$$

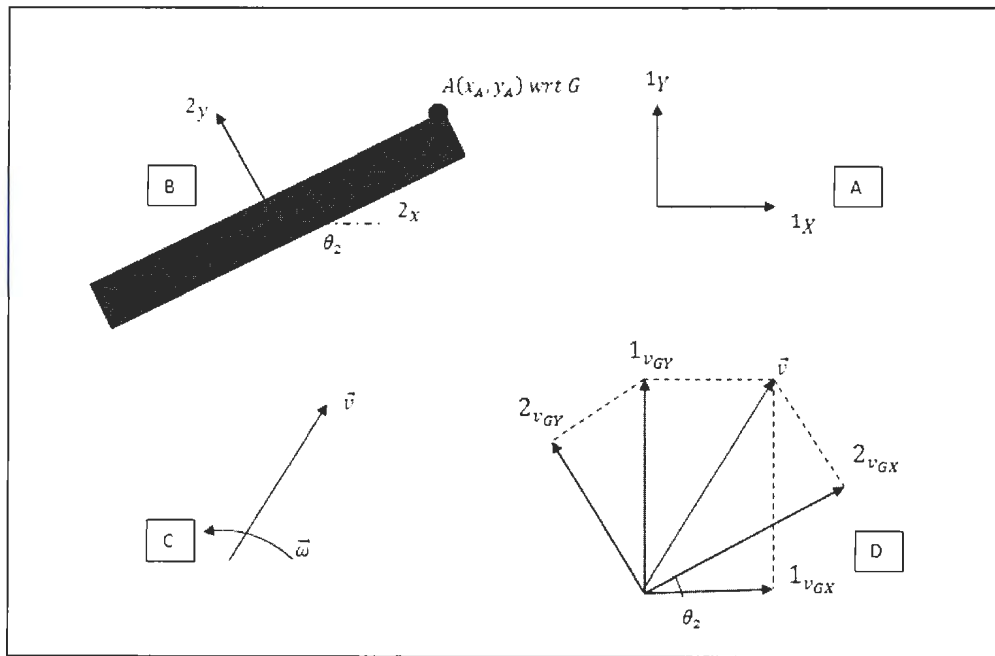


Figure 15: Generalized rigid body and frames of references

For a general vector r in a frame of reference 2,

$$\begin{aligned}\vec{r} &= r ({}^2\hat{i}) \\ \frac{d}{dt}(\vec{r}) &= \dot{r} ({}^2\hat{i}) + \vec{\omega} \times \vec{r}\end{aligned}$$

$$\vec{\omega} \times \vec{r} = \omega(\hat{k}) \times r({}^2i) = \omega r ({}^2j)$$

$$\frac{d}{dt}(\vec{r}) = \dot{r} ({}^2i) + r \omega ({}^2j) \quad (3.4.2)$$

For a point A located in rigid body as shown in Figure 16, the equations of motion are given. Here, G is the centroid of the body. Refer to page xii for the definition of the symbols used in this section.

$$\vec{v}_A = \vec{v}_G + \vec{v}_{A/G} \quad (3.4.3)$$

$$\vec{v}_{A/G} = \frac{d}{dt} \vec{r}_{A/G} = \frac{d}{dt} (x_A {}^2i + y_A {}^2j) \quad (3.4.4)$$

$$\omega \hat{k} \times \vec{r}_{A/G} = \frac{d}{dt} (x_A {}^2i + y_A {}^2j) \quad (3.4.5)$$

$$-\omega y_A \hat{k} + \omega x_A \hat{j} = \frac{d}{dt} (x_A {}^2i + y_A {}^2j) \quad (3.4.6)$$

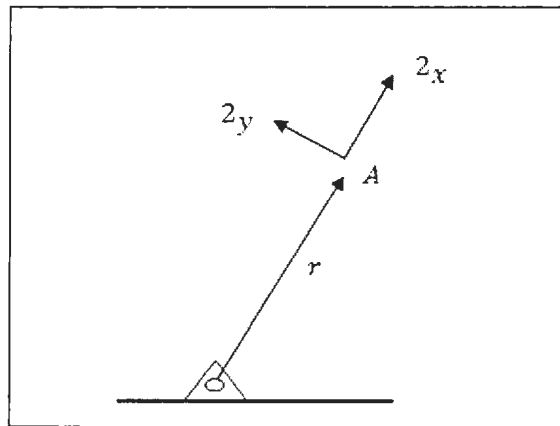


Figure 16: Generalized vector A

Now, to transform these coordinates in a body-fixed frame to inertial frame of reference, transformation matrices are used. Continuing the previous example to go from reference frame 2 to 1 shown in Figure 15 (D), the following transformation matrices are obtained.

$$\begin{bmatrix} {}^2i \\ {}^2j \end{bmatrix} = \begin{bmatrix} \cos \theta_2 & \sin \theta_2 \\ -\sin \theta_2 & \cos \theta_2 \end{bmatrix} \begin{bmatrix} i \\ j \end{bmatrix}$$

$$\begin{bmatrix} i \\ j \end{bmatrix} = \begin{bmatrix} \cos \theta_2 & -\sin \theta_2 \\ \sin \theta_2 & \cos \theta_2 \end{bmatrix} \begin{bmatrix} {}^2i \\ {}^2j \end{bmatrix}$$

$${}^1\vec{v}_G = R_{12} {}^2\vec{v}_G \quad (3.4.5)$$

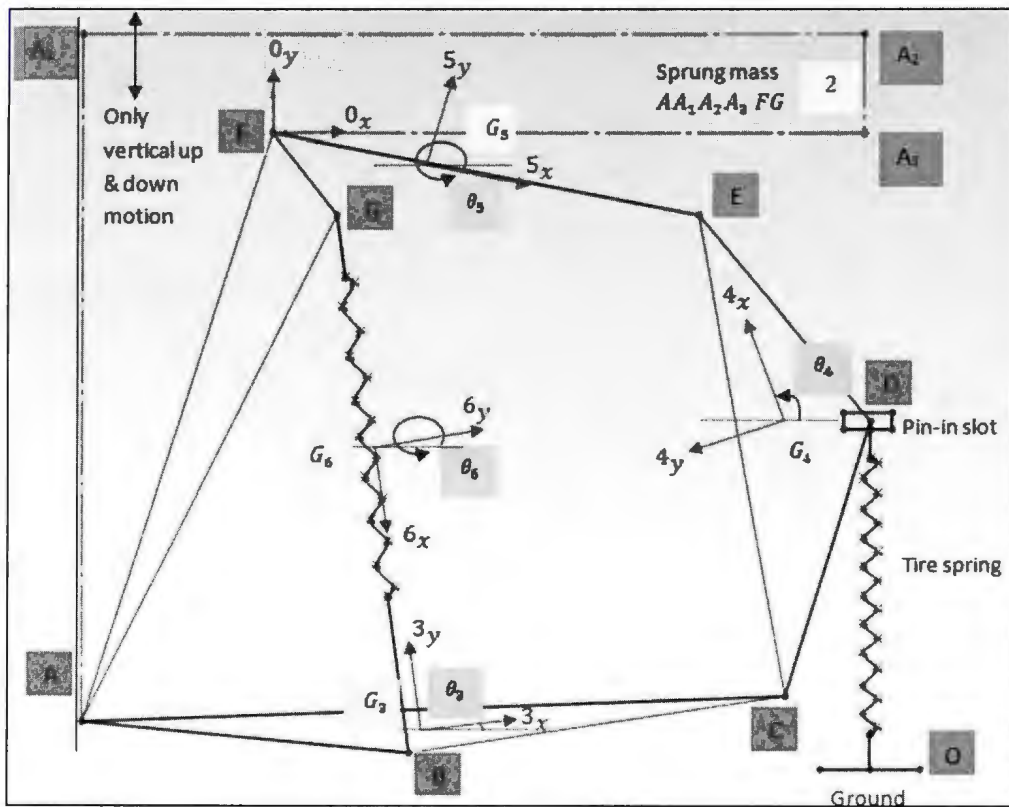


Figure 17: Co-ordinate system location for multi-body model

The location of the center of mass and the local coordinate system for the individual bodies have been labeled in Figure 17. The angles of orientation have also been shown in Figure 17.

Each rigid body has to be modeled using the approach described above. The global inertial coordinates are located at point F (0X , 0Y). At first, body 5 is being modeled where the velocity of centre of mass is being defined for (G_5), the coordinate frame (5X , 5Y) is described as shown in Figure 18 (in blue and labeled) and the initial orientation is given by θ_5 . Since in body-fixed coordinate systems only the velocity of the body is defined, points E and F in Figure 18 are located with respect to (G_5). For center of mass (G_5), the global coordinates is established by using transformation matrices to go from frame 5 to frame 1, and then it is integrated to get the inertial coordinates, which is done in block XY_G . Similarly, to find inertial coordinates for point F transformation matrices takes it from frame 5 to frame 1 and then it is integrated to get the inertial coordinates, which is done in block XY_F .

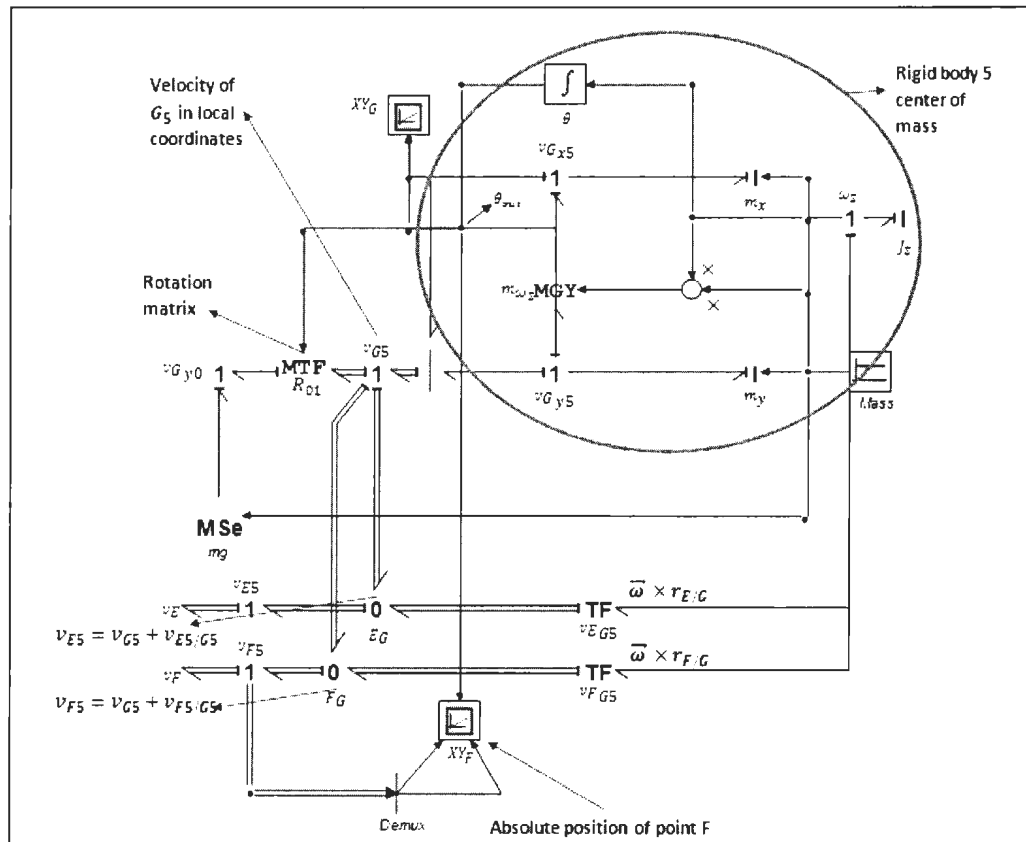


Figure 18: EJS for body 5 of multi-body quarter car model

This block has been compressed to represent other rigid bodies in the Figure 19 and the positions, orientations and velocities of each of these points have been defined in a similar manner. The Euler's equation of motion generated for a rigid body as shown in Equation 3.4.1 can be represented in bond graph by Euler Junction Structure (EJS). The rigid bodies are joined so that it represents the SLA suspension. There are parasitic elements used in various places in this bond graph formulation of SLA suspension system. This is done in order to avoid bond graph causality and to reduce errors in the simulation.

The point F is shared by body 5 and also body 2. So, the velocities of point F should be the same at both these bodies. They are joined to each by simulating a pin joint. For this a transformation matrix is used i.e. a modified transformer in bond graph notation to alter from frame 5 to frame 2. The x-component of the velocity of point F is equal to the velocity of x component of point A. Point A can only move vertically to simulate a quarter car model. So, the x-component of body 2 is restricted from moving in the x direction which can be defined by using a zero flow source Sf . The y-component of the velocity of point F is equal to the velocity of y-component of point A. The sprung mass is concentrated on the y-component of point A and it has also been used to include gravity on the suspension system. On the opposite side of body 5, the velocity of point E has been equated to that of body 4 by using a modified transformer. Here also, body 4 and body 5 are joined to each through pin-joints, which is represented by point E. The angle of orientation for the transformation matrix is the difference of θ_5 and θ_4 .

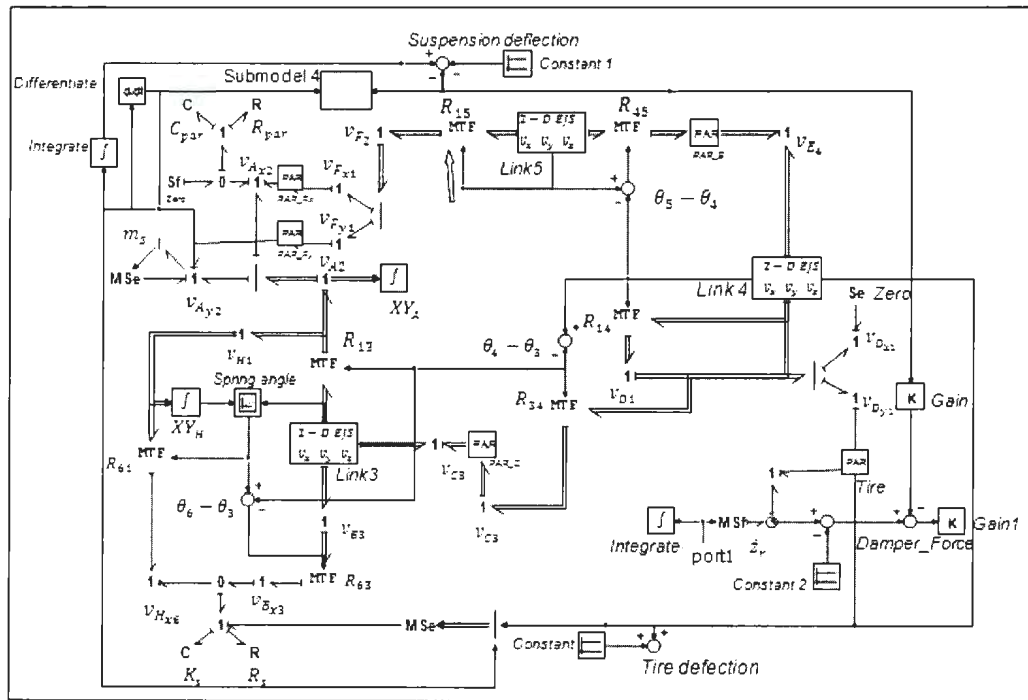


Figure 19: Full multi-body quarter car model

The EJS sub-model for body 4 contains the center of mass (G_4) in body-fixed coordinates and then transformation matrices are used to turn them into inertial coordinates as shown in Figure 20 in block MTF (R_{01}). Using the center of mass (G_4) the velocities of the three different points on the body are also defined, namely C, D and E. For points E and C, the global coordinates are calculated using the transformation matrices and integration of the x and y components of the velocities. The velocity of point D is changed from frame 4 to frame 1. Using a demultiplexer, the x and y components of the velocities of D can be separated, where the x-component has no effort applied on it, and so it is valued at zero. The y-component is where the tire is attached and provides vertical translation only. At this location, there is pin-in-slot joint, so that the body E can make transverse motion whereas the road displacement remains vertical.

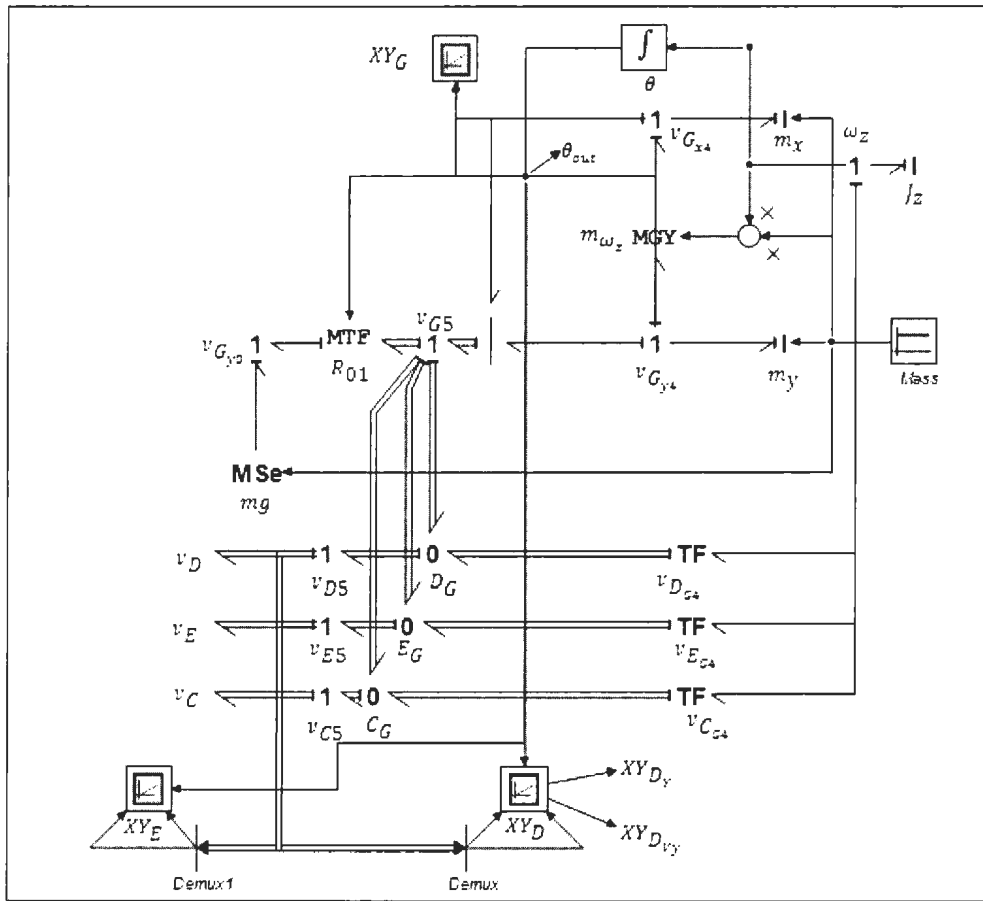


Figure 20: EJS sub-model body 4

The tire sub-model consists of a capacitance C and a resistance R , which represent the spring and damping values of the tire, respectively as shown in Figure 21. The road perturbation is also experienced by the tire and it is joined to the ground at point O .

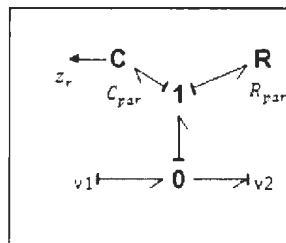


Figure 21: Tire sub-model

Similarly, the EJS sub-model for body 3 contains the center of mass (G_3) in body-fixed coordinates and then transformation matrices are used to change them into inertial coordinates as shown in Figure 22. It also contains the velocities of the different points on body 3, namely A, B and C which are defined using the center of mass (G_3). The inertial coordinates of the point B and C are calculated by applying the transformation matrix to the velocities of points B and C and then integrating them.

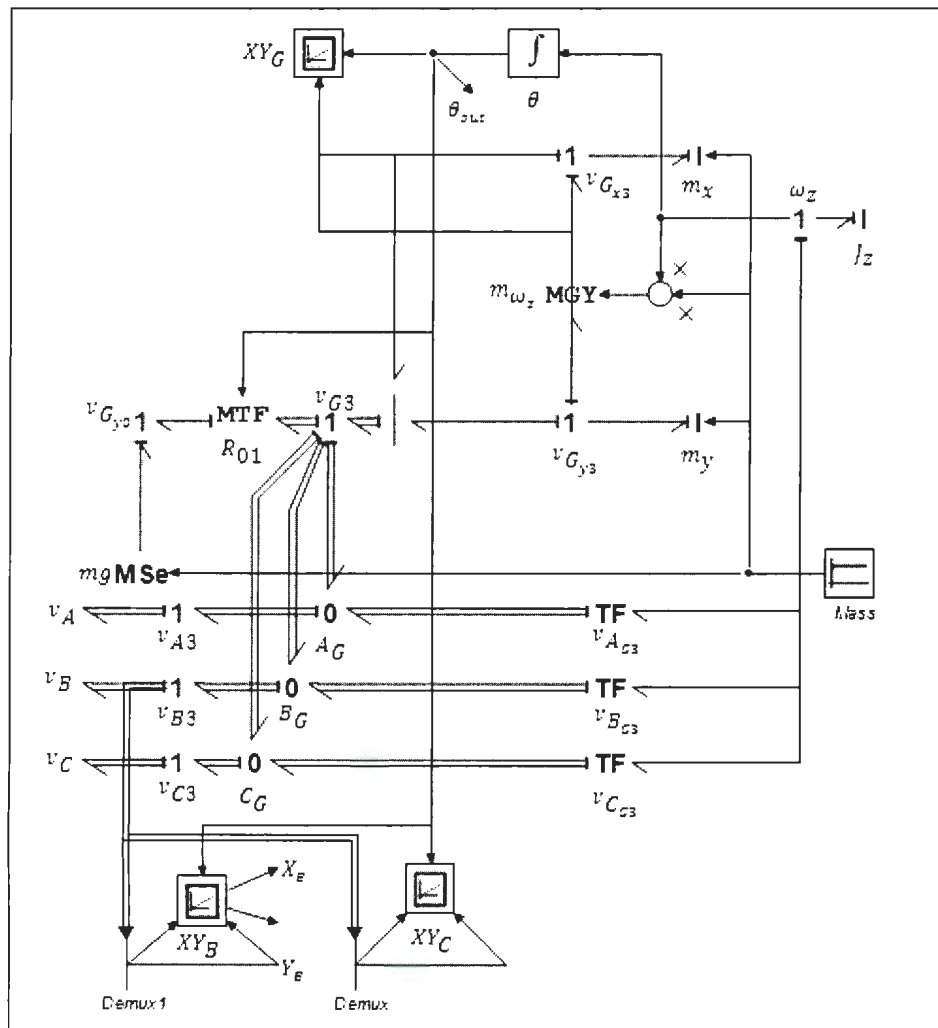


Figure 22: EJS submodel body 3

As shown in Figure 23, the suspension (spring and damper) is located between points B and G. The velocity of point G is defined in frame 1, which is transformed to frame 6, defined for the suspension components. Similarly, the point B in frame 3 is transformed into frame 6 using transformation matrix and the orientation is defined as the difference of θ_6 and θ_3 . The 0-junction between v_{Gx6} and v_{Bx6} , is where the spring and damper values are given. The suspension elements are rigidly joined between points B and G.

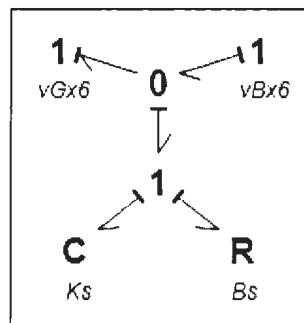


Figure 23: Suspension (spring and damper)

The states that are being investigated are the suspension deflection, sprung mass velocity, tire deflection and unsprung mass velocity, described in detail in Chapter 4. The suspension deflection is calculated by the difference in the position of the sprung mass and the unsprung mass denoted by x_{Ay} and XY_{Dy} respectively. The sprung mass velocity is calculated by the 1-junction v_{Ay} . The tire deflection is given by the state of the spring C_s and the unsprung mass velocity is calculated by the 1-junction v_{Dy} .

The simulation parameters for the suspension system have been entered into the model. The suspension system starts from an equilibrium position which means that the vehicle is resting on the road with initial compression in the spring. The parameters for the multi-body model such as link lengths, initial angles and mass properties have been determined

and listed in Table 1. Solidworks [23] was used to determine the initial positions and orientations of the linkages.

Table 1: Simulation parameters for quarter car model

Simulation Parameters	
Parameters	Value
Sprung mass of the vehicle, m_s	400 kg
Unsprung mass of the vehicle, m_u	30 kg
Suspension stiffness coefficient, k_s Coil spring	156000 N/m
Suspension damping coefficient, b_s Linear damper	6216 Ns/m
Tire stiffness, k_t	4000000 N/m

A string model for the quarter car has been constructed using Solidworks [23] and the initial coordinates and angles have been found using this model, depicted in Figure 24. The initial position and orientation of the vehicle are generated taking into account the spring and tire compression at equilibrium and the vehicle at rest on the road surface.

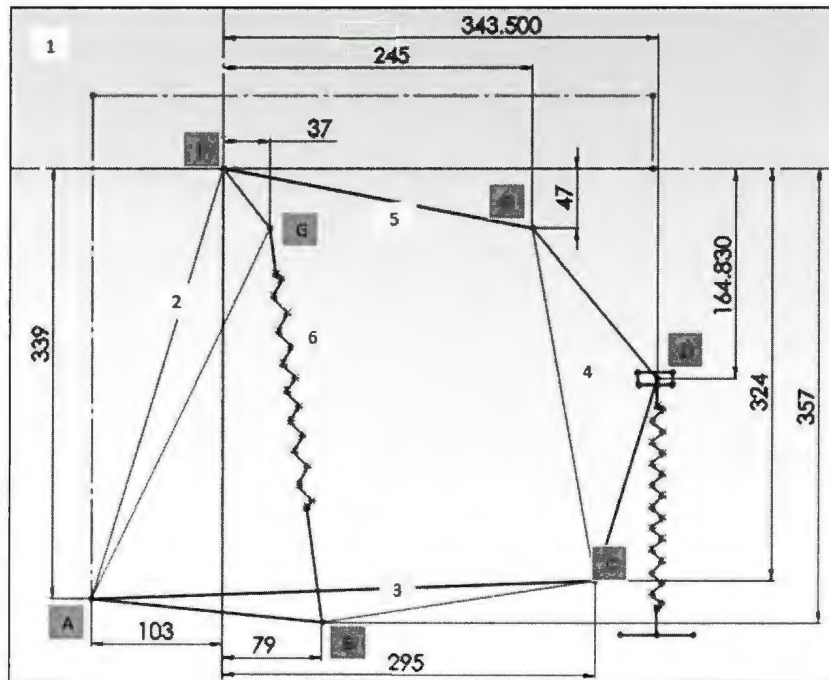


Figure 24: String multi-body quarter car model (Solidworks)

Additional initialization parameters for the particular multi-body model set-up have been listed in Table 2.

Table 2: Initialization parameters for the multi-body model

Multi-body Parameters	
Parameters	Value
Sprung mass of the vehicle, (AFG)	400 kg
Mass of link 3, (ACB)	10 kg
Mass of link 4, (ECD)	10 kg
Mass of link 5, (EF)	10 kg
Initial angle, θ_3	-3.279 rad
Initial angle, θ_4	-1.401 rad
Initial angle, θ_5	-0.1257 rad
Inertial coordinates of CM of G_3	(81.07,-333.32) mm
Inertial coordinates of CM of G_4	(291.01,-168.1) mm
Inertial coordinates of CM of G_5	(123.55,-17.26) mm

Figures 25 and 26 show the simulation results for a multi-body (MB) quarter car model in a passive state with a sinusoidal road input of 5 cm as shown in Figure 55 (Chapter 5). The sprung mass acceleration has been plotted as shown and the four suspension states described in Section 4.1 have also been shown. 20-Sim [21] was used to generate the simulation results using backward differentiation formula with a tolerance of 10^{-5} units.

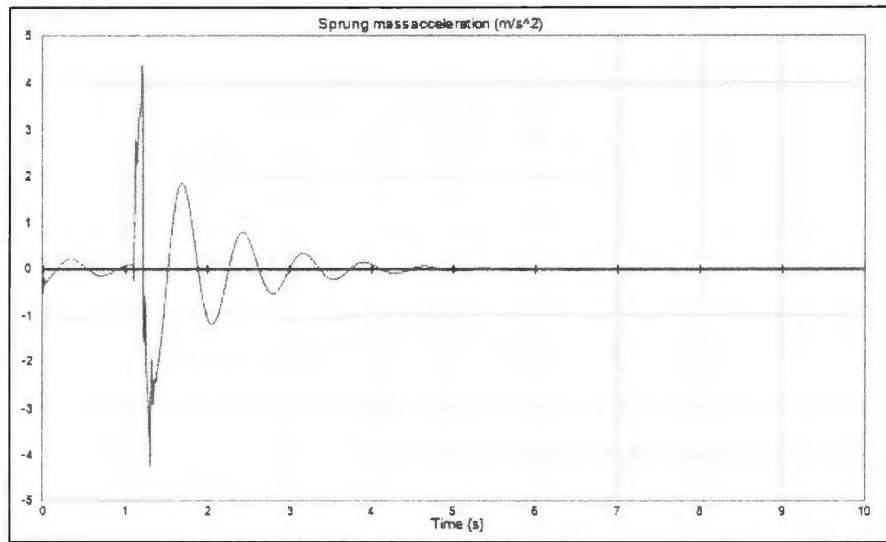


Figure 25: Sprung mass acceleration MB model – Passive mode

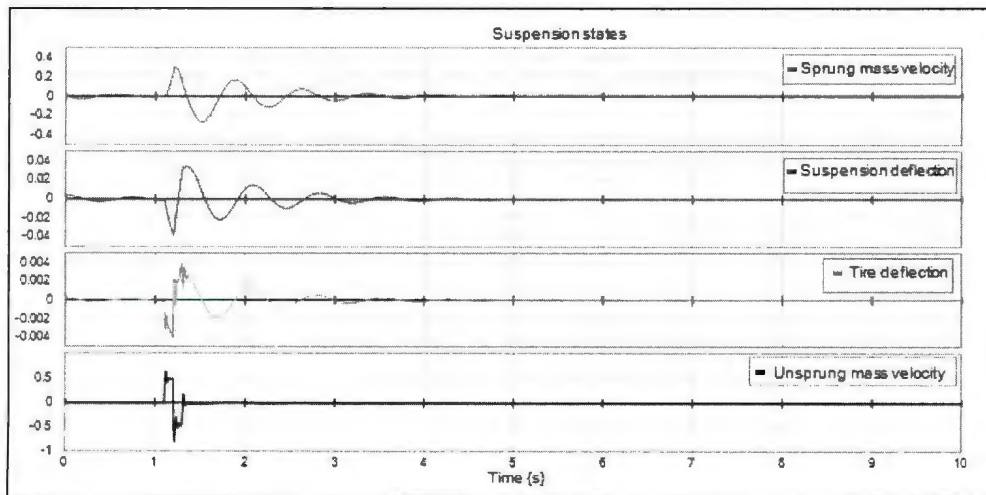


Figure 26: Suspension states MB model – Passive mode

3.4.1 Non-linear Component Addition

The multi-body quarter car model possesses a non-linear geometry in itself, which is the main inspiration of this thesis to investigate its differences from a linear quarter car. The multi-body model can have non-linearity in its components as well. A large suspension deflection introduces non-linearity in the multi-body quarter car model. A slow sinusoidal road input of 15 cm with the sprung mass at rest, reveals non-linearity in the suspension spring as shown for force-displacement curve (Figure 27) since spring is activated by a rotating link and the wheel deflection is not linearly proportional to the spring deflection. Here as the spring reaches its limits of travel, it introduces non-linearity in the suspension.

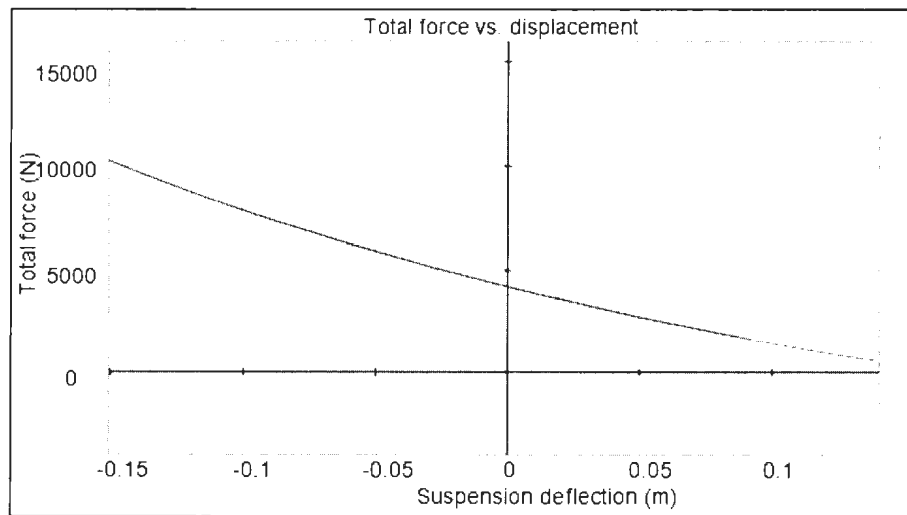


Figure 27: Non-linearity due to large suspension deflection

There can be non-linearity in the multi-body model by having non-linear spring and damper components. A cubic spring and a bi-linear damper have been added in the suspension to increase the complexity of the model. A cubic spring which is linear around the original suspension stiffness of $k_2 = 156000 \text{ N/m}$ has been introduced in the

suspension. The stiffness coefficient for the cubic spring is $k_1 = 42600000 \text{ N/m}$. The equation for the cubic spring applied to the 20-Sim model is given by the following formula.

$$\text{Force} = k_1 x^3 + k_2 x$$

Here, $x \text{ (m)}$ is the state of the spring C . Figure 28 shows total force-displacement curve of the multi-body model with non-linear spring and damper.

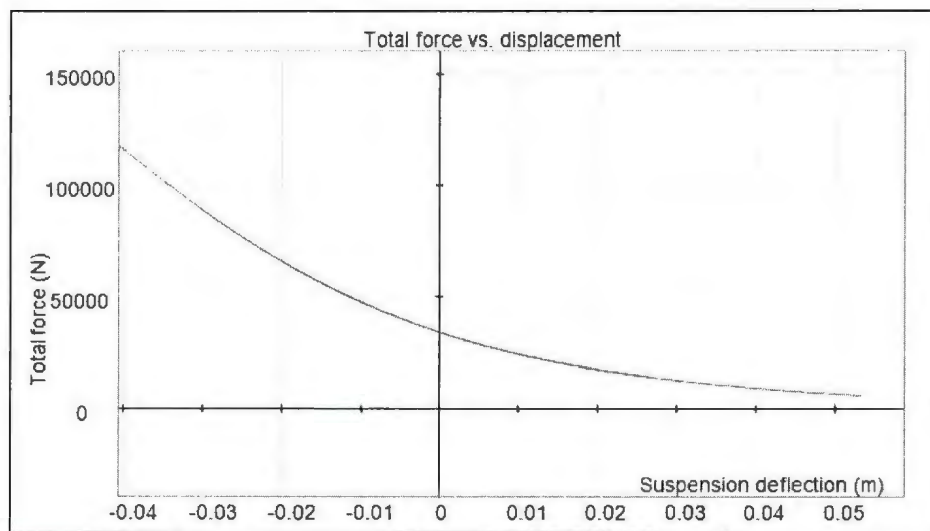


Figure 28: Effect of non-linear spring on MB model

A bi-linear damper has also been introduced in the suspension. A bi-linear damper has two different values for jounce and rebound. The bi-linear damper is also calculated by taking the average of the original damping coefficient of 6216 Ns/m . The rebound has higher damping coefficient than the jounce stage in a bi-linear damper applied to vehicle model. During the jounce stage, the damper has to support the body mass while the spring force is increasing whereas during the rebound stage it has to support the body mass and

increased energy in the suspension spring [5]. The slope for the rebound stage is 7800 Ns/m and for the jounce stage is 5300 Ns/m .

$$\text{Force} = v * B$$

Here, $v \text{ (m/s)}$ is the velocity experienced by the damper and $B \text{ (Ns/m)}$ is the damping coefficient. Figure 29 is shown here for the bi-linear damper for two different values of damping coefficients.

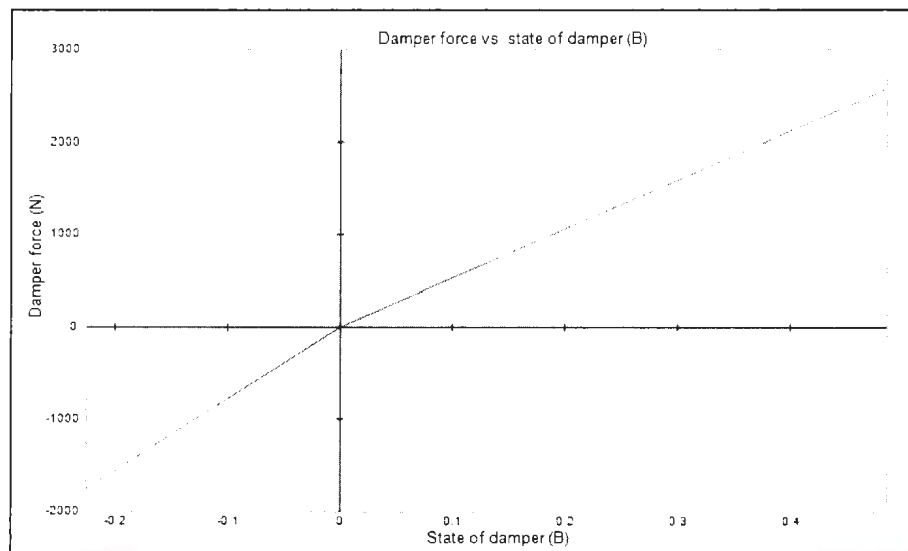


Figure 29: Bi-linear damper for MB model

3.5 Conclusion

This section is complete with the detailed description of multi-body quarter car model in bond graph methodology. After a brief introduction to the bond graph methodology, the multi-body model was created using bond graph elements and the various components of the model have been described. Using body-fixed frame of reference and inertial frame of reference the local and global coordinates of the various links and bodies have been

described. A string model created in Solidworks is used to estimate the initial positions and orientations of the bodies have been depicted. Geometrical non-linearity has been described for the non-linear suspension model. Non-linear spring and damper components have also been introduced in this chapter in the form of a cubic spring and a bilinear damper to simulate non-linearity in the components of the multi-body model. The next chapter is used to develop a linear quarter car model using bond graph method and using the multi-body model to characterize the suspension elements to find the apparent stiffness and damping coefficient. The natural frequencies of the linear quarter car model developed in 20 Sim is compared with the state space model developed in MATLAB to show that there is no discrepancies in the bond graph model. After the model is complete, comparison of the linear quarter car model is made with the multi-body quarter car model in passive state.

Chapter 4: Equivalent Quarter Car Suspension Model

4.1 Overview

A non-linear multi-body quarter car model can be transformed into a linear unidirectional quarter car model to remove the inherent nonlinearities in the system. This quarter car model as shown in Figure 30 represents the suspension system at each wheel. It has a linear spring k_s , damper b_s and a force actuator F_a for active suspension systems. The sprung mass m_s is the mass of the vehicle at each corner of the car. The unsprung mass m_u consists of all the suspension, axle and tire. The tire stiffness k_t represents the bounce of the tire.

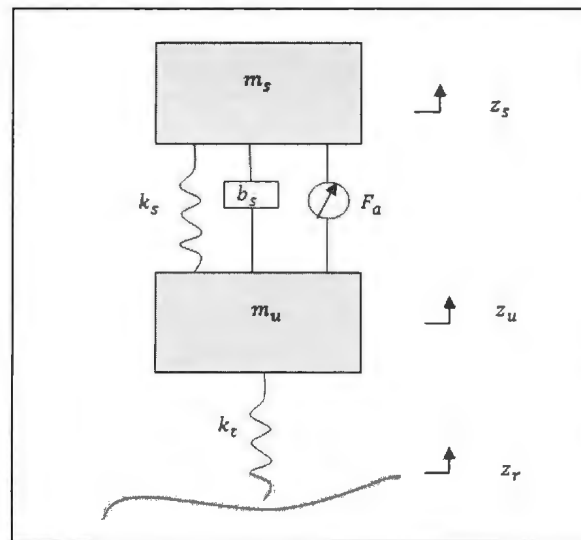


Figure 30: 2 DOF quarter car model

4.2 MATLAB/Simulink model for quarter car

A Simulink model was generated using these equations [1],

$$m_s \ddot{z}_s + b_s(\dot{z}_s - \dot{z}_u) + k_s(z_s - z_u) = F_a \quad (4.2.1)$$

$$m_u \ddot{z}_u + k_t(z_u - z_r) - b_s(\dot{z}_s - \dot{z}_u) - k_s(z_s - z_u) = -F_a \quad (4.2.2)$$

The state space equation can be written as

$$\{\dot{x}\} = [A]\{x\} + [B]F_a + [L]\dot{z}_r \quad (4.2.3)$$

$$\{y\} = [C]\{x\} \quad (4.2.4)$$

where, $x = \{x_1 \ x_2 \ x_3 \ x_4\}^T$

$$A = \begin{bmatrix} 0 & 1 & 0 & -1 \\ -\frac{k_s}{m_s} & -\frac{b_s}{m_s} & 0 & \frac{b_s}{m_s} \\ 0 & 0 & 0 & 1 \\ \frac{k_s}{m_u} & \frac{b_s}{m_u} & -\frac{k_t}{m_u} & -\frac{(b_s + b_t)}{m_u} \end{bmatrix}$$

$$B = \begin{bmatrix} 0 \\ 1 \\ -\frac{1}{m_s} \\ 0 \\ \frac{1}{m_u} \end{bmatrix}$$

$$L = \begin{bmatrix} 0 \\ 0 \\ -1 \\ 0 \end{bmatrix}$$

$$A = \begin{bmatrix} 0.00 & 1.00 & 0.00 & -1 \\ -390 & -16 & 0.00 & -16 \\ 0.00 & 0.00 & 0.00 & 1 \\ 4727 & 188 & -47273 & -188 \end{bmatrix} \quad B = \begin{bmatrix} 1 \\ 0.0025 \\ 0 \\ -0.0303 \end{bmatrix} \quad C = \begin{bmatrix} 1 & 0 & 0 & 0 \\ 0 & 1 & 0 & 0 \\ 0 & 0 & 1 & 0 \\ 0 & 0 & 0 & 1 \end{bmatrix} \quad D = 0$$

(4.2.5)

Eq. 4.2.5 is inserted into Eq. 4.2.3 and Eq. 4.2.4. These equations are used to make a Simulink model using state space method. As shown in Figure 31, the gain blocks are used for defining the individual matrices A, B, C, D and L. Following the equation formulation from Eq. 4.2.5, the blocks are set up to give the output. This makes up the plant model using the state space method.

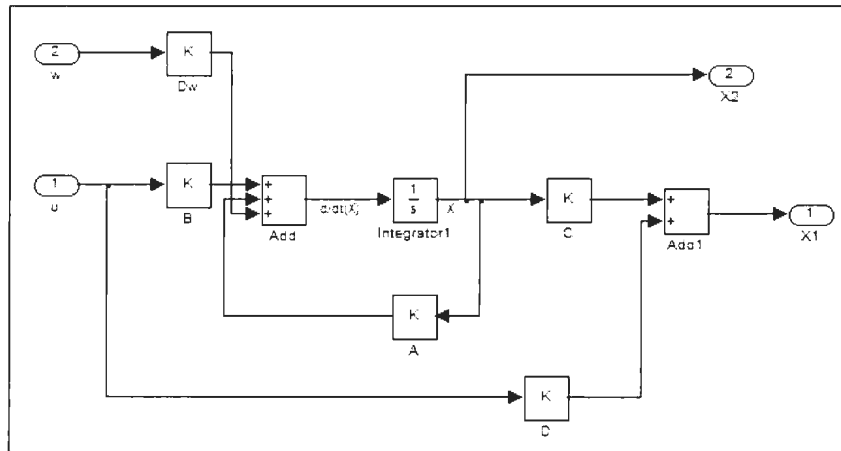


Figure 31: Simulink model with state-space matrix design

The purpose of generating a Simulink model is to verify the bond graph model with the state space model. As shown in Section 4.5, these models are compared with each other by generating their resonant frequencies. Once the bond graph model is verified with the Simulink model, then further analysis can be performed since the multi-body model also has to be consistent with the linear quarter car model. Also, the active suspension system can be designed for both the quarter car and multi-body models using bond graph once the verification is done.

4.3 Bond graph model for quarter car

A bond graph model was also generated for the linear quarter car model. Figure 32 shows the bond graph implementation of the quarter car. To analyze the bond graph model, it can be reduced and numbered so that it is easier to refer to particular bonds and variables.

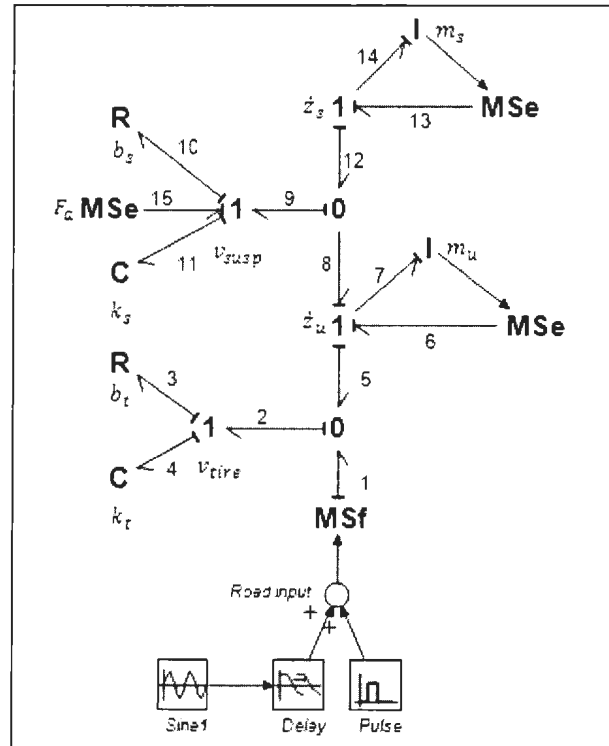


Figure 32: Notation for bond graph equation formulation

As earlier mentioned, the states for measurement are suspension deflection, sprung mass velocity, tire deflection and unsprung mass velocity. In bond graph, these four states are defined as state of suspension spring k_s defined by its displacement q_{11} , sprung mass momentum p_{14} , state of tire spring k_t defined by its displacement q_4 and unsprung mass momentum p_7 . The bond graph method for calculation of the suspension states has been included in the Appendix D for reference.

4.4 Method of determining quarter car parameters

The quarter car parameters have been determined using various methods. The suspension stiffness k_s used in the quarter car model is not equal to the coil spring stiffness in the multi-body suspension model. Similarly the damping coefficient b_s used in the quarter car model is not the same as the damping value used in the multi-body suspension model.

To determine these parameters, the multi-body model was used for characterization of the coil spring and jounce damper used in the model. With the sprung mass fixed, the tire underwent vibration at different frequencies and magnitudes. The spring stiffness was determined using a slow sinusoidal test. The slope of the force-displacement plot (Figure 33) provided the spring stiffness k_s for the quarter car model. A slow sinusoidal test (0.01 rad/s and 0.05 m amplitude) was performed to see the total force-displacement curve. Using a slow sinusoidal test, the damping effects of the system can be eliminated and the graph provides the stiffness coefficient without any contribution due to damping. The data was fitted into a linear regression equation generated in Excel and the suspension stiffness was found to be 31580 N/m . The offset of 4095 N is contribution due to the initial spring compression that the vehicle undergoes at equilibrium position.

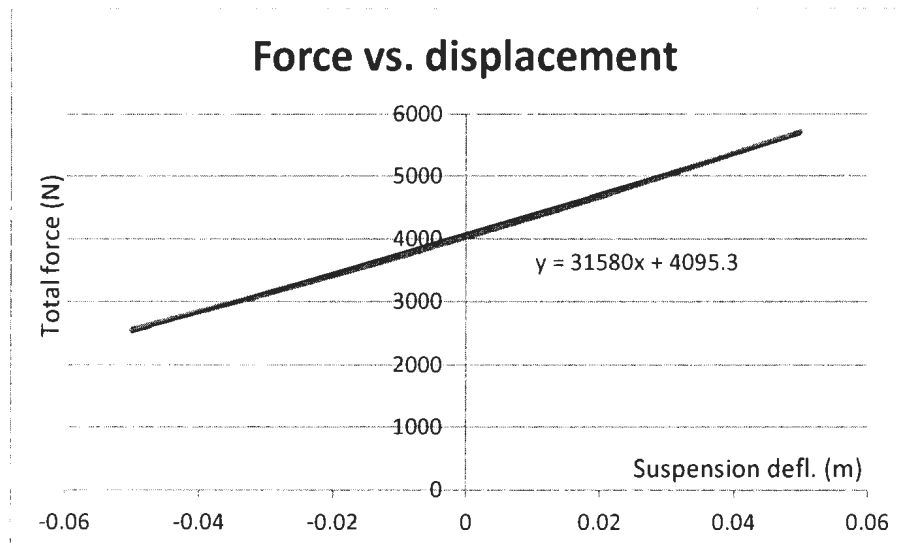


Figure 33: Slow sinusoidal test for stiffness coefficient

Another test was performed at a higher frequency with a sinusoidal input (20 rad/s and 0.05 m amplitude). This test contains the contribution of inertial and damping effects along with the spring characteristics. The results show that the suspension stiffness is very close to the slow sine test having a value of 31686 N/m as shown in Figure 34, calculated by fitting a linear regression equation. Here too the offset is due to the initial spring compression of the vehicle at equilibrium position.

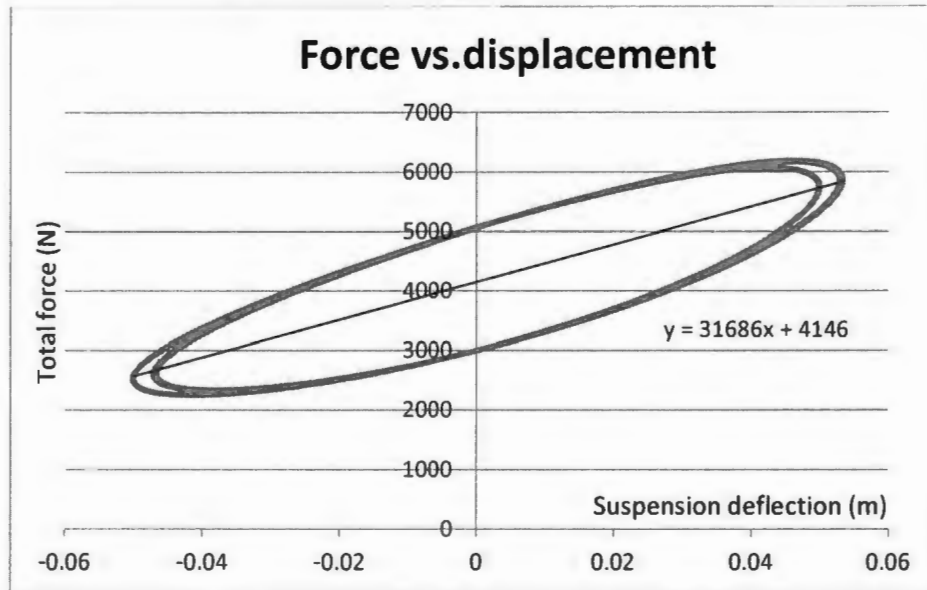


Figure 34: Sinusoidal test for stiffness coefficient

The damping coefficient was determined using two methods. First, the damper force was calculated by subtracting the spring force from the total force experienced by the tire. The damper force was plotted against the displacement which provided the work diagram as shown in Figure 35. The energy dissipated over a complete cycle in a harmonically induced motion is given by

$$\Delta U = \pi C \omega X^2$$

The area under the work diagram (ellipse) gives the energy dissipated per cycle for the sinusoidal input given in this case. The area of the ellipse is calculated to be 62.8 m^2 for the work diagram in Figure 35. Using the area, the damping coefficient can be estimated by

$$C = \frac{A}{\pi \omega X^2}$$

where, C – damping coefficient, Ns/m

ω – angular frequency, 20 rad/s

A – area of the work diagram, 62.8 m²

X – suspension deflection, 0.025 m

The damping coefficient is found to be 1600 Ns/m.

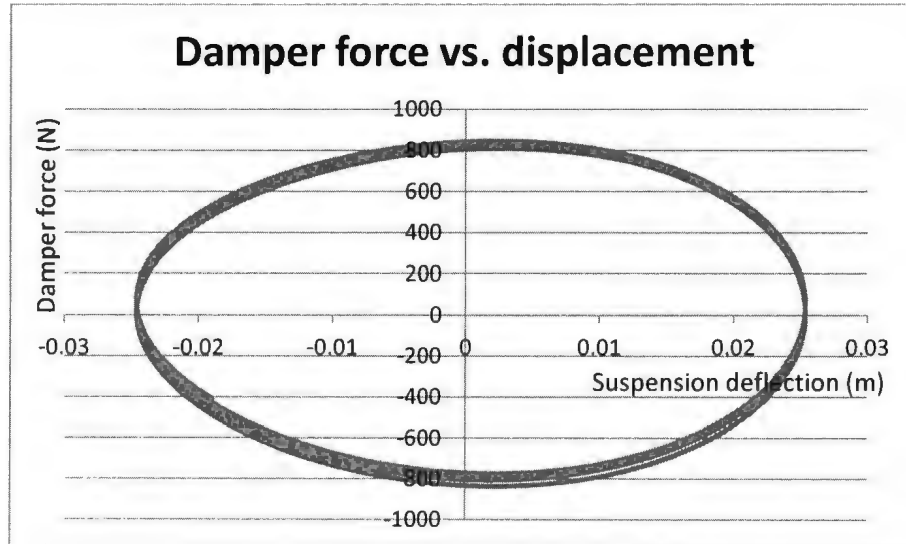


Figure 35: Work diagram for damping coefficient

The other method was to plot the damping force-velocity curve, which gave the damping coefficient of the system. Figure 36 shows the damping coefficient value to be 1618 Ns/m , which is in close proximity to the value found by the previous method. The damping coefficient is calculated by fitting a linear regression equation on the data.

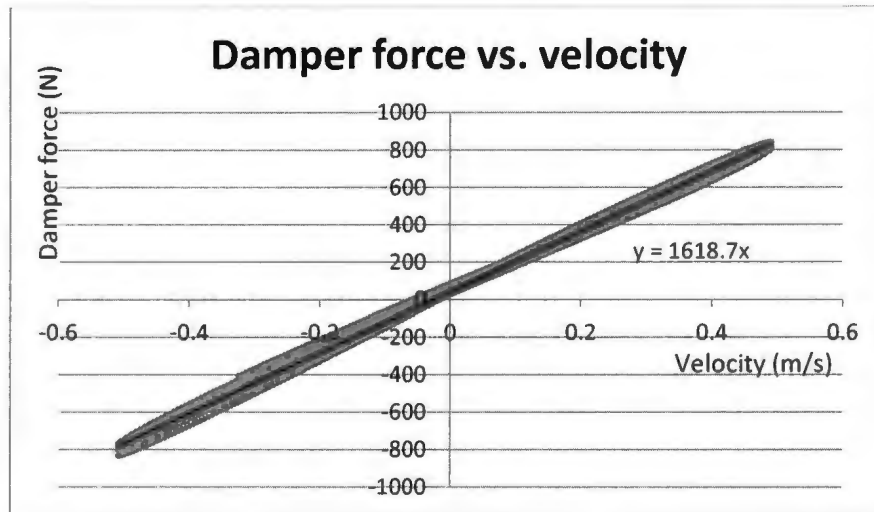


Figure 36: Force-velocity deflection curve for damping coefficient

The finalized parameters for the quarter car are provided in Table 3.

Table 3: Quarter car parameters

Simulation Parameters	
Parameters	Value
Sprung mass of the vehicle, m_s	400 kg
Unsprung mass of the vehicle, m_u	30 kg
Suspension stiffness coefficient, k_s	31580 N/m
Suspension damping coefficient, b_s	1000 Ns/m
Tire stiffness, k_t	4000000 N/m

4.5 Simulation results for quarter car model

The natural frequencies for the quarter car are given by [1],

$$\omega_1 = \sqrt{\frac{k_s}{m_s}} = \sqrt{\frac{30581}{400}} = 8.74 \text{ rad/s}$$

$$\omega_2 = \sqrt{\frac{k_t}{m_u}} = \sqrt{\frac{400000}{30}} = 115.47 \text{ rad/s}$$

The critical damping is given by

$$b_c = 2\sqrt{m_s k_s} = 2\sqrt{400 * 30581} = 6994.97 \text{ Ns/m}$$

The relative damping can be calculated by

$$\xi = \frac{b_s}{b_c} = \frac{1000}{6994.97} = 0.1429 = 14.29 \%$$

Now, the simulation models should also be coherent and give similar natural frequencies and damping ratios.

First, the Simulink model is tested with the same parameters and the natural frequencies are obtained for the passive mode. Figure 37 shows that the natural frequencies and damping ratios for the particular frequencies. The linear system editor in the Simulink work environment gives information about the system model. Here, the frequency response plots for the state space model are generated in Simulink (Figure 32) that give information about the natural frequencies and damping ratios of the system.

$$\omega_1 = 8.38 \text{ and } \xi = 12.8$$

$$\omega_2 = 118 \text{ and } \xi = 14.1$$

The values are in close proximity to the calculated values. So, the Simulink model seems to be behaving according to the analytical solution.

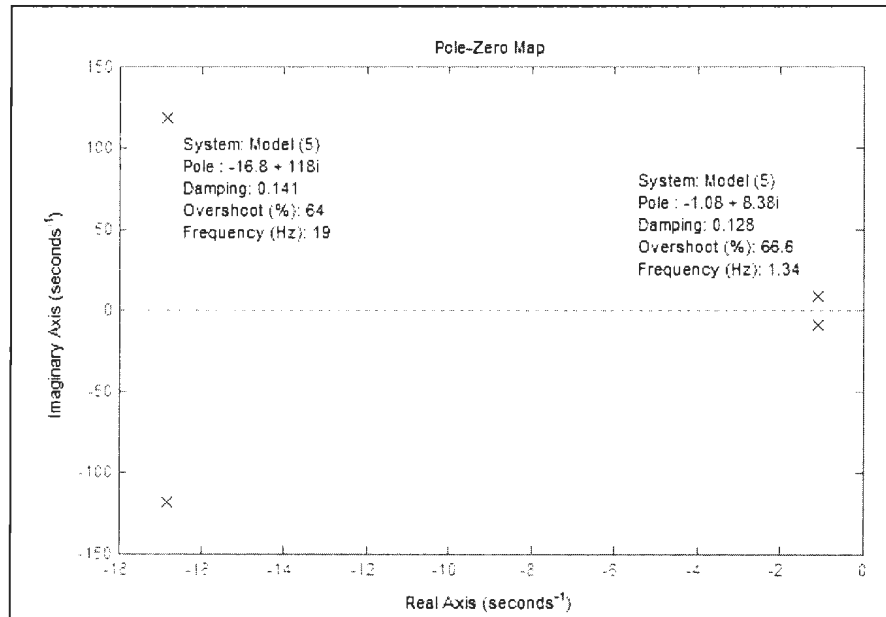


Figure 37: Pole-zero plots for Simulink model

Now, the 20-sim [21] model is tested in passive mode to see if the natural frequencies are matching with the analytical solution. The model linearization tool in 20-sim [21], provides the information about the frequency response of the system generated in bond graph method. The natural frequencies and damping ratios are shown in Table 4.

$$\omega_1 = 8.378 \text{ and } \xi = 12.82$$

$$\omega_2 = 118.3 \text{ and } \xi = 14.08$$

These values are in close proximity to the calculated values as well as to the Simulink model.

Table 4: Bond graph eigenvalues for quarter car

frequency {rad/s}	rel.damping	type	Δ gain {dB/dec}	Δ phase {deg}
1.542e-008	∞	lead	20	-90
8.378	0.1282	resonance	-40	-180
118.3	0.1408	resonance	-40	-180

system K =	2.017e-010
root-locus K =	-1.333e+004
u =	zrdot1\flow
v =	ks1\state

4.6 Comparison of Multi-body vs. Quarter Car Results

The passive states of the multi-body quarter car with no non-linearity and linear quarter car have been compared with each other. The road input is a 8 cm bump applied to both the models as shown in Figure 38.

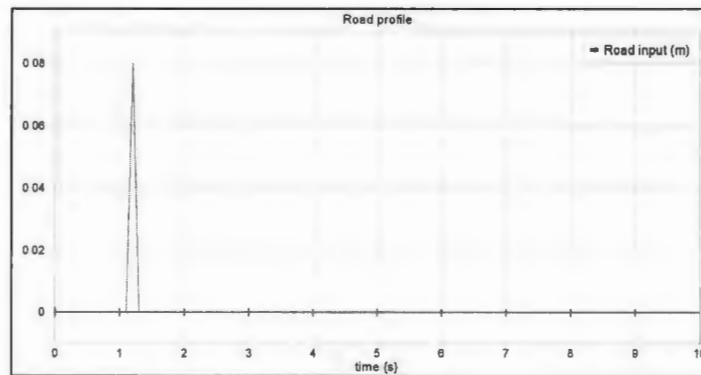
**Figure 38: Road input (8 cm)**

Figure 39 shows the sprung mass acceleration for the multi-body quarter car and the linear quarter car. The linear quarter car and multi-body model have comparable responses.

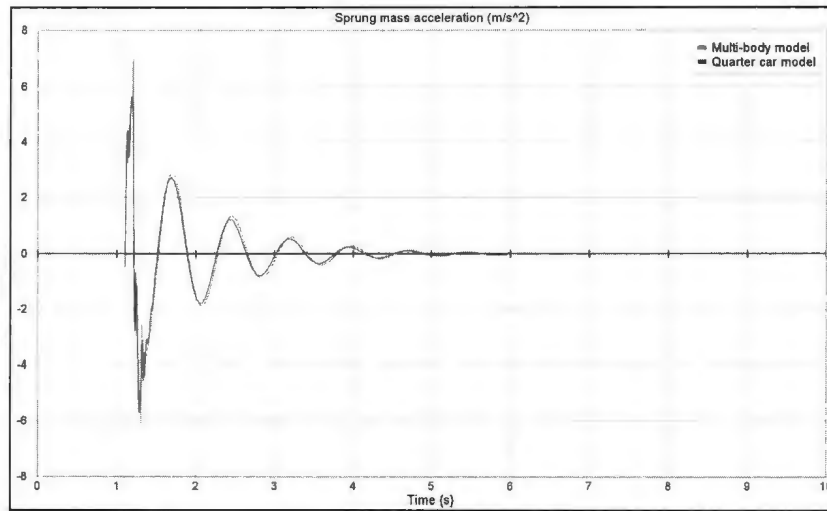


Figure 39: Sprung mass acceleration for MB & QC model (Passive mode)

Figure 40 shows the suspension deflection for both the models. The suspension deflection in both cases is almost the same in terms of peak response.

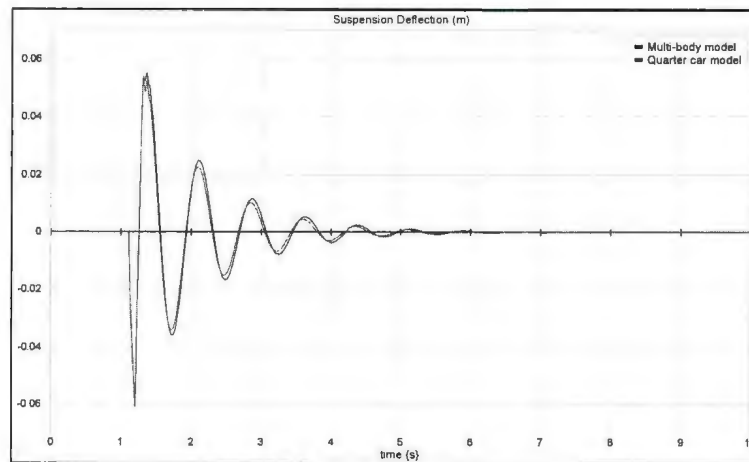


Figure 40: Suspension deflection for MB & QC model (Passive mode)

The tire deflection performs worse for the linear quarter car in comparison to the multi-body model as shown in Figure 41.

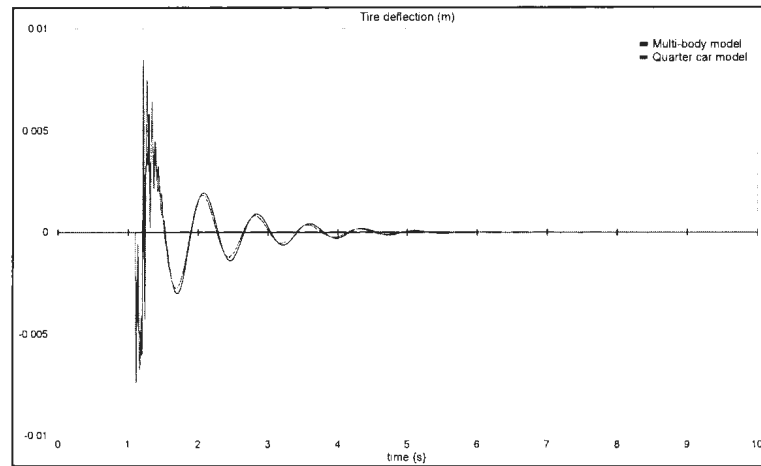


Figure 41: Tire deflection for MB & QC model (Passive mode)

4.7 Conclusion

The suspension states for both the models are behaving in a similar manner and there appears to be minor discrepancy in the model. The validation of both the models was necessary so that further controller development can be performed on it without any problems. As shown in Appendix A, a MATLAB/SimMechanics [22] based multi-body quarter car model was also developed before using the bond graph method but was unsuccessful in the controller implementation stage due to inherent problems in the system model, which were hard to identify due to the structure of the simulation environment.

This chapter develops a state space quarter car model and models it in MATLAB/Simulink environment. A bond graph based linear quarter car model has also been developed using 20-Sim in this chapter and compared with the Simulink model to confirm that the bond graph model is working in the same way as the state space model.

Both these models are compared in frequency domain and analytical calculations also show the validity of the models. Further, multi-body model and quarter car model developed in bond graph are compared with each other to show that they have similar system response in passive state. The next chapter describes in detail the LQR controller analytically and its implementation on the linear quarter car model and multi-body quarter car model. Four different case studies are developed and simulations are performed to compare the models to their active and passive states as well with each other.

Chapter 5: Active Suspension Controller Design and Simulation

5.1 Overview

A system provides some kind of output when an input signal is applied to it. The need to obtain a desirable system response necessitates the need to apply a controller to the model. A system where there is no feedback is called an open loop system whereas a closed loop system is the one where the output can be measured and then a feedback signal is fed back to compare it with the desired response [7]. Such closed loop systems form the basis of feedback systems.

In vehicle dynamics, predominantly in the academic research domain and usually not in the industrial domain, controllers are applied to the system models to reduce the vibrations experienced by the passengers in a vehicle and also maintain a good road holding. Ride quality and road holding are two competing criteria for evaluating the performance of active suspension system. Ride quality is assessed by measuring the suspension travel and/or body acceleration and road holding is assessed by measuring the wheel travel. The performance of one is at the expense of the other. For example, in a passive suspension when the vehicle has a soft suspension, it will absorb all the vibrations due to ruggedness of the road and provide a smooth ride. But this is at the expense of suspension reaching its limits of travel or degraded vehicle performance. Soft suspension is best for mountainous roads. When the suspension is made stiff, the response from road perturbations is felt much faster so that the driver can adjust accordingly and it reduces unwanted movement of the vehicle like nose-dive or rear-end squat [36]. Stiff suspensions are best for smooth roads. But having a stiff suspension can make ride

bumpier. So, there has to be a balance in maintaining the ride quality and road holding requirements.

A passive system can only provide limited performance due to the fixed spring and damper properties. In an active suspension system, an actuator applies force in tandem with the passive suspension which enhances the performance of the vehicle by suppressing the additional vibrations induced on the passengers while keeping the vehicle on track. This is attained by applying a controller to a model in a simulation environment. Several different types of controllers have been applied in literature [8, 10, 11 and 15]. In this chapter a linear quadratic regulator (LQR) controller is designed to be applied on a system model to provide ride quality and road holding benefits. For that reason, an optimal performance criterion (cost function) is established so that the ride comfort and road holding requirements are sufficiently satisfied [33]. The cost function consists of the sum of the deviations of the data from the desired values. The controller regulates the values of the key states by varying their weighting factors in the LQR algorithm, the details of which are provided in Section 5.2. The literature review has suggested that the linear LQR controller is tested mostly on the linear quarter car model or other vehicle models such as half car and full car models. But when there is non-linearity in the vehicle models due to geometry or components, then the performance of the linear controller has not typically been investigated in the literature. In this research, a multi-body model with varied levels of nonlinearities (Chapter 3) is developed and the linear controller performance is tested in the frequency and time domain. The active and passive states of the multi-body model as well as the quarter car model are compared with each other using the linear controller. The controller performance of both the models is also evaluated

against each other in active state. Four case studies have been summarized in Figure 42, which shows the variation of non-linearity in the multi-body model.

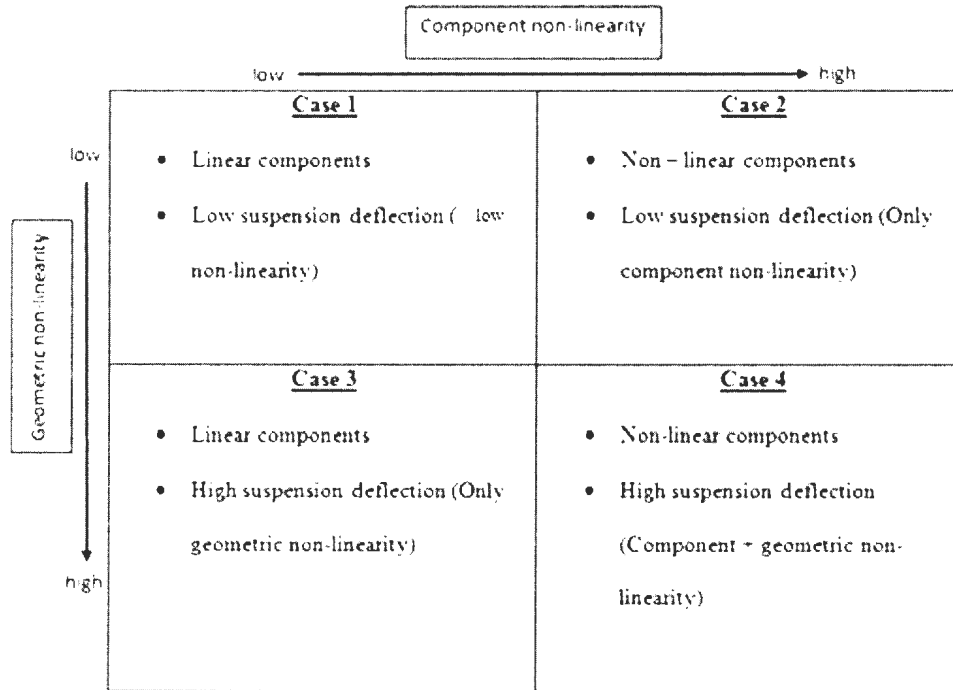


Figure 42: Overview of cases for studying active suspension system

5.2 LQR Controller Design

A classic example of controlling a system which consists of two points in space is that the shortest distance between two points is straight line [32]. This is the optimal path that can be traversed requiring minimal effort. Optimal control is based on such a theory. There has been lot of theorem on optimal control [1, 4 and 7] where different applications have been described. An optimal control method has been described with system equations and a cost function to be minimized. By obtaining the optimal gain K , the control force u can be calculated and applied in a feedback loop to provide optimal performance.

The state space model developed in Section 4.2 for the quarter car can be used equivalently to design the LQR controller. Here we consider a general state space model [4].

$$\dot{x} = [A]\{x\} + [B]\{u\} \quad (5.2.1)$$

where the control input vector is given by the optimal gain matrix K

$$u = -K\{x\} \quad (5.2.2)$$

In the case of quarter car model, u is the actuator force represented by F_a as shown in Section 4.2.

The objective function to be minimized is given by

$$J = \int_t^{t_f} (x^T Q x + u^T R u) dt \quad (5.2.3)$$

$$J = \int_t^{t_f} (x^T Q x + x^T K^T R K x) dt \quad (5.2.4)$$

Where t and t_f are the initial times and final times. Q is called the state weighting matrix and R is the control cost matrix. The matrix Q represents the transient cost energy and R represents the control energy. Both Q and R are square, symmetric and positive definite (or semi-definite) matrices. The objective function has to be minimized to obtain an optimal control matrix K for any initial state $x(t_o)$.

Substituting Eq. 5.2.1 into 5.2.2 gives,

$$\{\dot{x}\} = [A]\{x\} - [B]K\{x\} \quad (5.2.5)$$

$$= (A - BK)x \quad (5.2.6)$$

For convenience the matrix symbols are removed. The closed loop poles $(A - BK)$ are assumed to be stable, with real negative poles.

$$A_{CL} = (A - BK) \quad (5.2.7)$$

A_{CL} is the closed loop state dynamics matrix.

The state transition matrix φ_{CL} of the closed loop system represented by Eq. 5.2.6 can be defined as

$$x(t) = \varphi_{CL} x(t_0)$$

The objective function (Eq. 5.2.3) can be written as

$$J = \int_t^{t_f} x^T \varphi_{CL}^T (Q + K^T R K) \varphi_{CL} x dt \quad (5.2.8)$$

$$J = x^T P x \quad (5.2.9)$$

where P is a positive definite real symmetric matrix since both Q and R matrices are symmetric. Eq. 5.2.9 shows that the objective function is a quadratic function of the initial state. Hence, the name of the controller is termed as Linear Quadratic Regulator. On partially differentiating Eq. 5.2.8, we get the following

$$\frac{\partial J(t, t_f)}{\partial t} = -x^T (Q + K^T R K) x \quad (5.2.10)$$

On partial differentiation of Eq. 5.2.9, we get the following

$$\frac{\partial J(t, t_f)}{\partial t} = \dot{x}^T P x + x^T \frac{\partial P(t, t_f)}{\partial t} x + x^T P \dot{x} \quad (5.2.11)$$

$$= x^T [(A - BK)^T P + \frac{\partial P(t, t_f)}{\partial t} + P(A - BK)] x \quad (5.2.12)$$

Equating Eq. 5.2.10 and Eq. 5.2.12, we get

$$\begin{aligned} -[Q + K^T R K] &= [(A - BK)^T P + \frac{\partial P(t, t_f)}{\partial t} + P(A - BK)] \\ -\frac{\partial P(t, t_f)}{\partial t} &= [(A - BK)^T P + P(A - BK)] + [Q + K^T R K] \end{aligned} \quad (5.2.13)$$

To solve this first order differential equation, we need an initial condition i.e. obtained by putting $t = t_f$, which results in $P(t_f, t_f) = 0$.

To find the solution to the linear optimal problem such that we can find the optimal gain matrix K , the objective function J is minimized, subject to initial condition. So Eq. 5.2.13 becomes

$$[(A - BK)^T P + P(A - BK)] = -[Q + K^T R K] \quad (5.2.14)$$

Since Q and R are positive semi-definite matrices, P must be positive semi-definite too, which implies that the minimum will occur when,

$$K = R^{-1} B^T P \quad (5.2.15)$$

This is the optimal gain matrix K . The optimal control law is given by

$$u = -K\{x\} = -R^{-1} B^T P \{x\} \quad (5.2.16)$$

Eq. 5.2.14 reduces to

$$A^T P + PA - PBR^{-1} B^T P + Q = 0 \quad (5.2.17)$$

This is called the matrix Riccati equation and provides an optimal solution to the control law $\{u\} = -K\{x\}$.

For active suspension design, the objective function (performance index) has been determined [47] and is given by

$$J = \int_0^{\infty} [\ddot{z}_s^2 + \rho_1(z_s - z_u)^2 + \rho_2 \dot{z}_s^2 + \rho_3(z_u - z_r)^2 + \rho_4 \dot{z}_u^2] dt \quad (5.2.18)$$

The sprung mass acceleration can be written in terms of the standard state vectors as defined in Section 4.2

$$\ddot{z}_s^2 = 1/m_s^2[k_s^2 x_1^2 + b_s^2 x_2^2 + b_s^2 x_4^2 + F_a^2 + 2 k_s b_s x_1 x_2 - 2 k_s b_s x_1 x_4 - 2 b_s^2 x_2 x_4 - 2 k_s x_2 F_a + 2 b_s x_4 F_a] \quad (5.2.19)$$

The performance index can be put in a standard matrix form,

$$\ddot{z}_s^2 + \rho_1(z_s - z_u)^2 + \rho_2 \dot{z}_s^2 + \rho_3(z_u - z_r)^2 + \rho_4 \dot{z}_u^2 = x^T Q x + 2 x^T N F_a + F_a^T R F_a \quad (5.2.20)$$

$$\text{where, } Q = \begin{bmatrix} \frac{k_s^2}{m_s^2} + \rho_1 & \frac{b_s k_s}{m_s^2} & 0 & -\frac{b_s k_s}{m_s^2} \\ \frac{b_s k_s}{m_s^2} & \frac{b_s^2}{m_s^2} + \rho_2 & 0 & -\frac{b_s^2}{m_s^2} \\ 0 & 0 & \rho_3 & 1 \\ -\frac{b_s k_s}{m_s^2} & -\frac{b_s^2}{m_s^2} & 0 & \frac{b_s^2}{m_s^2} + \rho_4 \end{bmatrix}$$

$$N = \begin{bmatrix} -\frac{k_s^2}{m_s^2} \\ \frac{b_s}{m_s^2} \\ 0 \\ \frac{b_s}{m_s^2} \end{bmatrix}$$

$$R = \left[\frac{1}{m_s^2} \right]$$

The performance index reduces to

$$J = \int_0^{\infty} (x^T Q x + 2 x^T N u + u^T R u) dt \quad (5.2.21)$$

And the solution to the control law is given by the feedback gain K

$$K = R^{-1}(B^T P + N) \quad (5.2.22)$$

where the first term $(R^{-1}B^T P)$ depends on the choice of the weights and the second term $(R^{-1}N)$ cancels out the passive force due to the spring and the damper.

The choice of weights depends on the requirement of the system; if the ride quality has to be dominant, then the sprung mass acceleration has high weighting compared to the other states. In case the road holding is given priority, then the tire deflection is highly weighted compared to the other states. Now, the controller is applied to both the models and analysed in the frequency and time domain.

5.3 Frequency Domain Analysis

The LQR controller is tested for two scenarios: ride quality and road holding using different values of weights for ρ_1, ρ_2, ρ_3 and ρ_4 .

The LQR controller is applied to the linear quarter car model and the active suspension system is compared with the passive suspension system. A road input of 5 cm is applied to both the models and the velocity of the car is 1.8 km/h. The road profile is shown in Figure 43.

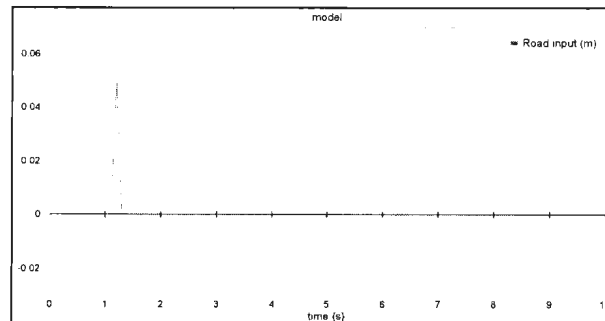


Figure 43: Road profile – 5 cm bump

Ride quality test for quarter car

For this case, the sprung mass is heavily penalized whereas the other states are not penalized as much. The weights used are $\rho_1 = 0.4, \rho_2 = 0.16, \rho_3 = 0.4, \rho_4 = 0.16$. From Section 4.5, the sprung mass acceleration had two resonant frequencies that occurred at 8 rad/s and 116 rad/s for the passive case.

Once the active controller is applied as shown in Figure 44, the first resonant frequency is suppressed whereas at the higher frequency, there is no change. The unsprung mass resonant frequency remains unchanged no matter how heavily the sprung mass acceleration is weighted [1].

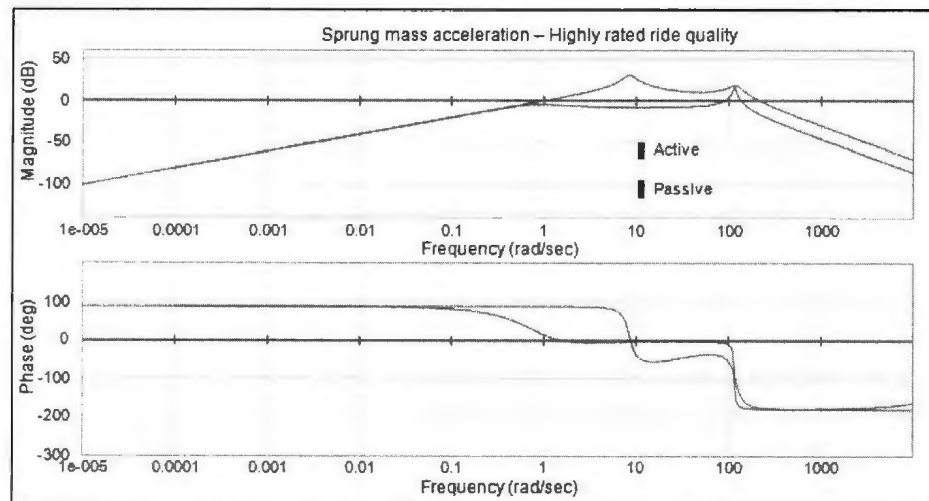


Figure 44: Sprung mass acceleration bode plot for QC model (highly rated ride quality)

For the moderately rated ride quality case, the sprung mass acceleration was weighted more compared to the other states but not too aggressively. The weights used are $\rho_1 = 400$, $\rho_2 = 16$, $\rho_3 = 400$, $\rho_4 = 16$. The higher resonant frequency remains unchanged whereas the lower resonant frequency vanishes as shown in Figure 45.

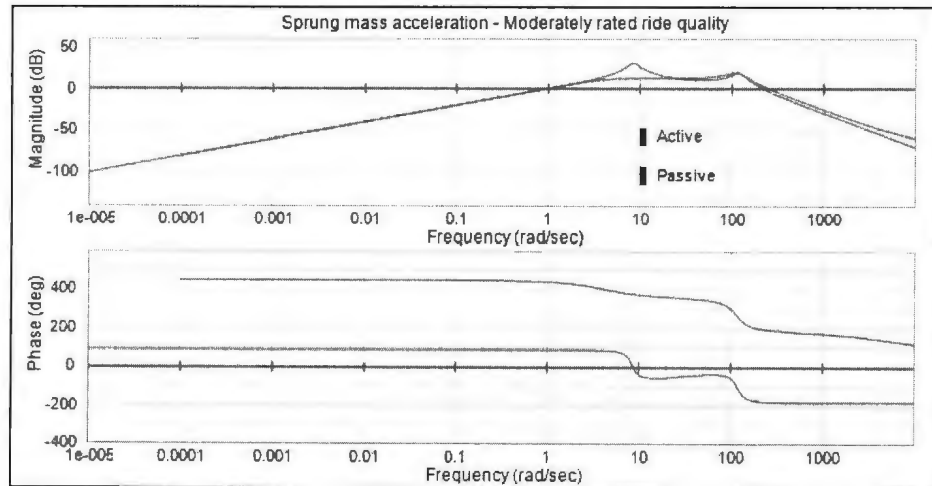


Figure 45: Sprung mass acceleration bode plot for QC model (moderately rated ride quality)

Road holding test for quarter car

In case of road holding, the suspension deflection and tire deflection were heavily weighted and other states were less weighted. The weights used are

$\rho_1 = 10000, \rho_2 = 100, \rho_3 = 100000, \rho_4 = 100$. The suspension deflection confirms improvement in suppressing both the resonant frequencies as shown in Figure 46.

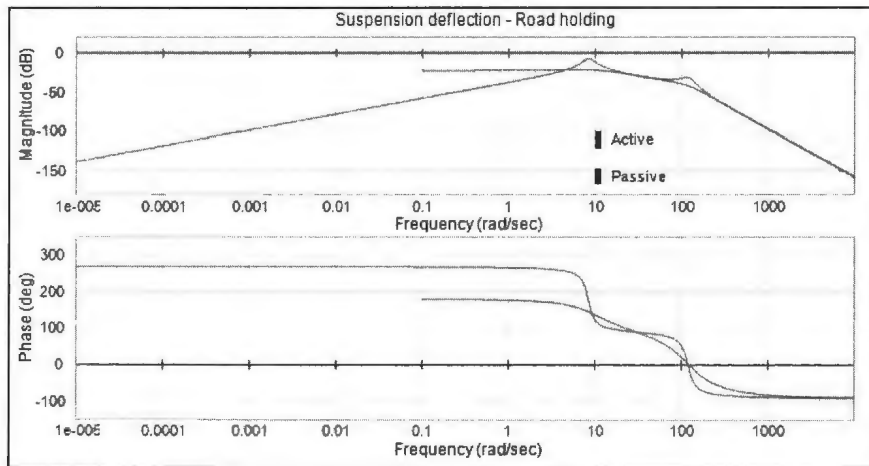


Figure 46: Suspension deflection bode plot for QC model (highly rated road holding)

The tire deflection is improved at both the resonant frequencies as shown in Figure 47.

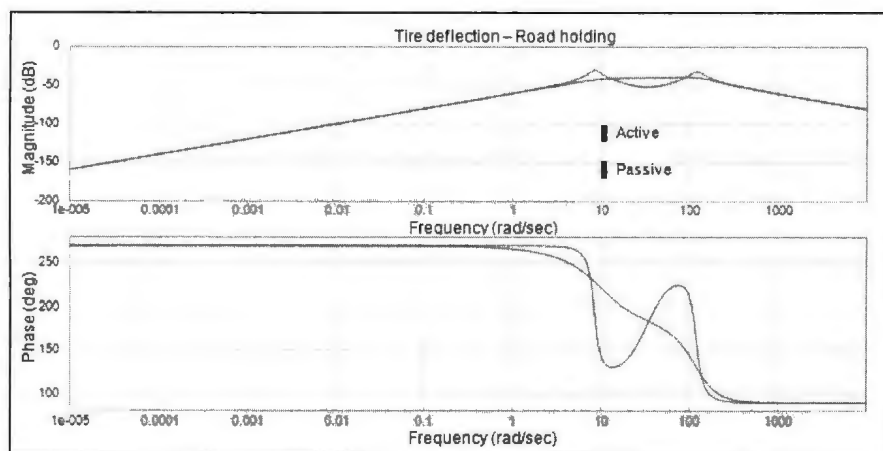


Figure 47: Tire deflection bode plot for QC model (highly rated road holding)

Now, the LQR controller can be applied to the multi-body quarter car model and the frequency domain analysis can be conducted. A test is conducted before the analysis to determine the actuator force that can be applied to the multi-body model in active state due to its kinematic difference from the unidirectional quarter car model.

5.3.1 Open loop test

Before the active suspension can be applied to the system model, the force actuator has to be parameterized for the multi-body model since it differs in kinematics from the linear model. As shown in Figure 48 (A and B), both the models differ from each other in terms of geometry.

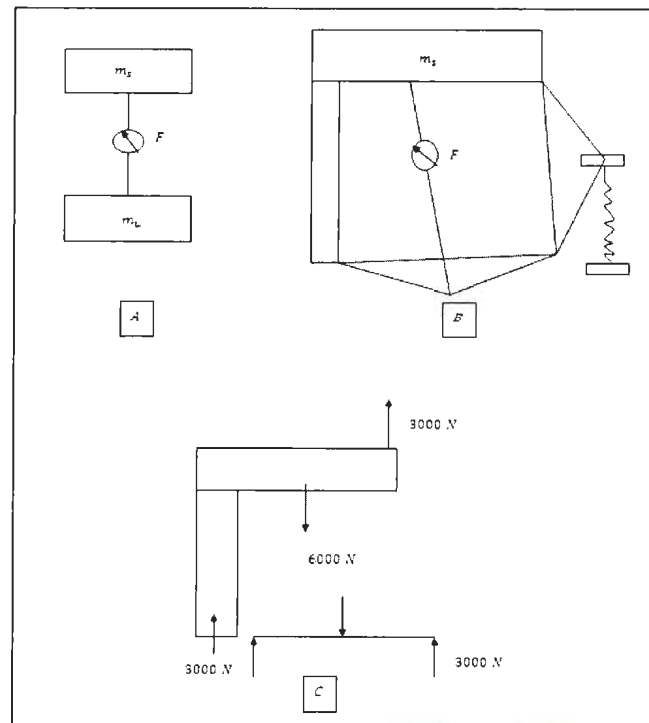


Figure 48: Open loop test illustration

For example, if the unsprung mass is moved 0.1 m up for the unidirectional quarter car model with a suspension stiffness of $k_s = 30000\text{ N/m}$, then the force can be calculated as shown,

$$\begin{aligned} F &= -k_s x & (5.3.1.1) \\ &= -30000 (0.1) \\ &= -3000\text{ N} \end{aligned}$$

But for the multi-body model if a force of 3000 N is applied on the unsprung mass, then it does not move the body by 0.1 m due to the difference in the amplitude of the force supplied by the actuator, which is almost halfway from the point of application of the force. This has been illustrated by the Figure 48 (C). So, an open loop test is conducted to determine the actuator force that would generate the same effort on the body as in the unidirectional quarter car model. At first, a step input of 1000 N is applied to the quarter car model and the sprung mass acceleration is observed. Figure 49 shows the sprung mass acceleration peak amplitude of 2.5 m/s^2 and -1.5 m/s^2 for negative peak amplitude.

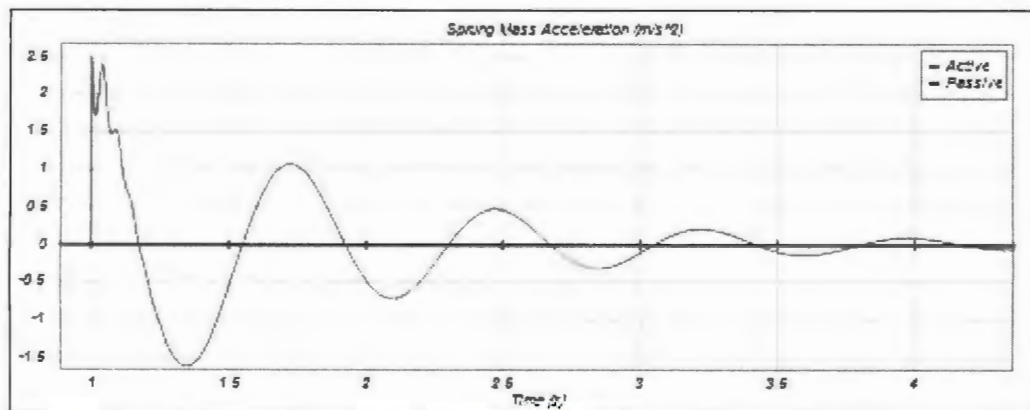


Figure 49: Open loop test for MB model

Now, the actuator force was varied for the multi-body model and it was determined that a force of 2300 *N* provides the same sprung mass acceleration when compared to the linear model as shown in Figure 50. The gain factor of 2.3 *units* is needed for the actuator force in multi-body model to provide comparable performance.

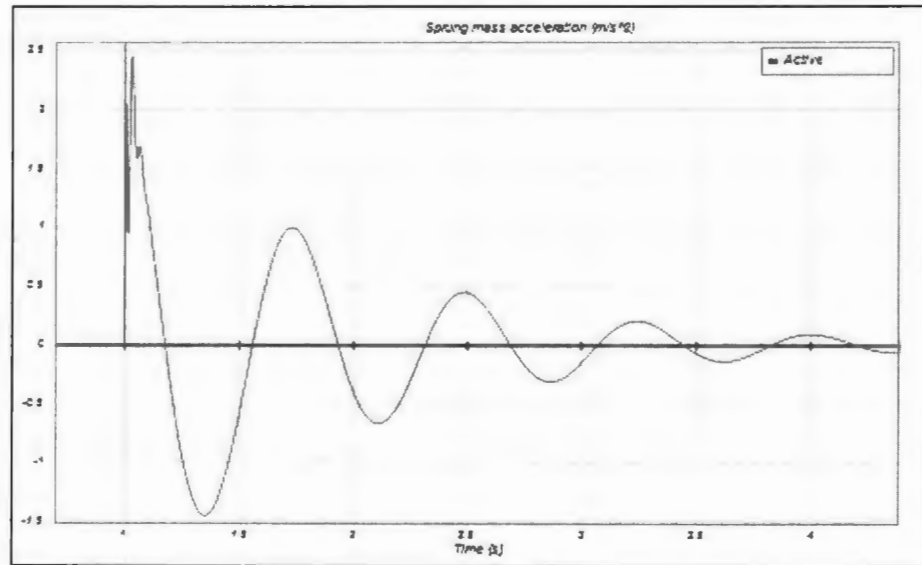


Figure 50: Open loop test (2) for MB model

Now, the LQR controller is tested for ride quality and road holding benefits for the multi-body model. The same weights are applied as with the linear quarter car case. In the passive mode, the resonant frequencies are found and they are similar to the ones obtained in the linear case at 8.3 rad/s and 150 rad/s as shown in Figure 51. The second resonant frequency is higher than the linear quarter car case. This could be due to the fact that the unsprung mass is not concentrated as a lumped mass but is combined mass of the links and bodies, which influence its natural frequency to occur at a higher magnitude.

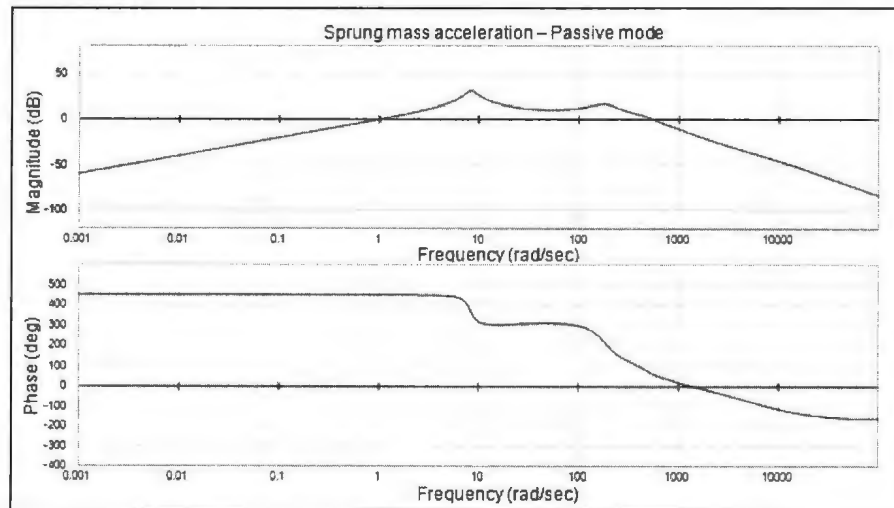


Figure 51: Sprung mass acceleration bode plot for MB model (Passive state)

Ride quality test for multi-body model

In the highly rated ride quality case, the plot shows that the sprung mass acceleration resonant frequencies still exist but now the first closed loop resonant frequency occurs at 2.6 rad/s and the second resonant frequency occurs at 145 rad/s . The peak frequencies are occurring at lower amplitude as shown in Figure 52.

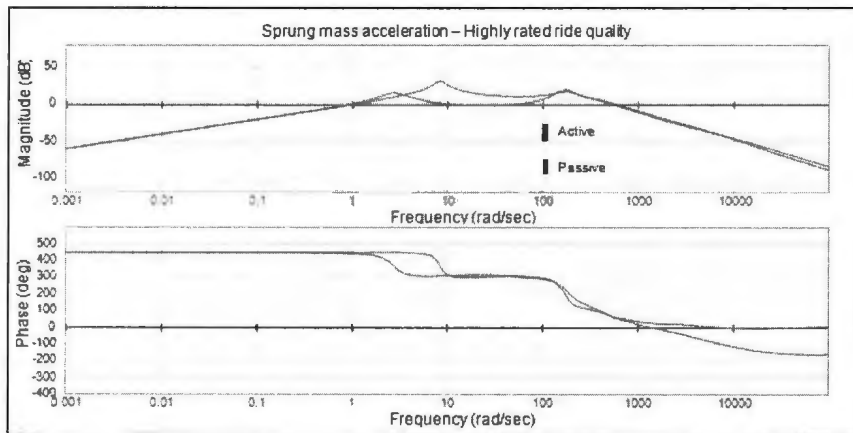


Figure 52: Sprung mass acceleration bode plot for MB model (highly rated ride quality)

In the moderately rated ride quality case, the sprung mass acceleration performs better.

Both the resonant frequencies are suppressed as shown in Figure 53.

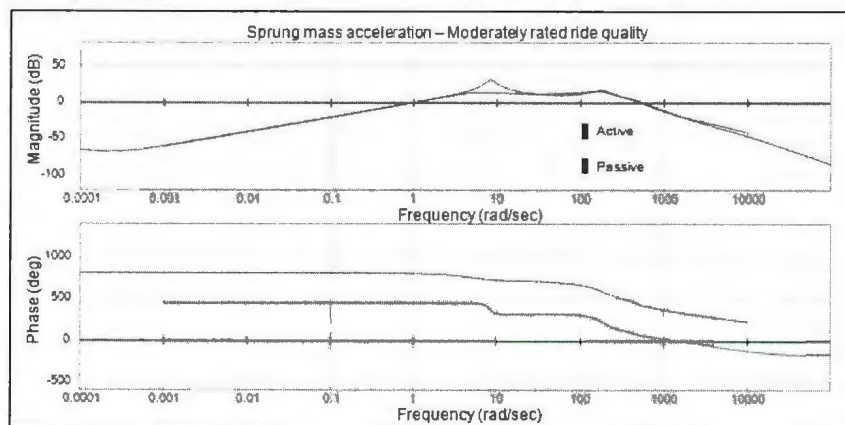


Figure 53: Sprung mass acceleration bode plot for MB model (moderately rated ride quality)

Road holding test for multi-body model

In the case of road holding, the LQR controller is analysed. Figure 54 shows that the unsprung mass resonant frequency is suppressed.

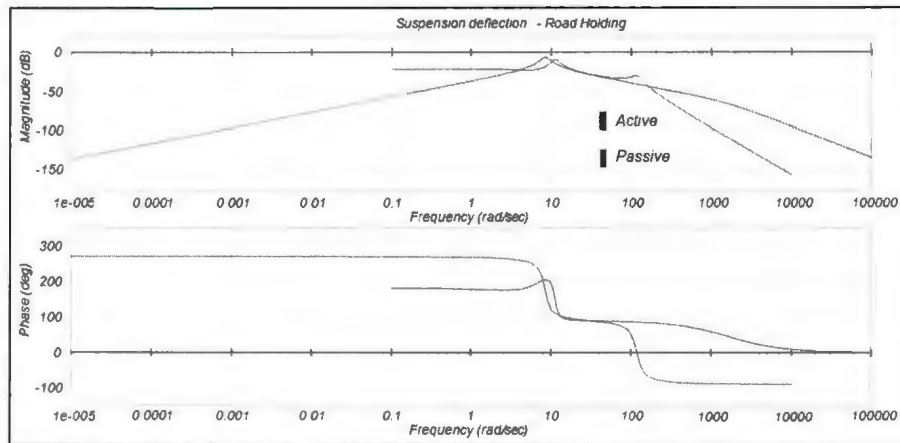


Figure 54: Suspension deflection bode plot for MB model (highly rated road holding)

In the case of tire deflection, both the resonant frequencies are also suppressed as shown in Figure 55.

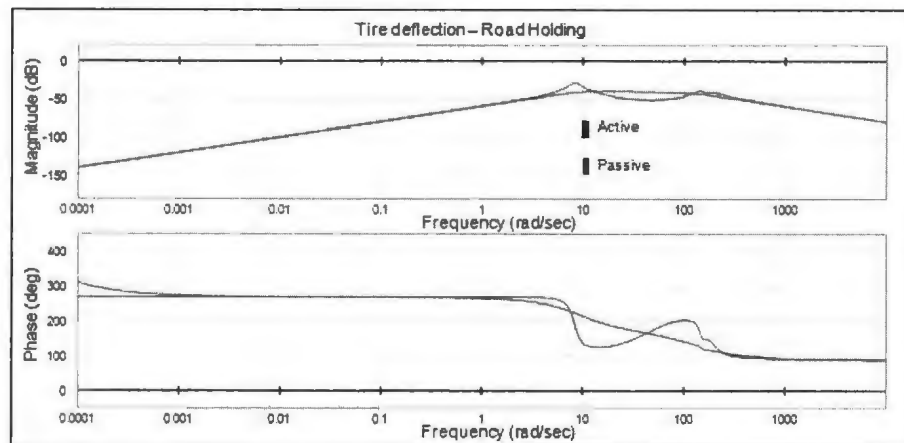


Figure 55: Tire deflection bode plot for MB model (highly rated road holding)

The frequency domain analysis shows that the linear LQR controller works well for the linear quarter car model overall but it does not work for the multi-body model in the highly rated ride quality scenario. Hence, the time domain analysis of the four cases will not include highly rated ride quality scenario in the comparison study. Only in the first case, the highly rated ride quality scenario is analysed and the suspension states are shown to compare its results with the passive mode in the time domain.

5.4 Time Domain Analysis

The time domain comparison of the effectiveness of the LQR controller is performed for the linear quarter car and multi-body model. The states that are analysed are sprung mass acceleration, sprung mass velocity, suspension deflection, tire deflection and unsprung mass velocity. Before we compare the multi-body model with the linear quarter car model, the passive and active states of both the models are analysed to see if the LQR controller works.

Case 1: Linear components with low suspension deflection (5 cm)

In this case, the multi-body model has linear components and the suspension deflection is low because of a low amplitude road input. The road profile is a 5 cm bump and the velocity of the car is 0.5 m/s as shown in Figure 56.

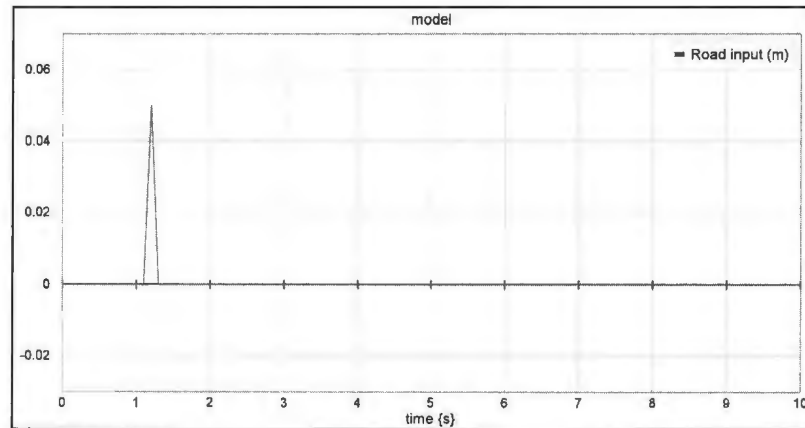


Figure 56: Road profile – 5 cm bump

Active vs. Passive modes

The LQR controller is applied to the linear quarter car model and the multi-body model and the effectiveness of the controller is analysed by comparing their active and passive states. Both the ride quality and road holding scenarios are presented here.

Ride quality

The LQR controller is applied to both the models for the highly rated ride quality scenario. The sprung mass acceleration is shown in Figure 57 for both the models. There is a marked improvement in the response when the active and passive modes are compared with each other for both the models. There is 41 % improvement in the positive peak amplitude and 48 % improvement in the negative peak amplitude in the active state for the multi-body model. There is 89 % improvement in the positive peak amplitude and 85 % improvement in the negative peak amplitude in the active state for the linear quarter car model.

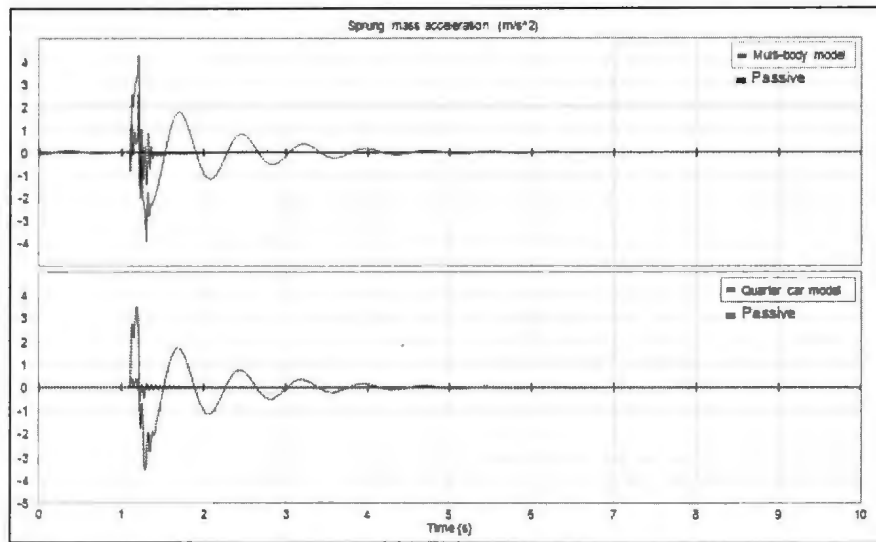


Figure 57: Case 1 – Sprung mass acceleration for MB and QC models (highly rated ride quality)

The four suspension states for the linear quarter car are shown in Figure 58. The controller shows improvement in all the states in the active state. However, the tire deflection and unsprung mass velocity have become highly noisy. This could be due to high gains obtained by the weighting of these states.

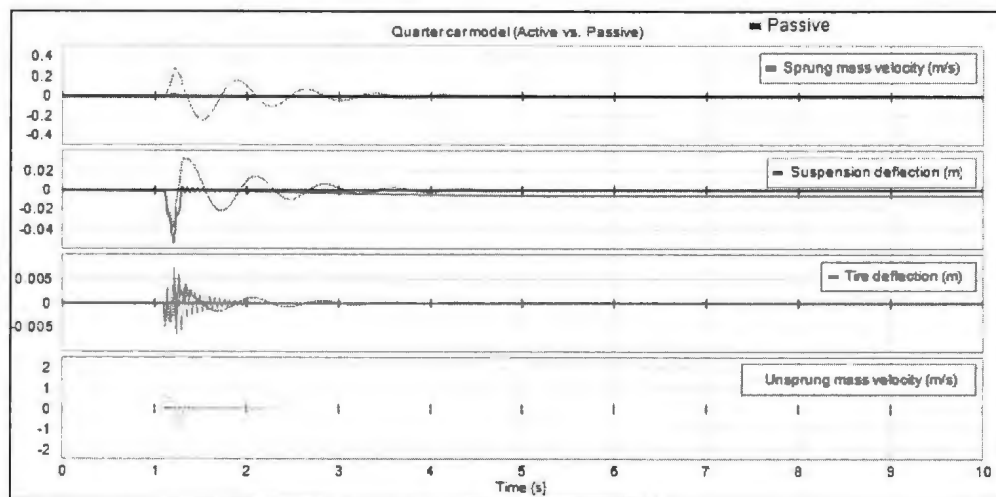


Figure 58: Case 1- QC model active vs. passive states (highly rated ride quality)

The active and passive states are analysed for the multi-body model for the highly rated ride quality scenario. Figure 59 shows that the multi-body models active states are working much better than the passive state. The sprung mass velocity and suspension deflection have reduced amplitudes in the positive and negative peaks. However, the tire deflection and unsprung mass velocity have become noisy.

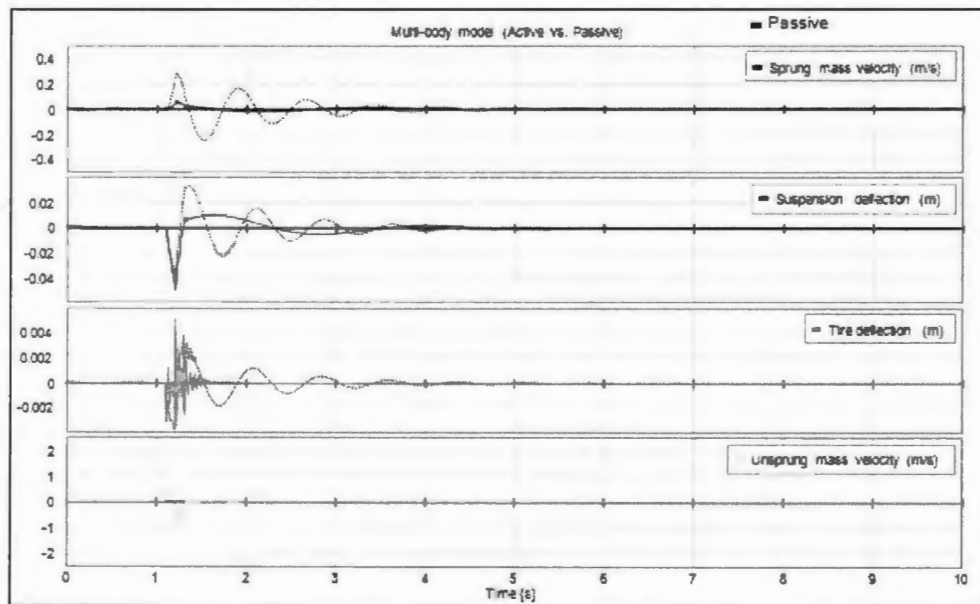


Figure 59: Case 1- MB model active vs. passive states (highly rated ride quality)

Now, the LQR controller for both the models is rated against each other. In the case of highly rated ride quality, the performance index for both the models is shown in the Figure 60. The performance index for the quarter car is much lower in comparison to that for the multi-body model. This shows that the quarter car is providing better performance for highly rated ride quality scenario.

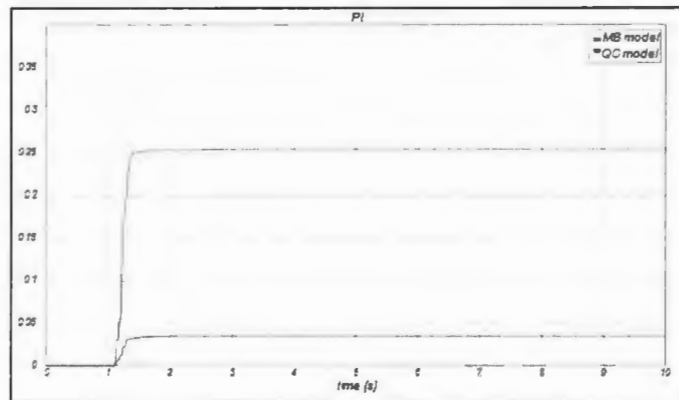


Figure 60: Case 1 - PI (highly rated ride quality)

The sprung mass accelerations for both the models are shown in Figure 61. The quarter car model performs significantly better than the multi-body model in terms of peak amplitude.

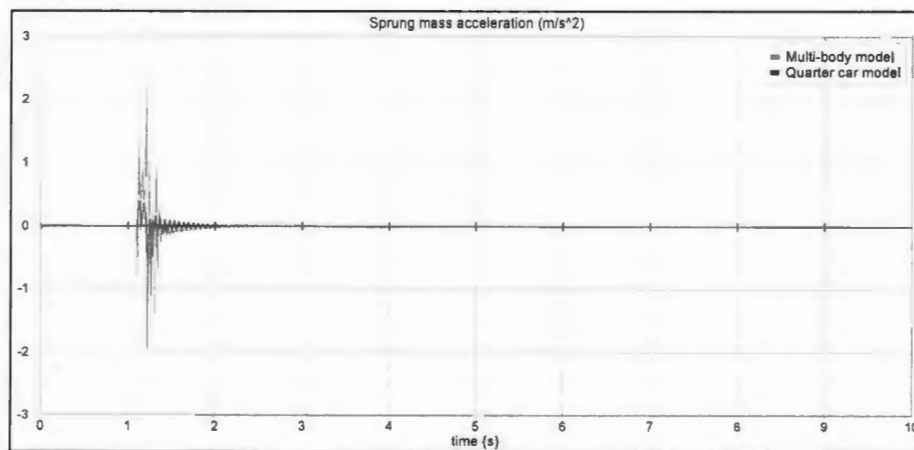


Figure 61: Case 1 - Sprung mass acceleration (highly rated ride quality)

The other suspension states are shown in Figure 62 for both the models. The suspension states of sprung mass velocity and suspension deflection seem to be performing better for the quarter car model compared with the multi-body model. The tire deflection and

unsprung mass velocity are better for the multi-body model as compared to the quarter car model.

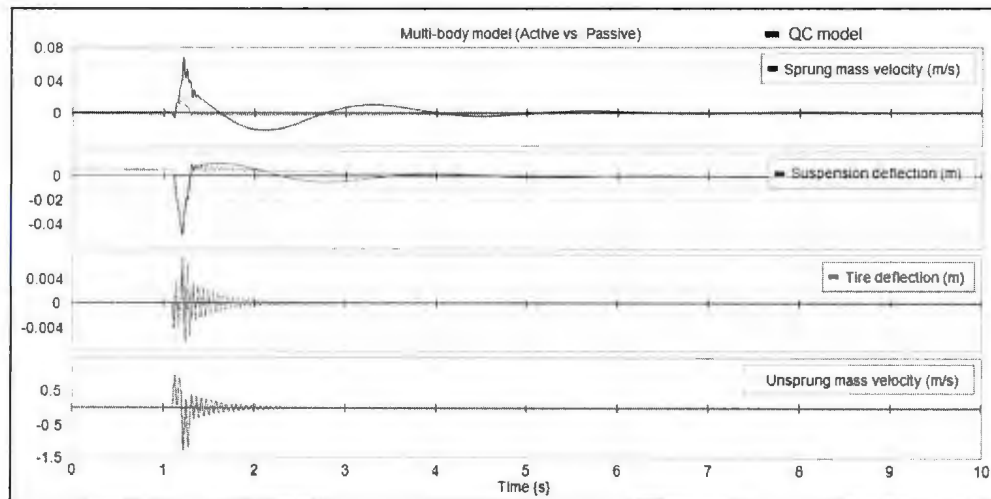


Figure 62: Case 1 – MB vs. QC model in active state (highly rated ride quality)

Now, the moderately rated ride quality scenario is tested for both the models. The active and passive states for the linear quarter car and multi-body are shown in Figure 63. The sprung mass acceleration for the multi-body model has an improvement of 41 % in the positive peak amplitude and 10 % in the negative peak amplitude in the active suspension system as compared to the passive state. The linear quarter car model has an improvement of 19 % in the positive peak amplitude but a 20 % degradation in the negative peak amplitude in the active suspension system compared with the passive state for the sprung mass acceleration.

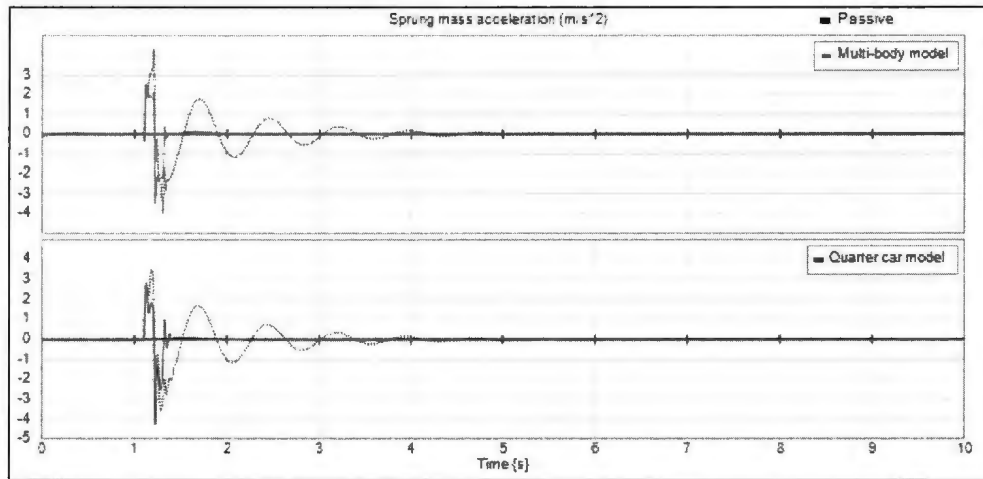


Figure 63: Case 1 - Sprung mass acceleration for MB and QC models (moderately rated ride quality)

The four suspension states are shown in Figure 64 for the linear quarter car in active and passive states. The active states are performing better in comparison to the passive state for the sprung mass velocity and suspension deflection. The tire deflection and unsprung mass velocity in the active state have similar response as the passive state but faster settling times.

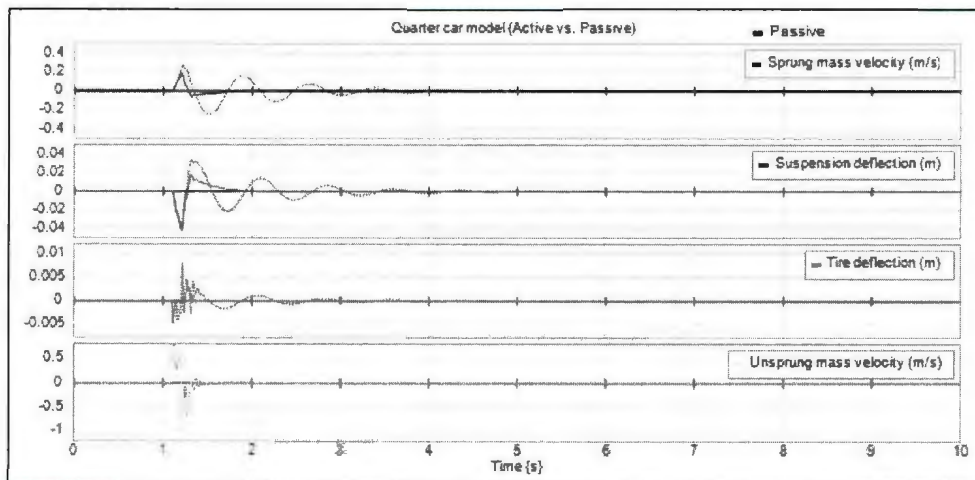


Figure 64: Case 1- QC model active vs. passive states (moderately rated ride quality)

The active and passive states are analysed for the multi-body model for the moderately rated ride quality scenario. Figure 65 shows that the active suspension states are working much better than the passive suspension states. There is less transients and faster settling times for all the suspension states in the active state.

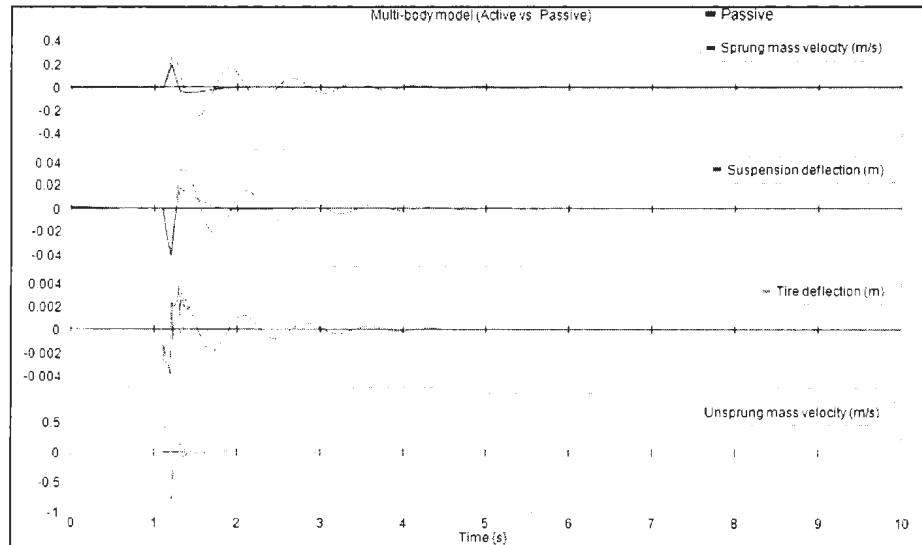


Figure 65: Case 1- MB model active vs. passive states (moderately rated ride quality)

Now, the LQR controller for both the models is rated against each other. In the case of moderately rated ride quality, the performance index for both the models is shown in Figure 66. The performance index for the quarter car is lower in comparison to that for the multi-body model. The performance index is 5.6 % better for the linear quarter car than the multi-body model.

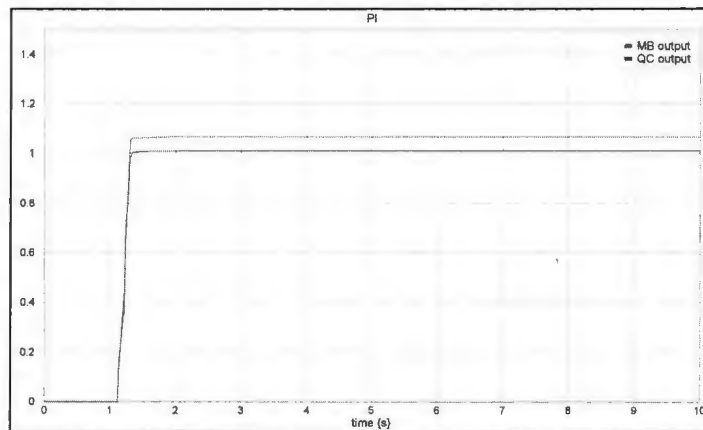


Figure 66: Case 1 - PI (moderately rated ride quality)

The sprung mass acceleration for the multi-body model has lower amplitude as compared to the linear quarter car model. There is a 12.7 % improvement in the positive peak and 21.2 % in the negative peak for the multi-body model when compared to the quarter car model, which can be seen in Figure 67. The moderately rated ride quality is working better for the multi-body model than the quarter car model.

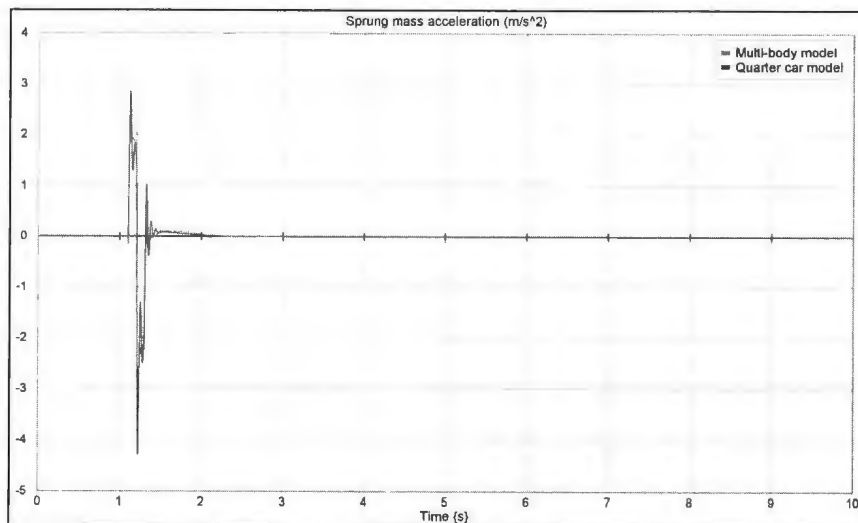


Figure 67: Case 1 - Sprung mass acceleration (moderately rated ride quality)

The other suspension states are shown in Figure 68 for both the models. The suspension states are comparable to each other for both the models.

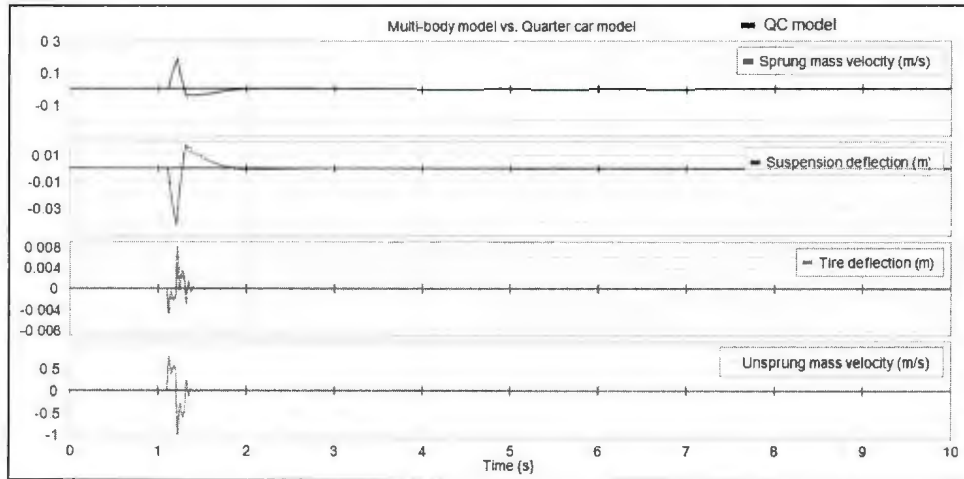


Figure 68: Case 1 - MB vs. QC model in active state (moderately rated ride quality)

Road holding

Now, the LQR controller is tested for the road holding scenario for both the models. Here, the linear quarter car's active and passive states are shown in Figure 69. There is improvement in the suspension deflection whereas the amplitude of the tire deflection deteriorates slightly.

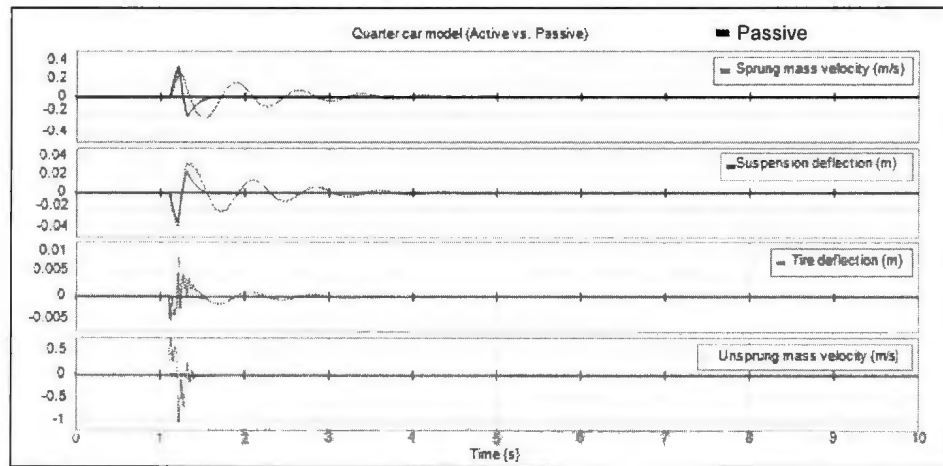


Figure 69: Case 1 – QC model active vs. passive states (road holding)

The active and passive states are analysed for the multi-body model for the highly rated road holding scenario. Figure 70 shows that there is 41.25 % improvement in the positive peak amplitude and 21.8 % in the negative peak amplitude for the suspension deflection in active state when compared to the passive state for the multi-body model. The amplitude of the tire deflection does not improve so much in terms of amplitude but it attains a faster settling time.

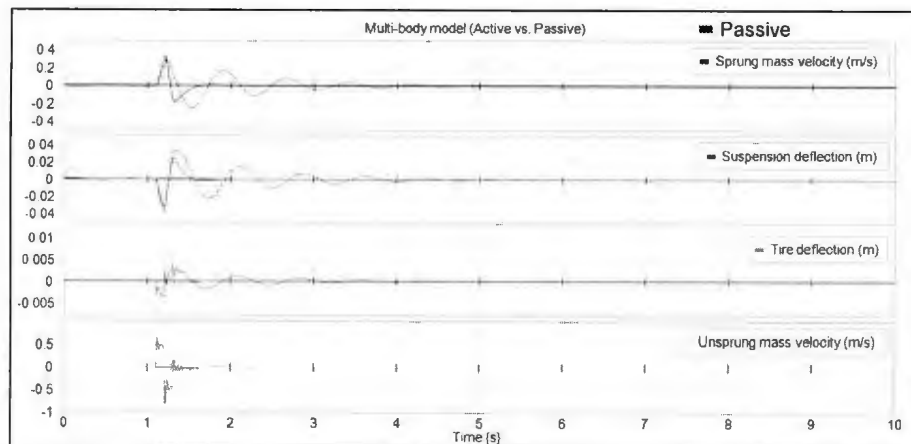


Figure 70: Case 1 - MB model active vs. passive states (road holding)

Now, the LQR controller for both the models is rated against each other. For highly rated road holding, the performance index of both the models remains very close to each other as shown in Figure 71.

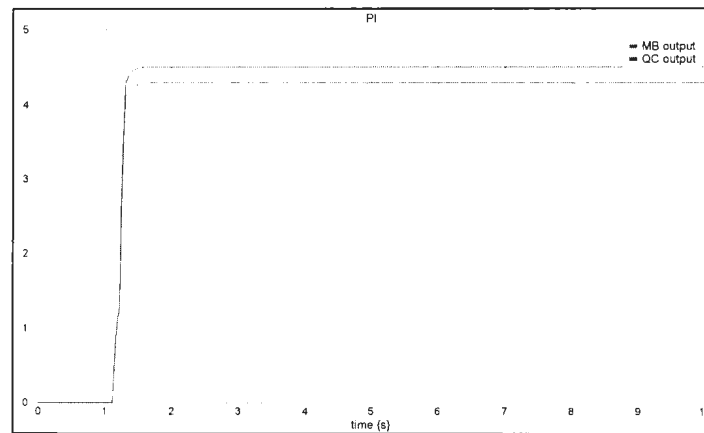


Figure 71: Case 1 - PI (road holding)

The two states that are worth to be noted for road holding case are suspension deflection and tire deflection. As shown in Figure 72, the suspension deflection is almost the same for both the models.

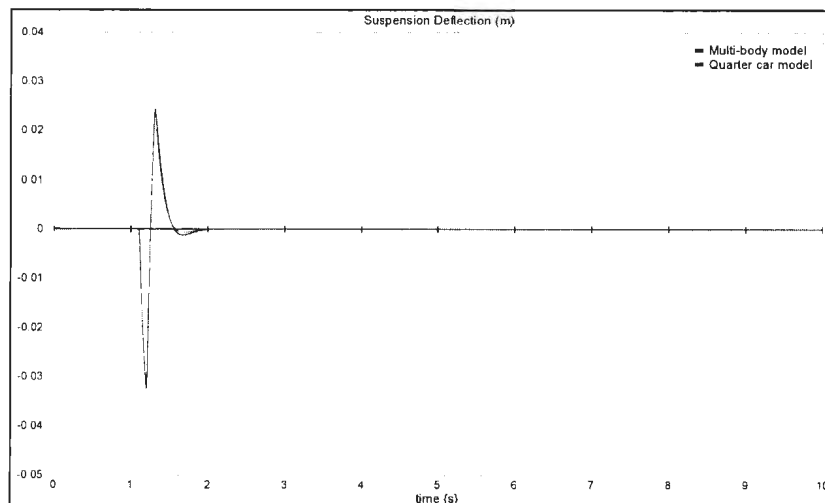


Figure 72: Case 1 - Suspension deflection (road holding)

The plots for tire deflection depict that the multi-body model has lower amplitude compared to the linear quarter car model. There is a 50 % improvement in the peak positive amplitude and 22 % in the negative peak amplitude of the multi-body model compared with the quarter car model as shown in Figure 73.

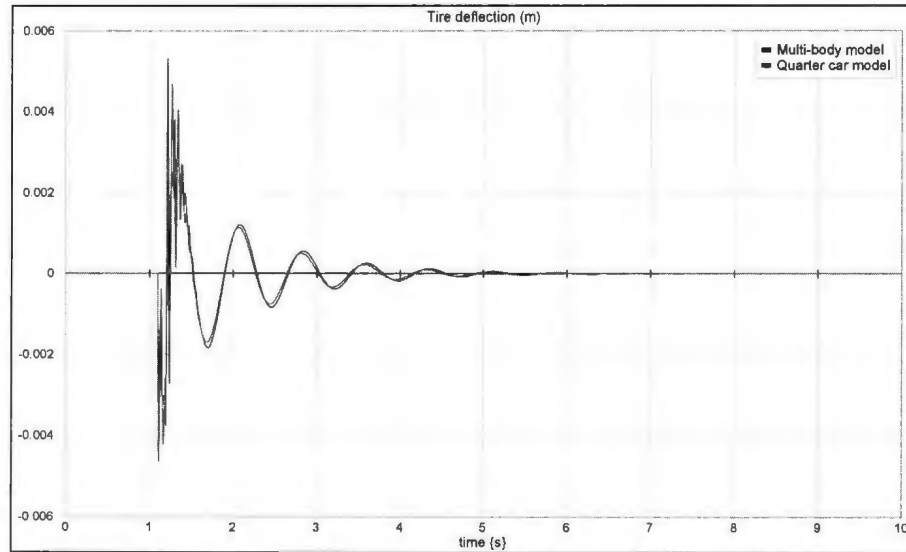


Figure 73: Case 1 - Tire deflection (road holding)

This case shows that the linear quarter car and the multi-body model are comparatively similar to each other when no non-linearity exists in the system. Also, the active states for both the models perform better than their passive states. For the ride quality cases, the moderately rated ride quality is working better for the multi-body model than for the linear quarter car model in low suspension deflection case. Aggressive weighting for the sprung mass acceleration for the LQR controller does not translate into better performance for the multi-body model. From this point on, the ride quality scenario will only be tested for the moderately rated ride quality.

Case 2: Non-linear components with low suspension deflection (5 cm)

In this case, non-linearity is introduced in the components for the multi-body model. There is a bilinear damper (*jounce* 5300 Ns/m and *rebound* 7800 Ns/m) and a cubic spring with a stiffness coefficient of 42600000 N/m ; the details of which have already been discussed in Section 3.4.1. The road input is a 5 *cm* bump and the velocity of the vehicle is 1.8 *km/h*. Also for this case, the LQR controller will not be analysed again for the linear quarter car since the additional non-linearity is only applied to the multi-body model and hence the comparison study will be same as performed in Case 1. The active and passive systems for the multi-body model are compared with each other.

Active vs. Passive modes

The LQR controller is applied to the multi-body model and the effectiveness of the controller is analysed by comparing the active and passive states. Both the ride quality and road holding scenarios are presented here.

Ride quality

For the moderately rated ride quality scenario, the LQR controller is applied to the multi-body model. The sprung mass acceleration is shown in Figure 74. There is a 27.7 % improvement in the positive peak and 29 % improvement in the negative peak in the active state for the multi-body model.

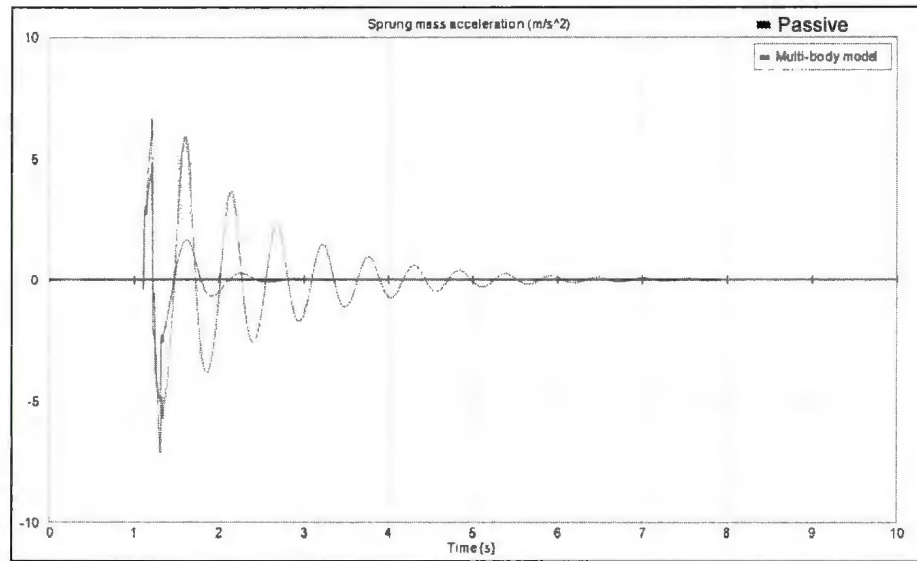


Figure 74: Case 2 – Sprung mass acceleration for MB and QC models (ride quality)

There is improvement in all the suspension states for the multi-body model as shown in Figure 75 in the active state when compared with the passive state.

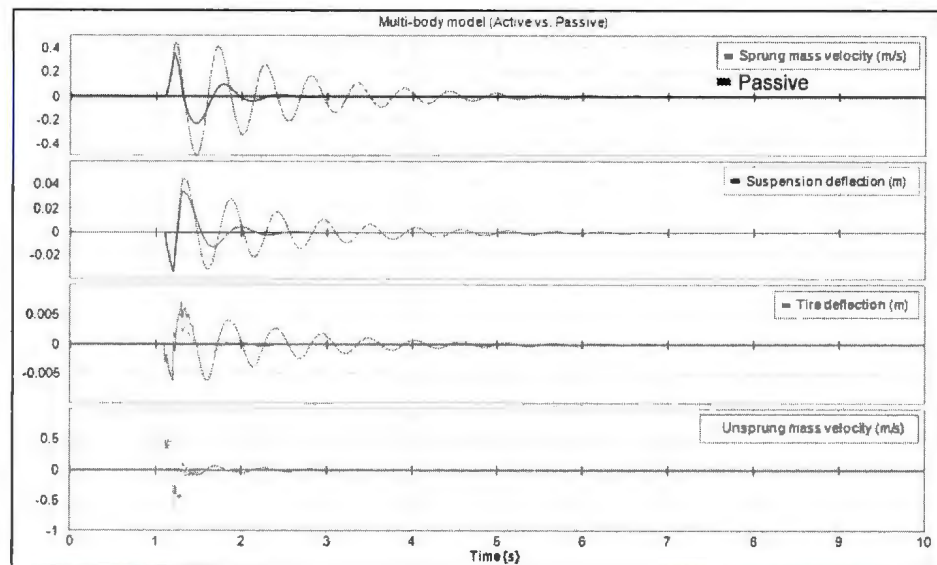


Figure 75: Case 2- MB model active vs. passive states (ride quality)

Now, the performance of the LQR controller for both the models is compared with each other. Figure 76 shows that in the moderately rated ride quality scenario, the performance index is better for the quarter car model than the multi-body model.

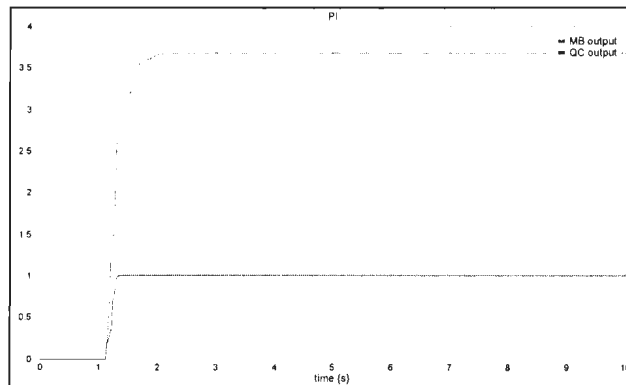


Figure 76: Case 2 - PI (ride quality)

The sprung mass acceleration does not seem to be performing better for the multi-body model either as shown in Figure 77. There is a 69 % deterioration of positive peak amplitude and 16.8 % for the negative peak amplitude for the multi-body model compared with the quarter car model.

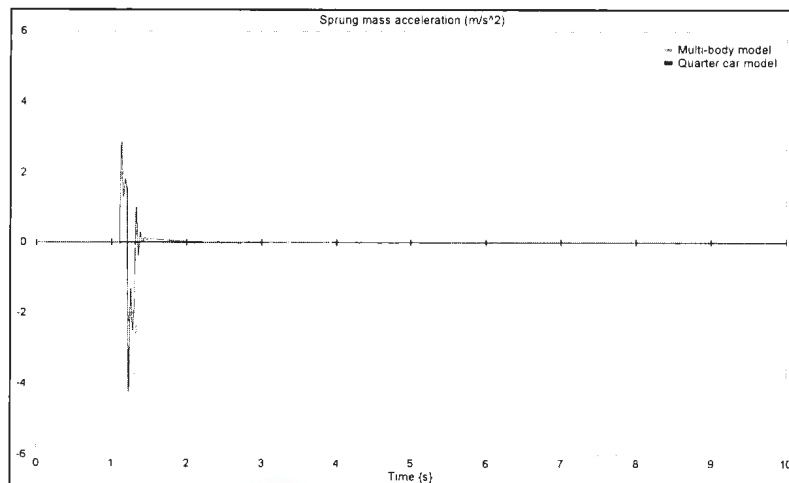


Figure 77: Case 2 - Sprung mass acceleration (ride quality)

The sprung mass velocity and suspension deflection performance deteriorates slightly for the multi-body model when evaluated against the linear quarter car model as shown in Figure 78. The tire deflection and the unsprung mass velocity are comparable for both the models.

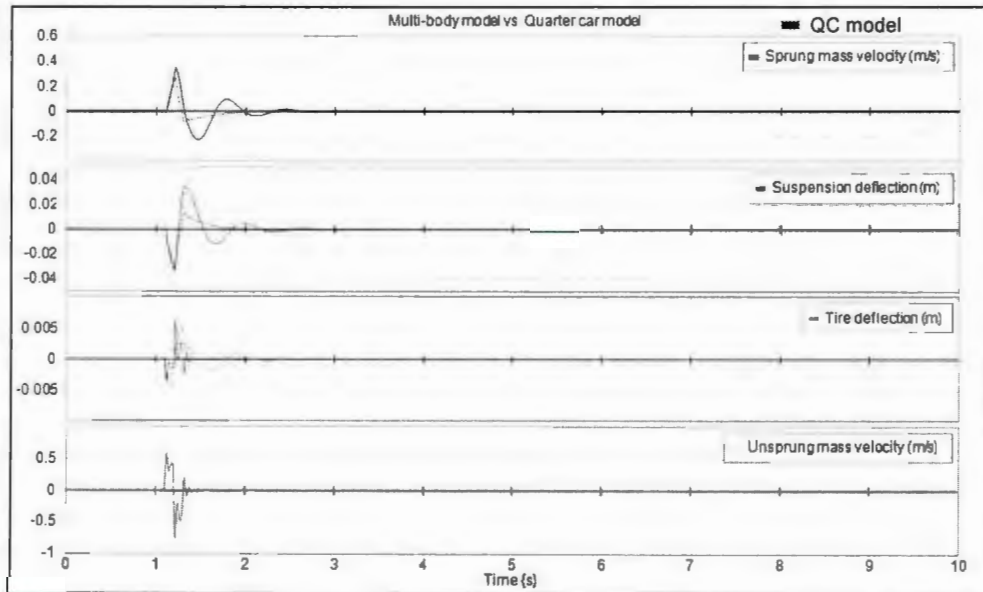


Figure 78: Case 2 – MB vs. QC model in active state (ride quality)

Road holding

Now, the LQR controller is tested for the road holding scenario for the multi-body model. Here, the multi-body model's active and passive states are shown in the Figure 79. The suspension deflection shows improvement of 33 % in the positive peak amplitude and 9 % in the negative peak amplitude in the active state compared to the passive state. The tire deflection in the active state has higher amplitude than the passive state but the transients die down quickly and it has less perturbations.

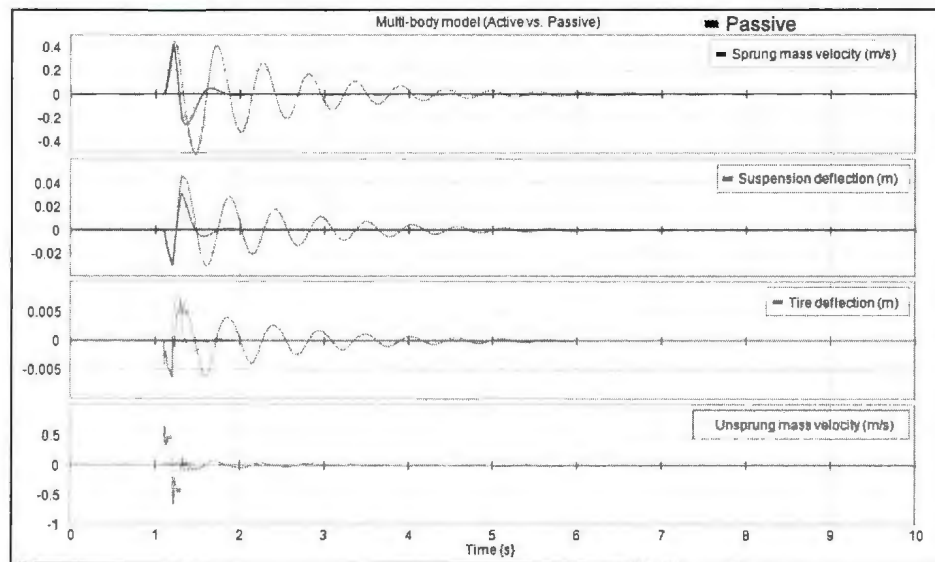


Figure 79: Case 2 - MB model active vs. passive states (road holding)

In the case of highly rated road holding, the controller performance index is slightly better for the quarter car model than the multi-body model. There is 40 % deterioration in multi-body model's performance index compared with quarter car. This is shown in Figure 80.

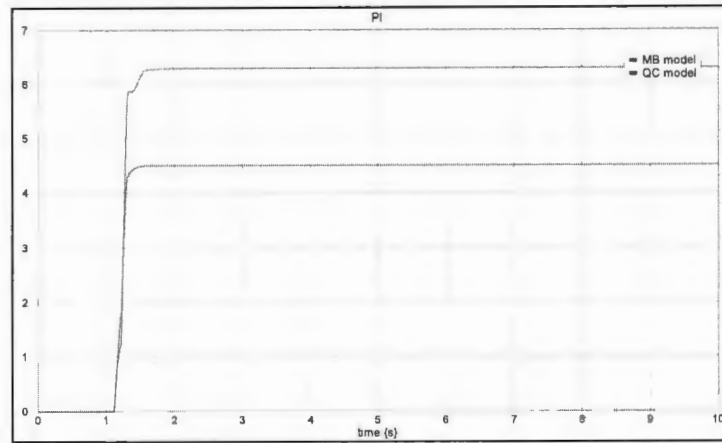


Figure 80: Case 2 - PI (road holding)

The suspension deflection is slightly worse for the multi-body model as compared to the quarter car model as shown in Figure 81. The positive peak amplitude degrades by 30 % but the negative peak amplitude improves by 10.3 % for the multi-body model when compared to the quarter car model.

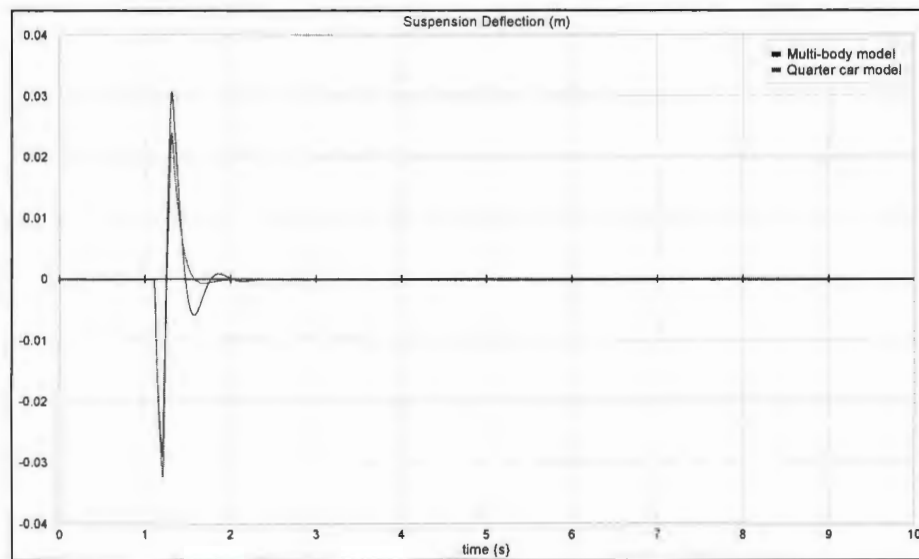


Figure 81: Case 2 - Suspension deflection (road holding)

The tire deflection is actually slightly better for the multi-body model as compared to the quarter car model as shown in Figure 82. There is a 28.6 % improvement in the positive peak amplitude and 66.6 % in the negative peak amplitude for the multi-body model evaluated against the quarter car model.

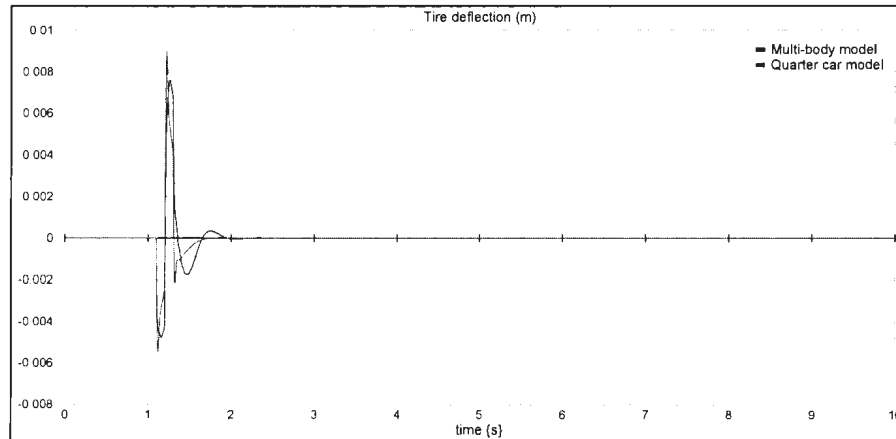


Figure 82: Case 2 - Tire deflection (road holding)

Even with the introduction of the non-linear elements in the multi-body model, the LQR controller performs better in ride quality and road holding scenarios in comparison to the passive state. However, the multi-body model does not fare well when compared to the linear quarter car model in terms of the active suspension states. This shows that the LQR controller's performance degrades when non-linearity is introduced in the system model and does not provide the same response as for the linear equivalent models.

Case 3: Linear components with high suspension deflection (16 cm)

In this case, the system undergoes high displacement i.e. the road input is a 16 cm bump and the velocity of the car is 1.8 km/h. This introduces geometric non-linearity in the multi-body model as the linkages have to travel beyond their normal limits. Figure 83 shows the road profile.

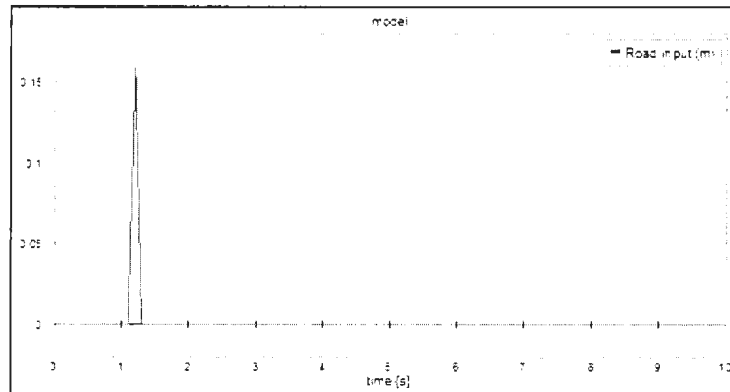


Figure 83: Case 3 - Road profile – 16 cm bump

Active vs. Passive modes

The LQR controller is applied to the linear quarter car model and the multi-body model and the effectiveness of the controller is analysed by comparing their active and passive states. Both the ride quality and road holding scenarios are presented here.

Ride Quality

For the moderately rated ride quality, the LQR controller is applied to both the models. The sprung mass acceleration is shown in Figure 84. There is a marked improvement in the response when the active and passive modes are compared with each other for both the models. There is 53 % improvement in the positive peak amplitude but 11 % deterioration in the negative peak amplitude in the active state for the multi-body model.

There is 18 % improvement in the positive peak but 20 % deterioration in the negative peak amplitude in the active state for the linear quarter car model.

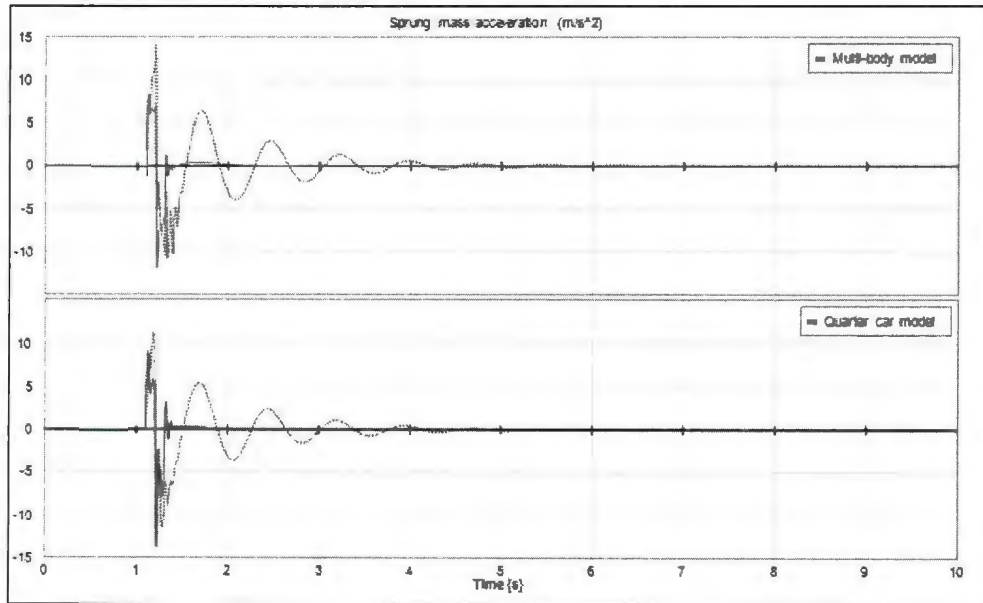


Figure 84: Case 3 – Sprung mass acceleration for MB and QC models (ride quality)

The four suspension states for the linear quarter car model are shown in Figure 85. There is considerable improvement in the sprung mass velocity and suspension deflection states in the active state.

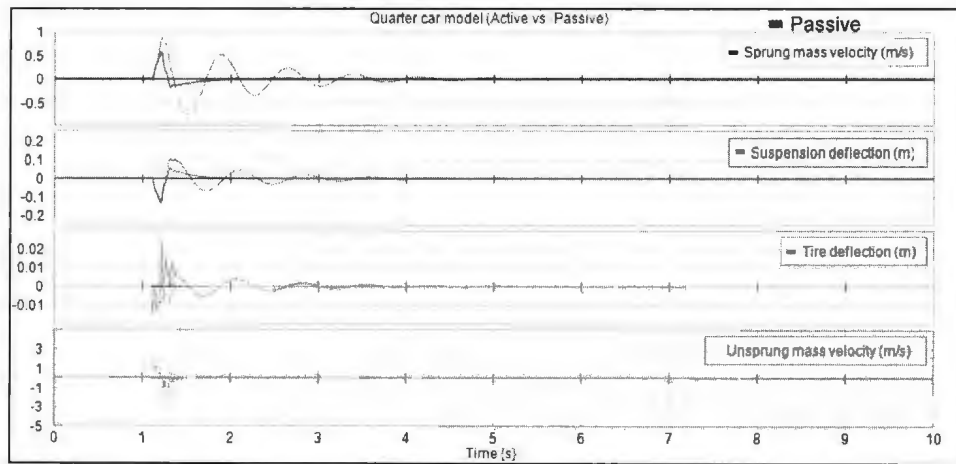


Figure 85: Case 3- QC model active vs. passive states (ride quality)

The active and passive states are analysed for the multi-body model for the moderately rated ride quality scenario. Figure 86 shows that the multi-body models active states particularly sprung mass velocity and suspension deflection are working much better than the passive state in suppressing the vibrations and faster settling times.

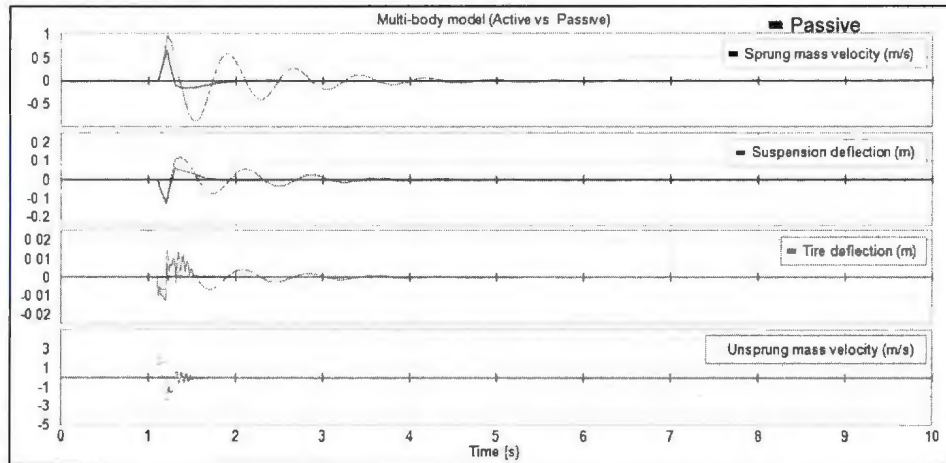


Figure 86: Case 3- MB model active vs. passive states (ride quality)

Now, the LQR controller for both the models is rated against each other. In the case of moderately rated ride quality, the performance index for both the models is shown in Figure 87. The multi-body model is 18 % better than the quarter car model.

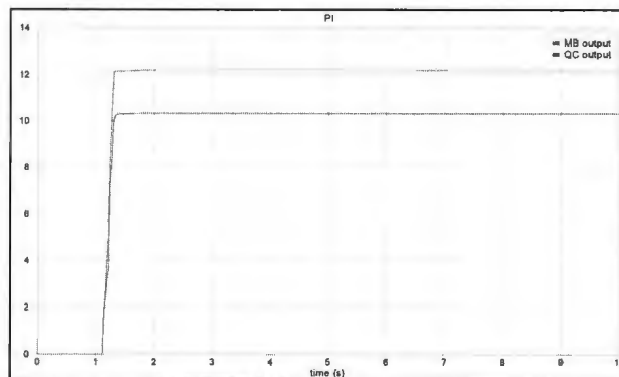


Figure 87: Case 3 - PI (ride quality)

The sprung mass acceleration for both the models is shown in Figure 88. The multi-body model performs slightly better than the linear quarter car model. The multi-body model performs 10.3% better than the quarter car model in the positive peak amplitude and 6.6% in the negative peak amplitude.

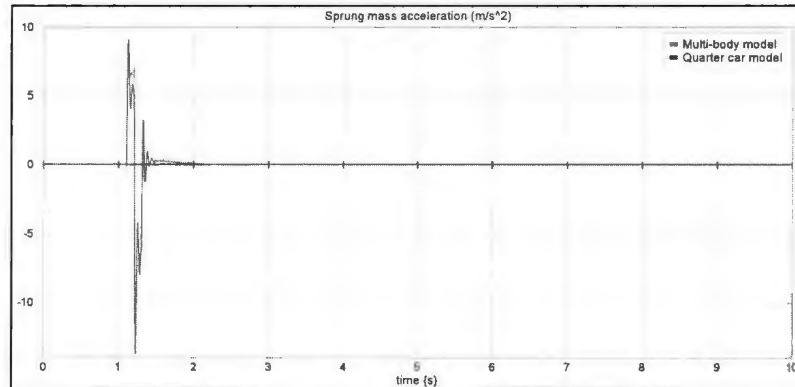


Figure 88: Case 3 - Sprung mass acceleration (ride quality)

The sprung mass velocities for both the models are comparable to each other. The other suspension states for the quarter car model perform better than the multi-body model as shown in Figure 89.

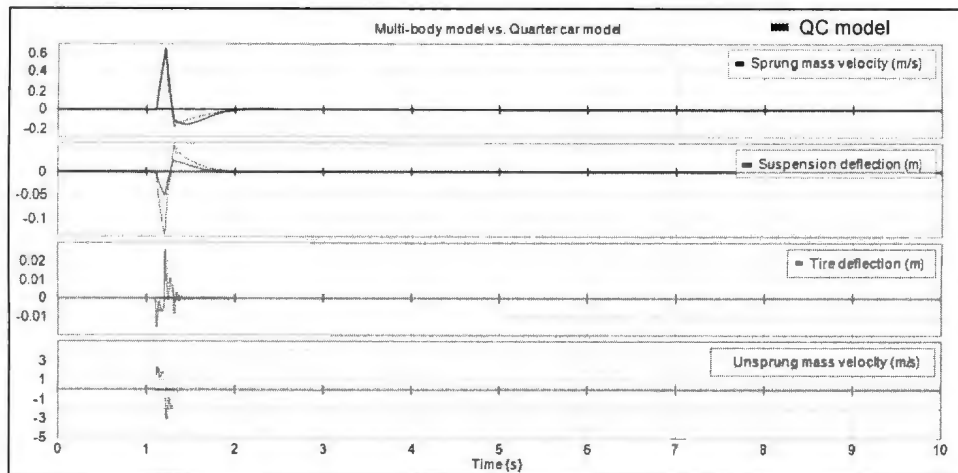


Figure 89: Case 3 – MB vs. QC model in active state (ride quality)

Road Holding

Now, the LQR controller is tested for the road holding scenario for both the models. Here, the linear quarter car's active and passive states are shown in Figure 90. The suspension deflection shows 28 % improvement in the positive peak amplitude and 15 % in the negative peak amplitude in the active state when compared to the passive state. The tire deflection in the active state has higher amplitude than the passive state but the transients die down quickly and it has less perturbations.

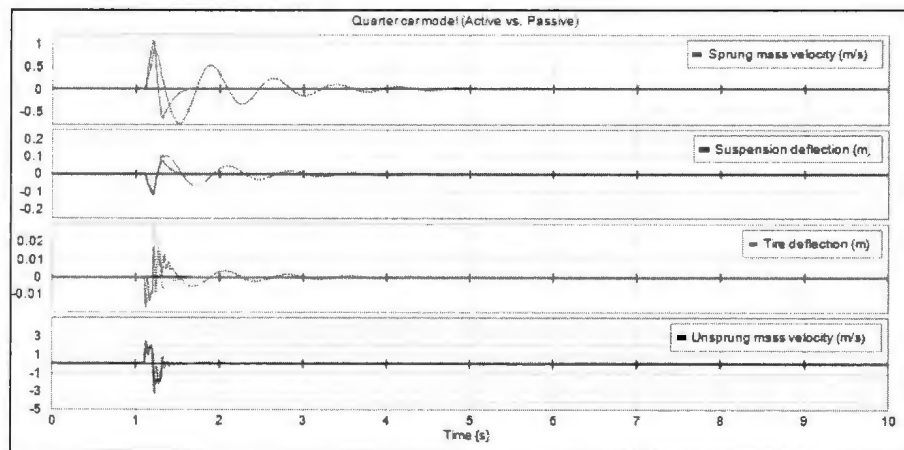


Figure 90: Case 3 – QC model active vs. passive states (road holding)

The active and passive states are analysed for the multi-body model for the highly rated ride quality scenario. For road holding, there is a 41 % improvement in the active state positive peak amplitude and 21 % in the negative peak amplitude for the suspension deflection when compared to the passive state for the multi-body model. The tire deflection shows higher amplitude in the active state but faster settling time and less transients. This is shown in Figure 91.

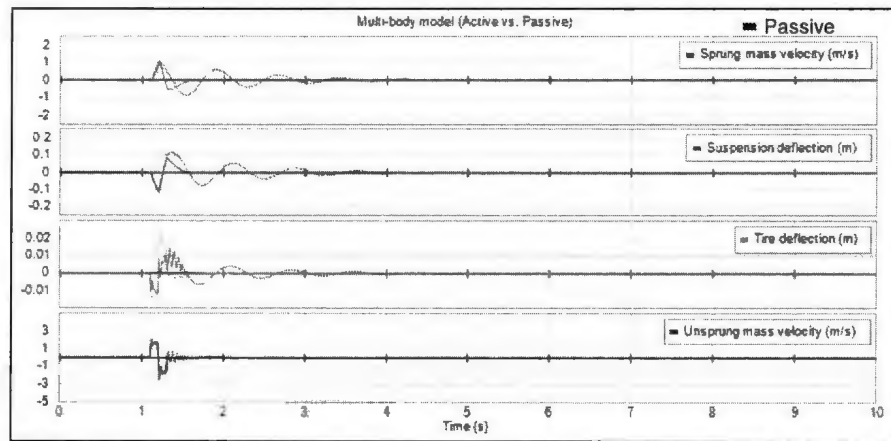


Figure 91: Case 3 - MB model active vs. passive states (road holding)

For highly rated road holding, the performance index is almost the same for both the models as shown in Figure 92. The quarter car model is 2 % better than the multi-body model in terms of their performance indices.

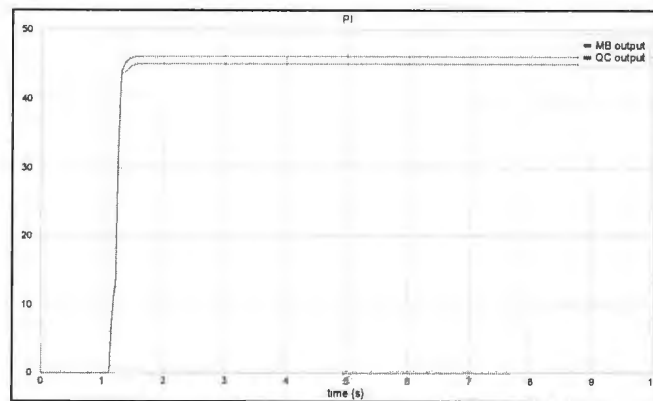


Figure 92: Case 3 - PI (road holding)

The suspension deflection for the linear quarter case performs just slightly better than the multi-body model case in terms of the amplitude. There is 8% degradation of the performance of multi-body model in positive peak amplitude when compared to the quarter car model and 9 % improvement in the negative peak amplitude as shown in the Figure 93.

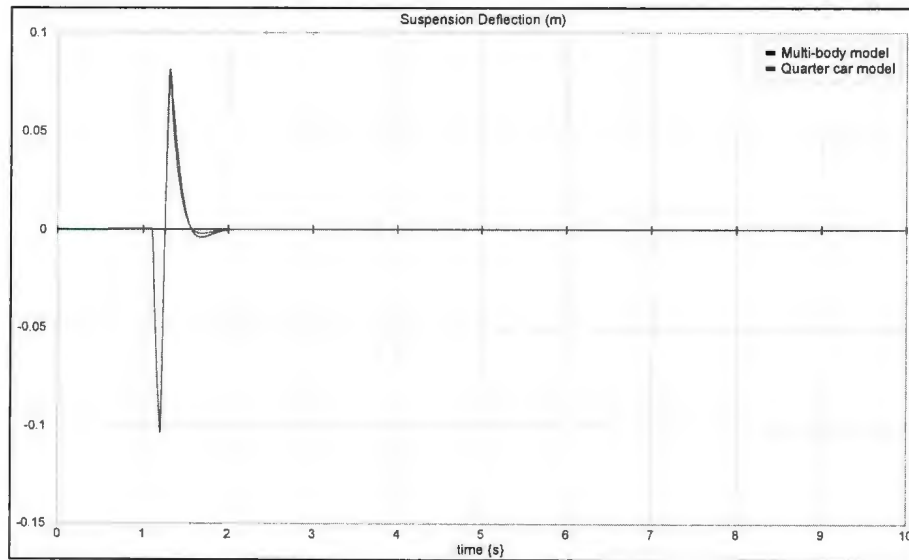


Figure 93: Case 3 - Suspension deflection (road holding)

The tire deflection is better for the multi-body model than the linear quarter car model. The peak positive amplitude of multi-body model is improved by 21 % and the negative peak amplitude by 17 % as shown in Figure 94.

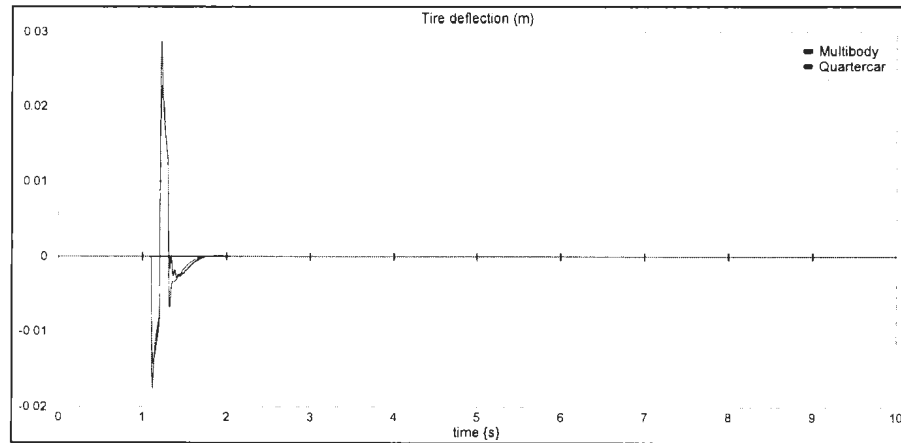


Figure 94: Case 3 - Tire deflection (road holding)

The LQR controller performs well for the multi-body model when the active and passive states are compared with each other for ride quality and road holding scenarios. The comparison study of multi-body model with the quarter car model also shows that the LQR controller works better for the linear model but the performance of the controller on the multi-body model is very similar to that of the linear model. This case shows that when there is high geometric non-linearity the linear controller still works well for a non-linear multi-body model.

Case 4: Non-linear components with high suspension deflection (16 cm)

In this case, there is a road input of 16 *cm* and there are nonlinearities in the spring and damper components, which have already been discussed in Case 2. This case contains nonlinearities of geometric and component nature. Since component non-linearity is not included in the linear unidirectional quarter car, the active and passive states are the same as in Case 3. The active and passive system of the multi-body model are analysed for ride quality and road holding scenarios.

Active vs. Passive modes

The LQR controller is applied to the multi-body model and the effectiveness of the controller is analysed by comparing the active and passive states.

Ride quality

For the moderately rated ride quality scenario, the LQR controller is applied to the multi-body model. The sprung mass acceleration is shown in Figure 95. There is a 21 % improvement in the positive peak and 47 % improvement in the negative peak in the active state for the multi-body model.

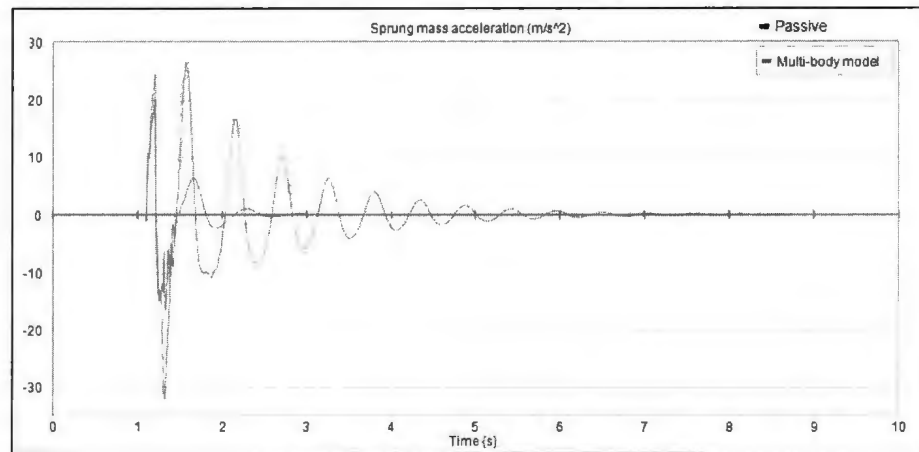


Figure 95: Case 4 – Sprung mass acceleration for MB and QC models (ride quality)

There is improvement in all the suspension states for the multi-body model as shown in Figure 96 in the active state when compared with the passive state.

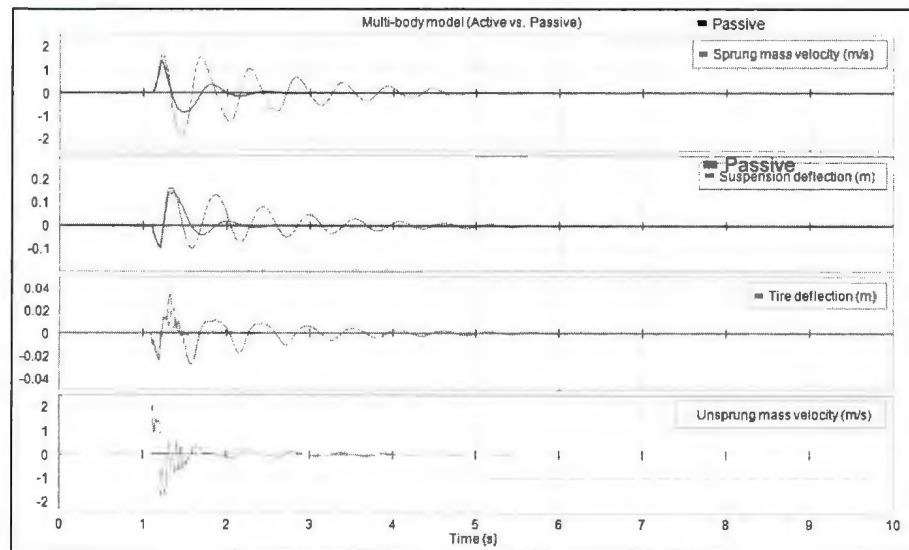


Figure 96: Case 4 - MB model active vs. passive states (ride quality)

In the moderately rated ride quality scenario, the performance index for the multi-body model is a lot worse than the linear quarter car model as depicted in Figure 97.

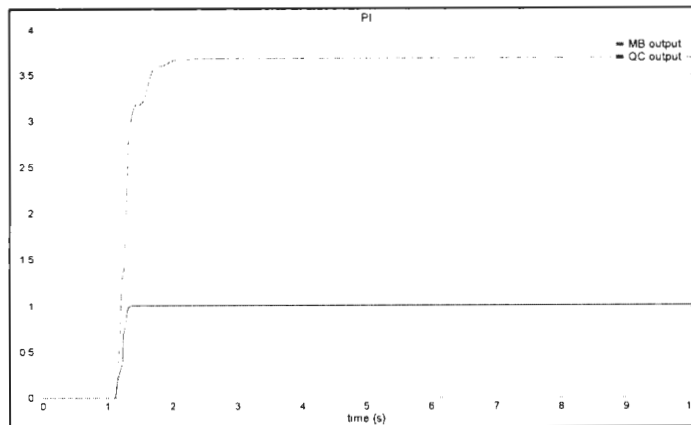


Figure 97: Case 4 - PI (ride quality)

The sprung mass acceleration does not seem to be performing better for the multi-body model either. There is a 119 % deterioration of positive peak amplitude and 37 % for the negative peak amplitude for the multi-body model when compared with the quarter car model as shown in Figure 98.

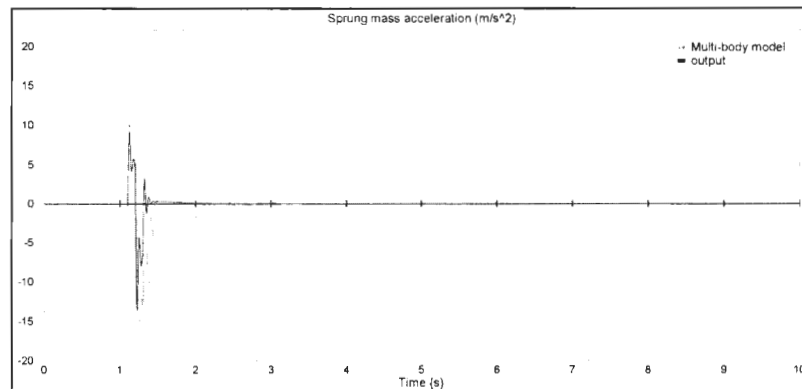


Figure 98: Case 4 - Sprung mass acceleration (ride quality)

The sprung mass velocity and suspension deflection performance deteriorates for the multi-body model when evaluated against the linear quarter car model as shown in the Figure 99. The tire deflection and the unsprung mass velocity are slightly better for the multi-body model than the other states.

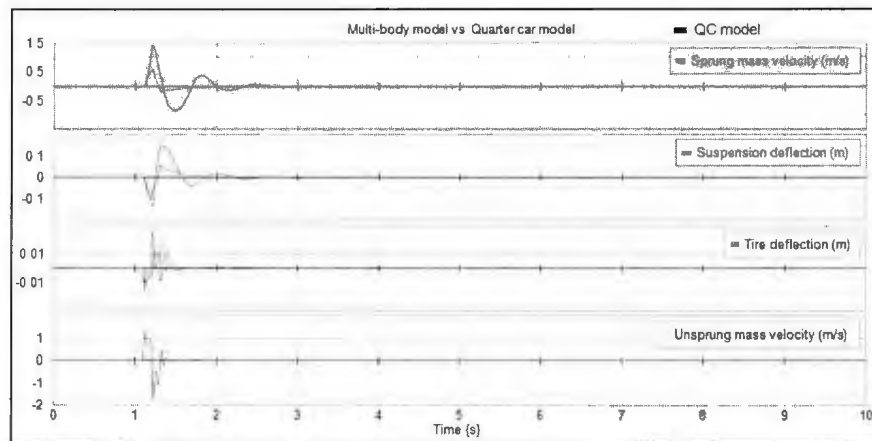


Figure 99: Case 4 – MB vs. QC model in active state (ride quality)

Road holding

Now, the LQR controller is tested for the road holding scenario for multi-body model. Here, the multi-body model's active and passive states are shown in Figure 100. The suspension deflection shows improvement of 25 % in the positive peak amplitude and 11 % in the negative peak amplitude in the active state compared to the passive state. The tire deflection in the active state has higher amplitude than the passive state but the transients die down quickly and it has less perturbations.

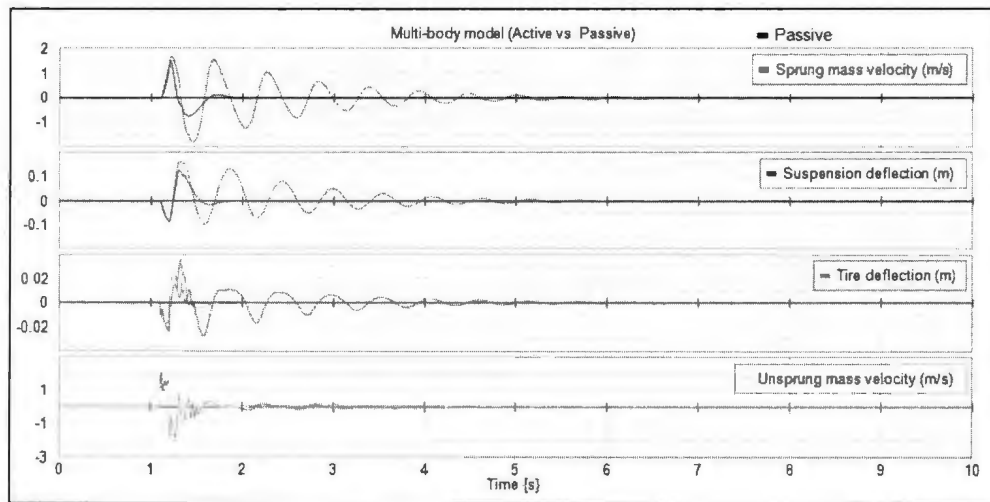


Figure 100: Case 4 - MB model active vs. passive states (road holding)

In the case of highly rated road holding, the controller performance index is slightly better for the quarter car model than the multi-body model. There is 40 % change in multi-body model performance index compared with quarter car. This is illustrated in Figure 101.

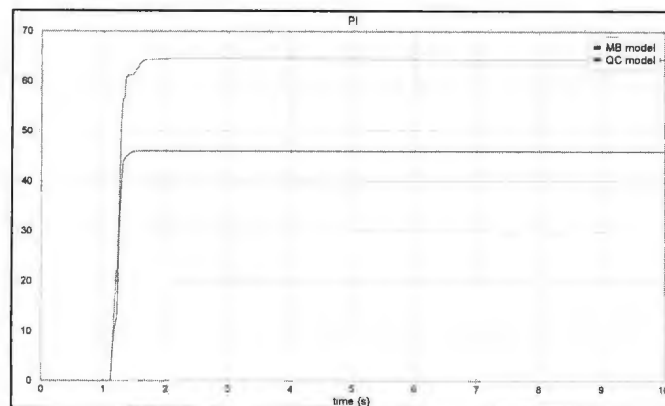


Figure 101: Case 4 - PI (road holding)

The suspension deflection is slightly worse for the multi-body model as compared to the quarter car model. Figure 102 shows that the positive peak amplitude degrades by 69 %

but the negative peak amplitude improves by 19 % for the multi-body model when compared to the quarter car model.

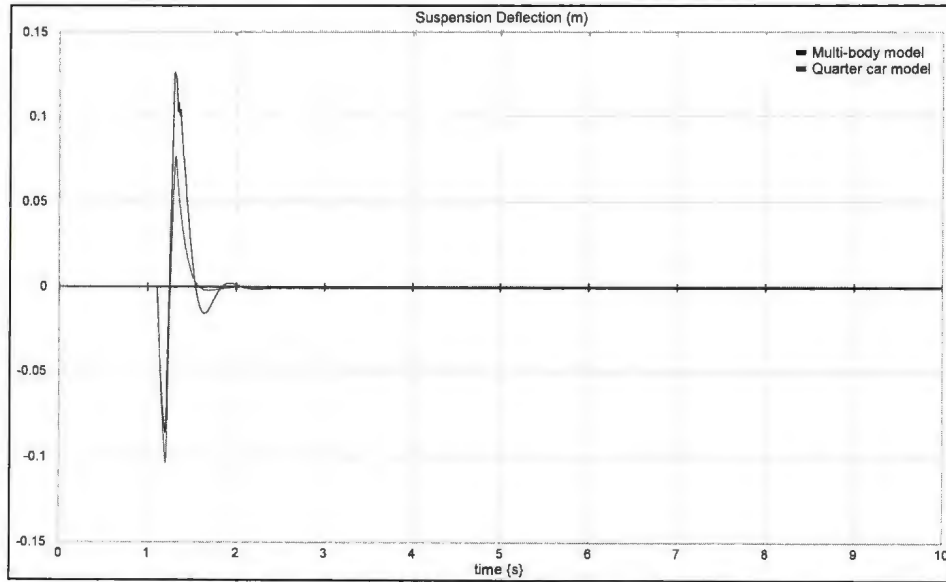


Figure 102: Case 4 - Suspension deflection (road holding)

The tire deflection is actually slightly better for the multi-body model as compared to the quarter car model. There is a 13 % improvement in the positive peak amplitude and 2 % in the negative peak amplitude for the multi-body model evaluated against the quarter car model as shown in Figure 103.

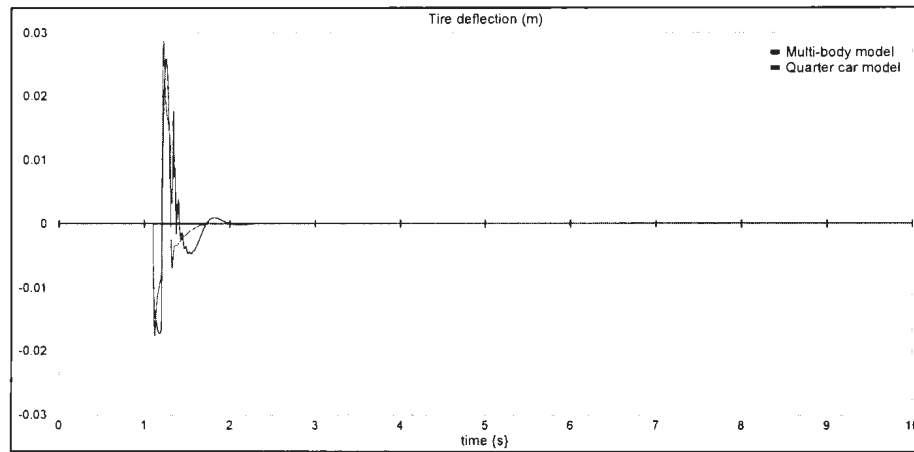


Figure 103: Case 4 - Tire deflection (road holding)

This case shows that when there is high non-linearity in the system model, the LQR controller does not perform so well for the active suspension system. Although there is improvement in the active state when compared with the passive state for the multi-body model, the linear controller does not work so well when compared to the linear quarter car. The non-linearity induced in the system due to the geometry and components seem to degrade the performance of the controller. This is the worst case scenario for the multi-body model and to improve the performance of the controller further studies have to be performed.

5.5 Summary of Results

The four cases discussed in previous sections have been summarized here in terms of the LQR controller performance for the ride quality and road holding scenarios. The moderately rated ride quality case is chosen for the ride quality scenarios.

The ratios of the positive peak amplitudes of the sprung mass acceleration have been chosen as the entity to compare the ride quality performance of the multi-body model

with the quarter car model and to compare the active and passive states of both the models. For the road holding, the ratios of the positive peak amplitudes of tire deflection or settling times have been chosen to compare the controller performance for both the models and their active and passive states.

$$\text{Passive vs. Active} \left[\frac{\ddot{z}_s \text{ or } z_{\text{tire}} (\text{passive})}{\ddot{z}_s \text{ or } z_{\text{tire}} (\text{active})} \right] > 1$$

$$\text{QC vs. MB model} \left[\frac{\ddot{z}_s \text{ or } z_{\text{tire}} (\text{QC model} - \text{active})}{\ddot{z}_s \text{ or } z_{\text{tire}} (\text{MB model} - \text{active})} \right] > 1$$

Table 5 and 6 show the ratios for the various cases for both ride quality and road holding scenarios.

Table 5: Ride quality (peak amplitudes) summary for four cases

Ride Quality (sprung mass acceleration)				
Peak amplitudes (m/s^2)	Case 1	Case 2	Case 3	Case 4
Active vs. Passive states (QC model)	1.24	1.23	1.24	1.23
Active vs. Passive states (MB model)	1.71	1.38	1.75	1.22
QC vs. MB model (Active state)	1.13	0.59	1.11	0.45

Table 6: Road holding (peak amplitudes) summary for four cases

Road Holding (tire deflection)				
Peak amplitudes (m)	Case 1	Case 2	Case 3	Case 4
Active vs. Passive states (QC model)	0.59	0.59	0.59	0.59
Active vs. Passive states (MB model)	0.56	0.942	0.61	1.38
QC vs. MB model (Active state)	1.34	1.18	1.27	1.11

For ride quality scenario, we can see from Table 5 that the multi-body model and the quarter car model have better performance in the active state as compared to their passive state in all the four cases. This shows that the LQR controller is working for both the models. The multi-body model performs better than the quarter car model in the active state when either there is low non-linearity (Case 1) or there is only geometric non-linearity (Case 3). For the other two cases (Case 2 and 4), component non-linearity is introduced in the multi-body model and so the controller performance degrades when compared to the linear quarter car model. So, the LQR controller does not work well with a multi-body model when there is component as well as geometric non-linearity present in the plant model.

For road holding scenario, we can see from Table 6 that the LQR controller fails to suppress the amplitude of the tire deflection in the active state for both the models as compared with their passive states. Only in Case 4, the multi-body model has better road holding in the active state as compared to its passive state in terms of peak amplitudes of

the tire deflection. As discussed in Section 5.4, even though the amplitudes of tire deflection are not suppressed for both the models, the vibrations are reduced and the system attains faster settling time. So the LQR controller is able to suppress the noisy vibrations induced on the system as well as attain equilibrium much quicker than its passive state. The LQR controller is working better for the multi-body model as compared to the quarter car model in all the cases for road holding scenarios in terms of suppressing the peak amplitudes.

Table 7: Road holding (settling times) summary for four cases

Road Holding (tire deflection)				
Settling time (s)	Case 1	Case 2	Case 3	Case 4
Active vs. Passive states (QC model)	11.58	11.58	11.58	11.58
Active vs. Passive states (MB model)	6.94	6.70	6.95	6.67
QC vs. MB model (Active state)	0.54	0.42	0.54	0.43

Table 7 provides the settling time ratios for the multi-body and the quarter car model. This table shows that even though there is less improvement in peak amplitudes of the tire deflection, the settling times is reduced considerable for all the cases. The active state is performing much better than the passive state for the quarter car as well as the multi-body models. Also Case 2 and 4, which contains non-linearity for the multi-body models have slower settling times than Case 1 and 3 which only has geometric non-linearity. When the comparison is made between the active states of the quarter car model and the multi-body

model, the quarter car model attains faster settling times and hence the ratio is less than 1 for all the cases.

5.6 Conclusion

The results show that the linear LQR controller works well for the multi-body model in all the cases for the ride quality scenarios but not as well for the road holding scenarios. Still the vibrations and settling time are reduced for the suspension states of the multi-body model in road holding as well as ride quality scenarios. When the component and geometric non-linearity increases for the multi-body model, the performance of the LQR controller is reduced for the ride quality scenario as evident from Case 1 and 3 when compared with Case 2 and 4. For the road holding scenario, the performance of the LQR controller is actually increased as the non-linearity increases for the multi-body model. But the highly rated ride quality scenario was abandoned for the multi-body model due to the controller instability. The proportional gains become too high and the controller performance degrades. However, this scenario works best for the linear quarter car model as seen in Case 1 for Section 5.4. So, the LQR controller does provide comparable performance for the LQR controller when the moderately rated ride quality scenario is compared for both the models.

The next chapter provides conclusion of the research conducted in this thesis.

Chapter 6: Conclusions and Future Work

6.1 Conclusion

The purpose of this thesis was to develop a non-linear multi-body quarter car model and a linear unidirectional quarter car model using bond graph method, design a linear controller and apply it to both the models. The performance of the linear controller designed with state space methods is tested on the non-linear multi-body model. The different streams have attained their own conclusions and would be discussed in detail along with scope of future work.

6.2 Quarter Car Model

The main objective of this research was to design and investigate the performance of a linear controller on a non-linear quarter car model and compare it with a linear unidirectional quarter car model. A multi-body SLA quarter car model using bond graph method was developed. Also, component non-linearity was appended in the SLA model to introduce complexities in the plant model. Simulations were performed to observe the suspension states in passive state and then the non-linear model was characterized to find the suspension parameters using force-deflection and force-velocity curves. The apparent suspension parameters were applied to the linear quarter car model developed in bond graph. Both the models were compared with each other in passive mode.

6.2.1 Future Work

Since a successful development of a multi-body quarter car model was accomplished, the study could be extended to develop half car models and full car models with added

complexities. Developing a half car model could provide the pitch and heave motions to the vehicle. When a full 7-DOF model is developed, pitch, roll, heave and vertical motions of each of the sprung mass could also be measured [1]. A Magic formula tire could be added to the half car and full car model to make the tires more realistic rather than just having stiffness and damping values.

6.3 Controller Design

A linear optimal LQR control was developed and applied to the linear quarter car model and the multi-body model. Their performance was compared in frequency and time domain for ride quality and road holding factors. Four case studies were formulated and simulation was performed on the multi-body model and compared to the linear quarter car model. The multi-body performance was good for low suspension deflection and linear components when compared with the linear quarter car model. The performance of the multi-body model degraded with added non-linearity in geometry and components when compared to a linear quarter car model, which showed the limitations of a linear LQR controller. The moderately rated ride factor performed much better than the highly rated ride factor for the multi-body model. The active multi-body model performed much better than the passive model in all ride quality and road holding cases.

6.3.1 Future Work

The study for linear controller design was accomplished for a multi-body quarter car model. Non-linear controllers like Model Predictive Control (MPC), Gain scheduling and Lypanov's based controllers can be designed to evaluate their performances on the multi-

body as well as quarter car models. The multi-body model could also be extended to preview control, the study of which has been performed by a previous student [40]. Once the non-linear controllers are applied and tested for a multi-body quarter car model, then the study could also include half car and full car models for controller performance. A comparison could be performed on the advantages of using non-linear controllers over linear controllers.

6.4 Validating Simulation Results

Once the experimentation is ready to be performed on a vehicle test-bed, the real feasibility of the simulation models can be verified. The simulation results can be validated by testing them on a unidirectional quarter car test-bed. After constructing a unidirectional quarter car test-bed and interfacing it with the required instrumentation for measurements, the test-bed can be used for real-time testing using dSPACE hardware. The road input can be provided by a MTS vibration machine [42] and the outputs can be displayed in real-time on MATLAB/Simulink. A voice coil for fully active suspension systems could be replaced with a semi-active damper for semi-active suspension system. The linear quarter car can be modified to include a scale wheel/tire. Dynamic similitude could be performed on the test rig to ensure that the test rig is scaled down version of a real suspension system. Once the active suspension implementation is complete on the linear unidirectional quarter car test rig, and then a non-linear SLA based quarter car test rig can be designed. The linear rails could be fabricated to include upper and lower control arms, joints and mountings to simulate a real suspension system. The linear controller can be tested on the both the rigs and comparison study can be performed

similar to the ones that have been achieved in simulation models in this thesis. This completes the scope of foreseeable future work related to the vehicle test-bed.

Contributions of this research towards vehicle dynamics,

1. A multi-body quarter car model with kinematic linkages was designed using bond graph method to investigate the performance of active suspension system. Earlier research was mostly restricted to controller performance in linear vehicle models. This study was performed to evaluate the linear controller performance on an inherently non-linear system. Component as well as geometric nonlinearities were introduced in the multi-body model to see the effects of controller performance.
2. A characterization method was devised to recover the apparent stiffness and damping coefficients from the non-linear multi-body model that could be applied to the linear quarter car models.
3. The LQR controller applied to the multi-body model and the linear quarter car model in frequency and time domain were compared against each other. The controller performance was also analysed in active and passive state for the multi-body model.

References

- [1] Rajamani, Rajesh. *Vehicle Dynamics and Control*. New York: Springer Science, 2006.
- [2] Karnopp, Dean C., Donald L. Margolis, and Ronald C. Rosenberg. *System Dynamics – Modeling and Simulation of Mechatronics Systems*. New Jersey: John Wiley & Sons, 2006.
- [3] Karnopp, Dean C. *Vehicle Stability*. New York: Marcel Dekker, 2004. Print.
- [4] Tewari, Ashish. *Modern Control Design with MATLAB and Simulink*. Chichester: John Wiley & Sons, 2002.
- [5] Happian-Smith, Jullian. *An Introduction to Modern Vehicle Design*. Oxford: Butterworth-Heinemann, 2001.
- [6] Wong, J.Y. *Theory of Ground Vehicles*. New York: John Wiley & Sons, 2008. Print.
- [7] Dorf, Richard C., and Robert H. Bishop. *Modern Control Systems*. Massachusetts: Addison-Wesley, 1994.
- [8] Hrovat, D. "Survey of Advanced Suspension Developments and Related Optimal Control Applications." *Automatica : the Journal of Ifac, the International Federation of Automatic Control*. 33.10 (1997): 1781.
- [9] Jahromi, K.E., D.G. Rideout, S.D. Butt , and F. Arvani. "Experimental Characterization of a Rubber Isolator for Dynamic Simulation of Vibration Attenuation in a Sonic Head Drilling Machine", Accepted for publication in *Proc. Canadian Machinery Vibration Association Machinery Vibration, Reliability and Maintenance Seminar and Annual General Meeting*, St. John's, NL. (2011).

- [10] Hrovat, D. "Optimal Active Suspension structures for quarter car vehicle models". *Automatica*. 26.5 (1990): 845-860.
- [11] Sharma, K, D A. Crolla, and D A. Wilson. "The Design of a Fully Active Suspension System Incorporating a Kalman Filter for State Estimation." *IEEE Conference Publication*. (1994): 344.
- [12] Sandu, C, E.R Andersen, and S Southward. "Multibody Dynamics Modelling and System Identification of a Quarter-Car Test Rig with Mcpherson Strut Suspension." *Vehicle System Dynamics*. 49 (2011): 153-179.
- [13] R. Ramli. M. Pownwall. M. Levesley. D.A. Crolla. "Dynamic Analysis of semi-active suspension systems using a co-simulation approach". John Wiley & Sons, 2004.
- [14] Mantaras, D. A, P. Luque, and C. Vera. "Development and Validation of a Three-Dimensional Kinematic Model for the Mcpherson Steering and Suspension Mechanisms." *Mechanism and Machine Theory*. 39.6 (2004): 603-619.
- [15] Esmailzadeh, E, and F Fahimi. "Optimal Adaptive Active Suspensions for a Full Car Model." *Vehicle System Dynamics*. 27.2 (1997): 89-107.
- [16] Brennan, S., and A. Alleyne. "A Scaled Testbed for Vehicle Control: The IRS". *Proceedings of the 1999 IEEE International Conference on Control Applications*. 1(1999): 327-332.
- [17] O'Brien, R. T., Jr., et al. "Scale-Model Vehicle Analysis using an Off-the-Shelf Scale-Model Testing Apparatus". *Proceedings of the American Control Conference*. 2004.
- [18] Liburdi, A. "Development of a Scale Vehicle Dynamics Test Bed." Windsor: University of Windsor. September 10, 2010. Thesis.

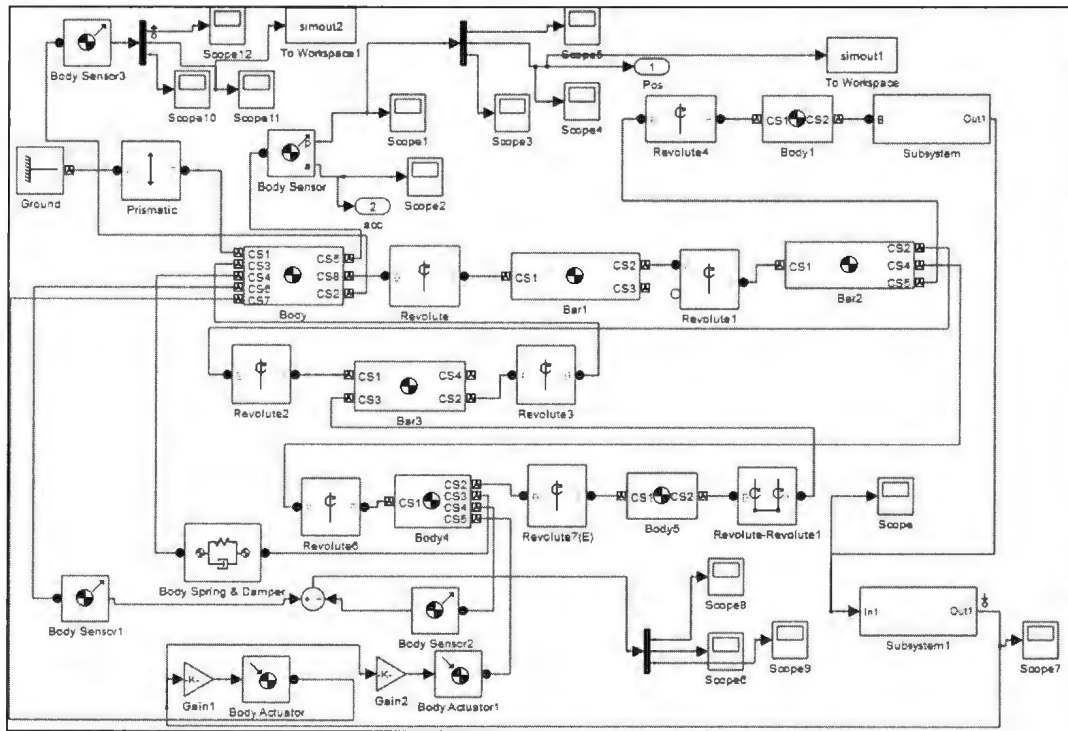
- [19] Verma, Rajeev, Domitilla Del Vecchio, and Hosam K. Fathy. "Development of a Scaled Vehicle with Longitudinal Dynamics of an HMMWV for an ITS Testbed." *IEEE/ASME Transactions on Mechatronics*. 13.1 (2008).
- [20] Mechanical Simulation Corp. CarSim, <http://www.carsim.com/products/carsim/index.php>. USA, 2012.
- [21] Controllab Products B.V. 20-Sim 4.1. <http://www.20sim.com/>. Netherlands. 2009.
- [22] Mathworks Inc. MATLAB. <http://www.mathworks.com/products/MATLAB/>. USA. 2009.
- [23] Dassault Systemes. SolidWorks Premium. <http://www.solidworks.com/>. USA. 2011.
- [24] Rideout, G. *Bond Graph Modeling- Multi-body model for quarter car*. Memorial University of Newfoundland. 2012.
- [25] Pacejka, H. B. "Modelling Complex Vehicle Systems using Bond Graphs." *Journal of the Franklin Institute* 319.1-2 (1985): 67-81.
- [26] Quijano, Nicanor, Kevin Passino, and Santosh Jogi. "A Tutorial Introduction to Control Systems Development and Implementation with dSPACE." USA. 2002.
- [27] Thomas, Annemarie. "dSPACE DS1103 Control Workstation Tutorial and DC Motor Speed Control. 2009.
- [28] Adibi-asl, Hadi, Geoff Rideout, "Bond Graph Modeling and Simulation of a Full Car Model with Active Suspension." *Proceedings of the 20th IASTED International Conference on Modelling and Simulation, Banff, AB, July 6-8 2009*.
- [29] Wan, Mark. "Suspension Geometry- Independent Suspensions" http://www.autozine.org/technical_school/suspension/tech_suspension2.htm#DW. 1997. 24 Aug. 2012.

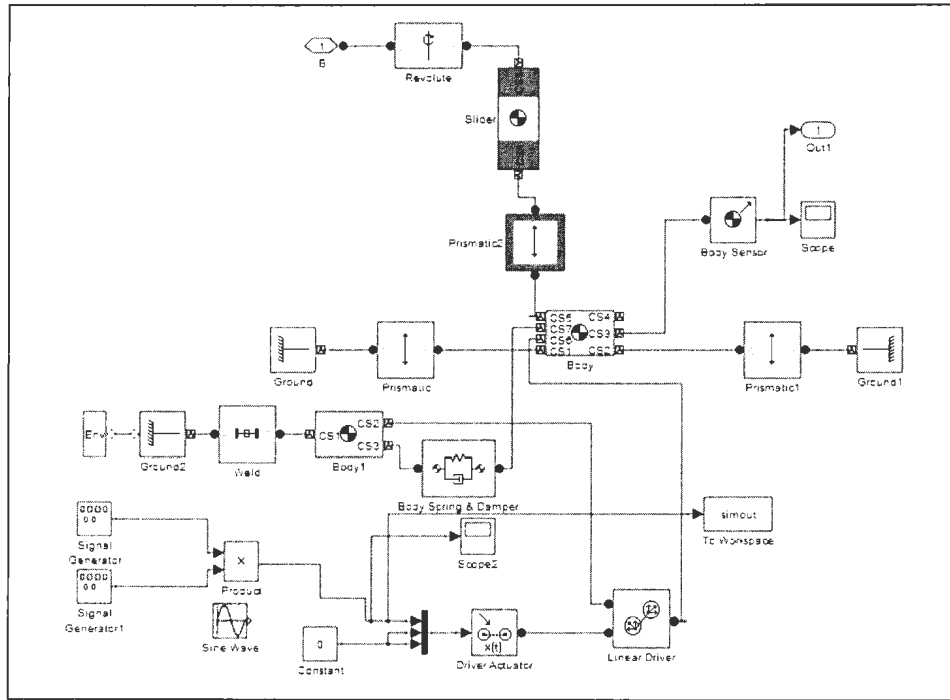
- [30] Margolis, Donald, and Taehyun Shim. "A Bond Graph Model Incorporating Sensors, Actuators, and Vehicle Dynamics for Developing Controllers for Vehicle Safety." *Journal of the Franklin Institute* 338.1 (2001): 21-34.
- [31] Filippini, German, et al. "Dynamics of Multibody Systems with Bond Graphs." *Mecanica Computacional* 26 (2007): 2943-2958.
- [32] Billingsley, John. *Essentials of Controls Theory and Applications*. FL: Taylor and Francis, 2010.
- [33] Hansen, Colin H., and Scott D. Snyder. *Active Control of Noise and Vibration*. London: E & FN Spon, 1997.
- [34] Broenink, J.D. "Introduction to Physical Systems Modeling with Bond Graphs." *SiE handbook on Simulation Methodologies*. (1999).
- [35] Rideout, G. *Simulating Coupled Longitudinal, Pitch and Bounce Dynamics of Trucks with Flexible Frames*. Memorial University of Newfoundland. Modern Mechanical Engineering. 2012.
- [36] Blue Ribbon Motoring. "Suspension Systems Tech Center." <http://www.autoanything.com/suspension-systems/50A26A163A1.aspx>. 19 September 2012.
- [37] Steidel, Robert F. *An Introduction to Mechanical Vibrations*. New York: John Wiley & Sons, 1989.
- [38] Firgelli Automations. "Linear Slides." <http://www.firgellilinearslides.com/40-inches-Large-Linear-Slides> 2012. Web. 28 September 2012.
- [39] Silicon Designs. "Advanced Accelerometer Solutions." <http://www.silicondesigns.com/product.html#SASMA>. 28 September 2012.

- [40] Wakeham, K. *Development of an Active Suspension Scale Vehicle Platform*. Memorial University of Newfoundland. 2011. Thesis.
- [41] dSPACE GmbH. "DS 1103 Hardware." <http://www.dspace.com/en/inc/home.cfm>. Web. 30 September 2012.
- [42] MTS Systems Corp. "Axial/Torsional Test Systems." <http://www.mts.com/en/products/producttype/test-systems/load-frames-multiaxial/axial-torsional/index.htm>. 30 September 2012.
- [43] Moticont. "Linear voice coils." <http://www.moticont.com/voice-coil-motor.htm>. Web. 30 September 2012.
- [44] Wikipedia. http://en.wikipedia.org/wiki/Main_Page. Web. 30 September 2012.
- [45] Nikravesh, P.E. *Computer Aided Analysis of Mechanical Systems*. New Jersey: Prentice Hall, 1988.
- [46] Carnegie Mellon. "Planar Joints." <http://www.andrew.cmu.edu/org/me-tutorials/PLANARJOINTS.htm>. 30 September 2012.
- [47] Butsuen, T. The design of semi-active suspension for automotive vehicles. PhD thesis, MIT. 1989.

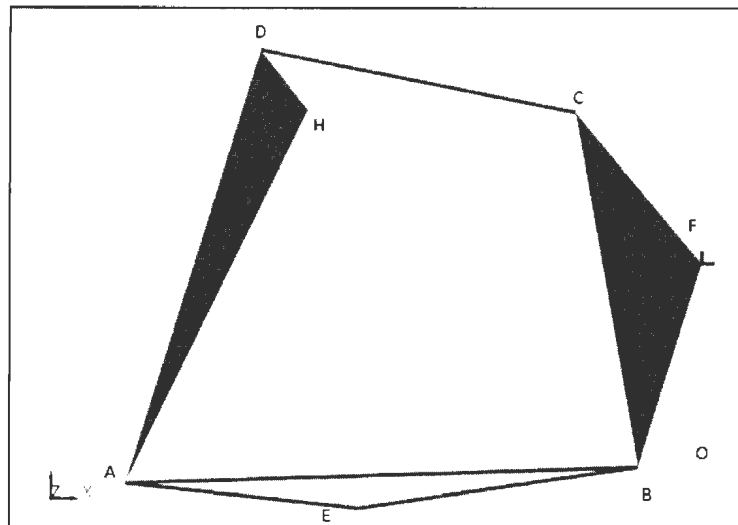
Appendix A Matlab/Simmechanics Multi-body Model

This Matlab/Simmechanics model was developed prior to the bond graph multi-body model. The purpose was to develop a multi-body quarter car model and design a controller for it. Although the model was generated successfully, the controller did not work on the model and it was giving unreliable results. So, this model was discarded after several modifications.





The multi-body model developed in Simmechanics had the following layout. A spring, damper and actuator system was attached from points E and H. A tire was attached between points F and O. The road input was giving at point O.



129

```
0 0 0 1;
```

```
4727 188 - 47273 - 188];
```

```
B = [0;
```

```
0.0025;
```

```
0;
```

```
-0.0303];
```

```
C = [1 0 0 0;
```

```
0 1 0 0;
```

```
0 0 0 1];
```

```
D = [0;
```

```
0;
```

```
-1;
```

```
0];
```

```
%Cost Function
```

```
%zsddot^2 + p1(susp.def.)^2 + p2(tire def.^2) + p3(control force)^2
```

```
%Weighting factors - heavily weighted susp/tire deflection
```

```
p1 = 10000;
```

```
p2 = 100;
```

```
p3 = 100000;
```

```
p4 = 100;
```

130

%Weighting factors – heavily weighted ride quality

% p1 = 400;

% p2 = 16;

% p3 = 400;

% p4 = 16;

$Q1 = [ks^2/ms^2 + p1 \ bs \ * \ ks/ms^2 \ 0 \ - \ bs \ * \ ks/ms^2;$

$\ \ bs \ * \ ks/ms^2 \ bs^2/ms^2 + p2 \ 0 \ - \ bs^2/ms^2;$

$\ 0 \ 0 \ p3 \ 0;$

$\ -bs \ * \ ks/ms^2 \ - \ bs^2/ms^2 \ 0 \ bs^2/ms^2 + p4];$

$N = [-ks/ms^2;$

$\ -bs/ms^2;$

$\ 0$

$\ bs/ms^2];$

$R = 1/ms^2;$

$S = N;$

%P = manipulated variables

%E = closed loop eigenvalues

%G = gain matrix

$[P, E, G] = care(A, B, Q1, R, S);$

Appendix C Bond Graph States

Bond graph method for calculation of suspension states has been described here.

The suspension deflection can be calculated in the following way

$$\begin{aligned}\dot{q}_{11} &= f_{11} \\ f_{11} &= f_9 \\ &= f_{12} - f_8 \\ &= f_{14} - f_7 \\ &= \frac{p_{14}}{I_{14}} - \frac{p_7}{I_7} \\ \dot{q}_{11} &= \frac{p_{14}}{m_s} - \frac{p_7}{m_u}\end{aligned}$$

The sprung mass velocity is given by

$$\begin{aligned}\dot{p}_{14} &= e_{14} \\ e_{14} &= e_{13} - e_{12} \\ &= -m_s g - e_{12} \\ e_{12} &= e_9 \\ e_9 &= e_{10} + e_{11} \\ &= \frac{q_{11}}{C_{11}} + f_{10} R_{10} \\ f_{10} &= f_9 \\ &= f_{12} - f_8 \\ &= f_{14} - f_7 \\ &= \frac{p_{14}}{I_{14}} - \frac{p_7}{I_7}\end{aligned}$$

$$\begin{aligned}\dot{p}_{14} &= -m_s g - \left[\frac{q_{11}}{C_{11}} + \left(\frac{p_{14}}{I_{14}} - \frac{p_7}{I_7} \right) R_{10} \right] \\ &= -m_s g - \left[q_{11} k_s + \left(\frac{p_{14}}{m_s} - \frac{p_7}{m_u} \right) b_s \right]\end{aligned}$$

The tire deflection is given by

$$\begin{aligned}\dot{q}_4 &= f_4 \\ f_4 &= f_2 \\ &= f_5 - f_1 \\ &= f_7 - f_1 \\ &= \frac{p_7}{I_7} - f_1 \\ \dot{q}_4 &= \frac{p_7}{m_u} - f_1\end{aligned}$$

Similarly, the unsprung mass velocity can be calculated by

$$\begin{aligned}\dot{p}_7 &= e_7 \\ e_7 &= e_6 + e_8 - e_5 \\ e_7 &= -m_u g + e_9 - e_2 \\ e_2 &= e_3 + e_4 \\ &= f_3 R_3 + \frac{q_4}{C_4} \\ f_3 &= f_2 \\ &= f_5 - f_1 \\ &= f_7 - f_1\end{aligned}$$

$$= \frac{p_7}{I_7} - f_1$$

$$\dot{p}_7 = -m_u g + \left[\frac{q_{11}}{C_{11}} + \left(\frac{p_{14}}{I_{14}} - \frac{p_7}{I_7} \right) R_{10} \right] \\ - \left[\left(\frac{p_7}{I_7} - f_1 \right) R_3 + \frac{q_4}{C_4} \right]$$

$$\dot{p}_7 = -m_u g + \left[q_{11} k_s + \left(\frac{p_{14}}{m_s} - \frac{p_7}{m_u} \right) b_s \right] \\ - \left[\left(\frac{p_7}{I_7} - f_1 \right) b_t + q_4 k_t \right]$$

